FEDERAL UNIVERSITY OF ITAJUBÁ

MECHANICAL ENGINEERING INSTITUTE

DEVELOPMENT OF A MULTI-OBJECTIVE OPTIMIZATION ALGORITHM BASED ON LICHTENBERG FIGURES

JOÃO LUIZ JUNHO PEREIRA

Itajubá - MG

2022

FEDERAL UNIVERSITY OF ITAJUBÁ

MECHANICAL ENGINEERING INSTITUTE

DEVELOPMENT OF A MULTI-OBJECTIVE OPTIMIZATION ALGORITHM BASED ON LICHTENBERG FIGURES

João Luiz Junho Pereira

A dissertation presented to the Postgraduate Program of Mechanical Engineering, from the Mechanical Engineering Institute of the Federal University of Itajubá, as a requirement to obtain the title of Doctor of Science in Mechanical Engineering.

Concentration area: **Design, Materials, and Processes**

Advisor: Prof. Dr. Guilherme Ferreira Gomes

Co-advisor: Prof. Dr. Sebastião Simões da Cunha Jr.

Itajubá - MG

2022

FEDERAL UNIVERSITY OF ITAJUBÁ

MECHANICAL ENGINEERING INSTITUTE

DEVELOPMENT OF A MULTI-OBJECTIVE OPTIMIZATION ALGORITHM BASED ON LICHTENBERG FIGURES

João Luiz Junho Pereira

Doctoral Dissertation to be examined on August 22, 2022, granting the author the title of **Doctor of Science in Mechanical Engineering.**

Examination Board:

Prof. Dr. Domingos Alves Rade (ITA)

Prof. Dr. Samuel da Silva (UNESP)

Prof. Dr. Anderson Paulo de Paiva (IEPG – UNIFEI)

Prof. Dr. Yohan Alí Diaz Mendéz (IEM – UNIFEI)

Prof. Dr. Sebastião Simões da Cunha Jr (IEM – UNIFEI)

Prof. Dr. Guilherme Ferreira Gomes (IEM – UNIFEI)

Itajubá - MG

2022

Dedication

I dedicate this work to all those who are on the frontier of knowledge and seek to expand it.

"I would give everything I know, for half of what I do not know"

René Descartes

Acknowledgements

I thank my father João Batista and my aunt Maria Mônica for all support and encouragement during my life. Nothing would be possible without you.

I thank my dissertation advisor, Professor Guilherme Ferreira Gomes, for all your support, patience, dedication, effort, and inspiration. Your success spills over to everyone around you. Thank you.

My dissertation co-advisor, Professor Sebastião Simões, for your technical support, friendship, patience, life advice, and motivation that will always bring good memories.

To all GEMEC colleagues for their friendship, trust and partnerships. In special: Matheus Brendon, Camila Diniz, Lucas Antônio, Ronny Francis, and Guilherme Oliver.

Finally, I thank my friends Leonardo Huhn and Matheus Ramos for being my brothers in life.

Abstract

This doctoral dissertation presents the most important concepts of multi-objective optimization and a systematic review of the most cited articles in the last years of this subject in mechanical engineering. The State of the Art shows a trend towards the use of metaheuristics and the use of a posteriori decision-making techniques to solve engineering problems. This fact increases the demand for algorithms, which compete to deliver the most accurate answers at the lowest possible computational cost. In this context, a new hybrid multi-objective metaheuristic inspired by lightning and Linchtenberg Figures is proposed. The Multi-objective Lichtenberg Algorithm (MOLA) is tested using complex test functions and explicit contrainted engineering problems and compared with other metaheuristics. MOLA outperformed the most used algorithms in the literature: NSGA-II, MOPSO, MOEA/D, MOGWO, and MOGOA. After initial validation, it was applied to two complex and impossible to be analytically evaluated problems. The first was a design case: the multi-objective optimization of CFRP isogrid tubes using the finite element method. The optimizations were made considering two methodologies: i) using a metamodel, and ii) the finite element updating. The last proved to be the best methodology, finding solutions that reduced at least 45.69% of the mass, 18.4% of the instability coefficient, 61.76% of the Tsai-Wu failure index and increased by at least 52.57% the natural frequency. In the second application, MOLA was internally modified and associated with feature selection techniques to become the Multi-objective Sensor Selection and Placement Optimization based on the Lichtenberg Algorithm (MOSSPOLA), an unprecedented Sensor Placement Optimization (SPO) algorithm that maximizes the acquired modal response and minimizes the number of sensors for any structure. Although this is a structural health monitoring principle, it has never been done before. MOSSPOLA was applied to a real helicopter's main rotor blade using the 7 best-known metrics in SPO. Pareto fronts and sensor configurations were unprecedentedly generated and compared. Better sensor distributions were associated with higher hypervolume and the algorithm found a sensor configuration for each sensor number and metric, including one with 100% accuracy in identifying delamination considering triaxial modal displacements, minimum number of sensors, and noise for all blade sections.

Keywords: Multi-objective Lichtenberg Algorithm, Multi-objective Optimization, Metaheuristics, Mechanical Engineering, Isogrid Structures, Sensor Placement Optimization.

Resumo

Esta tese de doutorado traz os conceitos mais importantes de otimização multi-objetivo e uma revisão sistemática dos artigos mais citados nos últimos anos deste tema em engenharia mecânica. O estado da arte mostra uma tendência no uso de meta-heurísticas e de técnicas de tomada de decisão a *posteriori* para resolver problemas de engenharia. Este fato aumenta a demanda sobre os algoritmos, que competem para entregar respostas mais precisas com o menor custo computacional possível. Nesse contexto, é proposta uma nova meta-heurística híbrida multi-objetivo inspirada em raios e Figuras de Lichtenberg. O Algoritmo de Lichtenberg Multi-objetivo (MOLA) é testado e comparado com outras metaheurísticas usando funções de teste complexas e problemas restritos e explícitos de engenharia. Ele superou os algoritmos mais utilizados na literatura: NSGA-II, MOPSO, MOEA/D, MOGWO e MOGOA. Após validação, foi aplicado em dois problemas complexos e impossíveis de serem analiticamente otimizados. O primeiro foi um caso de projeto: otimização multi-objetivo de tubos isogrid CFRP usando o método dos elementos finitos. As otimizações foram feitas considerando duas metodologias: *i*) usando um meta-modelo, e *ii*) atualização por elementos finitos. A última provou ser a melhor metodologia, encontrando soluções que reduziram pelo menos 45,69% da massa, 18,4% do coeficiente de instabilidade, 61,76% do TW e aumentaram em pelo menos 52,57% a frequência natural. Na segunda aplicação, MOLA foi modificado internamente e associado a técnicas de *feature selection* para se tornar o Seleção e Alocação ótima de Sensores Multi-objetivo baseado no Algoritmo de Lichtenberg (MOSSPOLA), um algoritmo inédito de Otimização de Posicionamento de Sensores (SPO) que maximiza a resposta modal adquirida e minimiza o número de sensores para qualquer estrutura. Embora isto seja um princípio de Monitoramento da Saúde Estrutural, nunca foi feito antes. O MOSSPOLA foi aplicado na pá do rotor principal de um helicóptero real usando as 7 métricas mais conhecidas em SPO. Frentes de Pareto e configurações de sensores foram ineditamente geradas e comparadas. Melhores distribuições de sensores foram associadas a um alto hipervolume e o algoritmo encontrou uma configuração de sensor para cada número de sensores e métrica, incluindo uma com 100% de precisão na identificação de delaminação considerando deslocamentos modais triaxiais, número mínimo de sensores e ruído para todas as seções da lâmina.

***Palavras-chave**:* Algoritmo multi-objetivo de Lichtenberg, Otimização multi-objetivo, Meta-heurísticas, Engenharia mecânica, Estruturas isogrid, Otimização da Alocação de Sensores.

CONTENTS

List of Figures

List of Tables

List of Symbols

$f(x)$	Objective function
X	Vector of decision Variables
i	Iteration
w	Weight
P_i	Score (TOPSIS)
Pop	Population
N_p	Number of Particles
R_c	Creation Radius
S	Stickiness coefficient
ref	Refinement
M	Figure Switching factor
N_{iter}	Number of iterations
$rand$	ramdom number between 0 and 1
φ	Angle between helical ribs [°]
δ_c	width of circular ribs [mm]
δ_H	width of helicoidal ribs [mm]
R^2	Indicator of model fit
E_1	Elasticity Modulus in longitudinal direction [GPa]
E_2	Elasticity Modulus in transverse direction [GPa]
G_{12}	Shear modulus in plane [GPa]
k	Number of design parameter
TW_T	Tsai-Wu under torsion efforts
TW_C	Tsai-Wu under compression efforts
λ_T	Buckling coefficient under torsion efforts
λ_C	Buckling coefficient under compression efforts
y	RSM response
α	Distance from center point
β	Constant coefficients
ω_n	Natural frequency [Hz]

m	Mass [g]
h	Thickness [mm]
$\overrightarrow{S_s}$	Selected Sensors Vector
$\overrightarrow{B}$	Binary Vector
ΔS	Triaxial Nodal Displacement
N_e	Element Number
α	Damage Rate
Φ	Mode Shape

List of Abbreviations and acronyms

MOP	Multi-objective Problem
NFL	No-free-lunch theorem
LA	Lichtenberg Algorithm
MOLA	Multi-objective Lichtenberg Algorithm
ZDT	Zitzler-Deb-Thiele test functions
NSGA-II	Non-Dominated Sorting Genetic Algorithm II
MOPSO	Multi-objective Particle Swarm Optimization
MOEA/D	Multi-objective Evolutionary Algorithm based on Decomposition
MOGWO	Multi-Objective Grey-Wolf Optimizer
MOGOA	Multi-objective Grasshopper Optimization Algorithm
SPO	Sensor Placement Optimization
CFRP	Carbon fiber-reinforced polymer
DoE	Design of Experiments
RSM	Response Surface Methodology
FEM	Finite Element Method
PF	Pareto Front
DM	Decision Maker
NBI	Normal Boundary Intersection
GA	Genetic Algorithm
MOEA	Multi-objective Evolutionary Algorithm
VEGA	Vector Evaluation GA
MOGA	Multi-objective GA
SPEA	Strength Pareto Evolutionary Algorithm
MOALO	Multi-objective Ant Lion Optimizer
OM	Orthogonal Method
FG	Functionally Graded
TOPSIS	Technique to Order of Preference by Similarity to Ideal Solution
ORC	Organic Rankine Cycles
DMS	Direct Multi-Search

SAW	Submerge Arc Welding
FCAW	Flux Cored Arc Welding
GMAW	Gas Metal Arc Welding
ANOVA	Analysis of Variance
FSW	Friction Stir Welding
ANN	Artificial Neural Network
NSTLBO	Non-dominated Teaching-Learning Based Algorithm
HMOGWO	Hybrid grey wolf optimizer
SHM	Structural Health Monitoring
LF	Lichtenberg Figure
PF	Pareto front
DLA	Diffusion Limited Aggregation
IGD	Inverted Generational Distance
SP	Spacing
MS	Maximum Spread
PSO	Particle Swarm Optimization
CCD	Central composite design
MRB	Main Rotor Blade
SC	Sensor Configurations
FS	Feature Selection
ADPR	Average Driving-Point Residue
EfI	Effective Independence
FIM	Fisher Information Matrix
MAC	Modal Assurance Criterion
DOF	Degrees of Freedon
IE	Information Entropy
KE	Kinetic Energy
MOSSPOLA	Multi-objective Sensor Selection and Placement Optimization LA-based
SVM	Support Vector Machine
FRF	Frequency Response Function
HV	Hypervolume
EA	Evolutionary Algorithm

Chapter 1

Introduction

Optimization can be described as a process of searching for the best solution within a set of possible solutions (ALEXANDRINO *et al*., 2020). In practical engineering problems, most applications are nonlinear, multimodal, non-convex, with complicated or nonexistent analytical solutions and must often serve more than one objective or function that may even be in conflict with each other, and they require sophisticated optimization tools to be determined (YANG, 2014; GOMES & GIOVANI, 2020).

It is possible to determine in mono-objective optimization which solution is better than other given one set of solutions. As result, a single solution is usually obtained and generally an efficient algorithm is required that has good exploitation and exploration capabilities. The former refers to the ability to improve the accuracy of solutions already found, while the latter refers to the ability to escape local optimal solutions (OLORUNDA & ENGELBRECHT, 2008; GOMES & ALMEIDA, 2020). However, in multi-objective optimization there is no direct method for determining if one solution is better than another, because the answer is a set of solutions that involves multiple conflicting objectives that must be considered simultaneously (GOMES, 2018).

Mechanical engineering is a vast and complex area with numerous possible applications for Multi-objective Optimization Problems (MOP). Nowadays, according to the author's best knowledge, there is no work in the literature that compiles the main applications and allows the researcher an overview of the subject in this area. The review works found, and some are even out of date, usually focus on the *i*) multi-objective optimization itself: Long *et al.* (2021), Gunantara

(2018), Wang *et al*. (2017b), Marler & Arora (2004) focusing on engineering in general; *ii*) in algorithms and where they have already been applied: Liu *et al.* (2020b) in meta-heuristics for discrete optimization, Mane & Rao (2017) in Evolutionary Algorithms, Tamaki *et al.* (1996) in Genetic Algorithms, Song & Gu (2004) in Particle Swarm Optimization, Leguizamón & Coello Coello (2011) in Ant Colony Optimization; or *iii*) specific cases: Ridha *et al.* (2021) in photovoltaic system, Kumar *et al.* (2021) in machining, Ojstersek *et al.* (2020) in production scheduling, Liu *et al*. (2020) in wind energy, Rangaiah *et al.* (2020) in chemical process engineering, Afshari *et al*. (2019) in concrete structures, Cui *et al*. (2017) in energy saving, Fadaee *et al*. (2012) in renewable energy.

One of the objectives of this Dissertation is to summarize the most cited applications in the last five years and some others which, although not so recent, have great relevance in mechanical engineering. The main focus is to highlight the most modern and efficient trends on algorithms and decision-making techniques used, indicating precisely the decision variables and objective functions. Some of the applications that can be found in this work are: *i*) problems in design optimization: meta-materials, functionally graded plates, airfoils, wind turbines, fan and pumps, security and support structures, suspensions, exchangers and expanders, beams, composites, etc. *ii*) problems in process engineering: welding, machining, and molding, and *iii*) problems in structural health monitoring.

The methods to approach these MOPs can be divided into optimization processes in which an operator can participate at any time: not participating, participating at the beginning of the optimization process, during or only at the end. Algorithms can be enumerative, deterministic, or stochastic (as in meta-heuristics) (COELLO *et al*., 2007). This study will discuss the advantages and drawbacks of these approaches and will justify what has been done in literature as to why meta-heuristics and *a posteriori* decision-making techniques have been more widely used. This increases the demand on algorithms, causing a dispute for an algorithm that achieves more solutions with more convergence, coverage, and at a lower computational cost.

Some behaviors found in nature are sources of inspiration for the development of algorithms that aim to obtain optimal solutions with these capabilities (MIRJALILI & LEWIS, 2016). Due to this characteristic, these algorithms are called meta-heuristics, and each one has its own parameters that regulate its optimization process (YANG, 2014; NABIL, 2016). Meta-heuristics generate random solutions in the search space for a given problem and continuously improve them through iterations, not just randomly, but with tradeoffs that depend on how each algorithm is created.

For Yang (2014), there are no good or bad algorithms, but rather ones that may be more appropriate for a given optimization problem. It is a difficult task for a single algorithm to face any type MOP with good balance of exploration, exploitation, convergence, coverage, and low computational cost at the same time. In this sense, the no-free-lunch (NFL) theorem was developed (JOYCE & HERRMANN, 2018). These facts suggest that there will always be room for developing new meta-heuristics capable of dealing with multi-objective optimization problems.

A metaheuristic in the mono-objective version was recently created and had the author of this Dissertation as one of the creators. Inspired by the physical phenomenon of radial intra-cloud lightning and Lichtenberg Figures, the Lichtenberg Algorithm (LA) (PEREIRA *et al*., 2021) has been successfully applied to identify cracks (PEREIRA *et al*., 2021b), damage in composites (PEREIRA *et al*., 2021c), optimize carbon fiber designs as isogrid lower limb prosthetics (FRANCISCO *et al*., 2020), and in other unpublished applications.

To the best knowledge of the author, the LA was the first published hybrid algorithm, as it combines trajectory and population optimization routines in the same optimizer. Meta-heuristics are usually classified into only one of two categories. Furthermore, it is a fully numerical algorithm, since the process of creating figures that guide the optimization trajectories is based on the theory of Diffusion Limited Aggregation (WITTEN & SANDER, 1981). There is no other way to create an algorithm inspired by lightning while dispensing with the use of internal sub calculations common to the overwhelming majority of other meta-heuristics, and so the algorithm proved to be fast, accurate, and efficient.

The main objective of this Dissertation is to bring all the details surrounding the evolution of LA into the Multi-Objective Lichtenberg Algorithm (MOLA). Furthermore, the algorithm will be validated via three groups of test functions: *i*) the first group is known as the Zitzler-Deb-Thiele test functions (ZDT) (ZITZLER *et al*., 2000), one of the most used test functions in literature, *ii*) CEC2009 test functions (ZHANG *et al*., 2008), which is considered to be the most challenging function group contained in literature on multi-objective optimization algorithms (MIRJALILI *et al*., 2016), and then iii) constrained engineering problems with explicit equations.

During the algorithm testing process, MOLA was compared against the most well known meta-heuristics in literature in recent years, the Non-Dominated Sorting Genetic Algorithm II (NSGA-II) (DEB *et al*., 2000), and the Multi-objective Particle Swarm Optimization (MOPSO) (MOSTAGHIM & TEICH, 2003). It will also be compared with the Multi-objective Evolutionary Algorithm based on Decomposition (MOEA/D) (ZHANG & LI, 2007), and two other more recent meta-heuristics, the Multi-Objective Grey-Wolf Optimizer (MOGWO) (MIRJALILI *et al*., 2016),

and the Multi-objective Grasshopper Optimization Algorithm (MOGOA) (MIRJALILI, *et al*., 2017). Pareto fronts comparison metrics will be used to assess performance.

Having made a detailed review of the state of the art of multi-objective optimization in mechanical engineering and proposed/validated a new multi-objective meta-heuristic, MOLA will be applied to two complex engineering problems that gradient-based optimization or requiring explicit equations methods would be unable to optimize. The first will be a design application for identifying geometric variables and the second will be an application for Sensor Placement Optimization (SPO).

The first complex application in this work is the design optimization of carbon fiber-reinforced polymer (CFRP) isogrid tubes considering six different structural responses, i.e., mass, Tsai-Wu failure index, and instability coefficient (under compression and torsion efforts), and natural frequency. These structures are highly complex and do not have explicit equations that model their responses. All works before used Design of Experiments (DoE) and Response Surface Methodology (RSM) to generate metamodels and then perform the optimization of their structural parameters.

One of the qualities of meta-heuristics is their ability to optimize systems that deliver answers from input variables, without necessarily using equations, such as finite element software or machine learning algorithms. This Dissertation brings the optimization of isogrid tubes for the first time using the direct link between MOLA (MATLAB®) and the finite element method (FEM) software (ANSYS APDL®), identifying the true behavioral nature of the Pareto fronts of these structures. The answers will be compared with the same problems using metamodels through Pareto fronts comparison metrics.

The second complex application is based on adapting MOLA to develop a SPO methodology that maximizes the acquired modal response and minimizes the number of sensors in a helicopter's main rotor blade. Although this trade-off is a SHM principle, there is no methodology in literature that opposes these objectives for any structure. Firstly, a real AS350 helicopter rotor blade was experimentally tested and a numerical model was elaborated in FEM. Then, MOLA undergoes internal modifications and is associated with feature selection techniques to become the Multi-objective Sensor Selection and Placement Optimization based on the Lichtenberg Algorithm (MOSSPOLA).

It has as one of the objectives the number of sensors and the other, one of the 7 best-known metrics in SPO: Kinetic Energy, Effective Independence, Average Driving-Point Residue, Eigenvalue Vector Product, Information Entropy, Fisher Information Matrix, and Modal Assurance

Criterion. All results will be analyzed and the best and most appropriate sensor configuration found will be validated in a blade damage identification study.

Figure 1.1 summarizes the development of the dissertation: *i*) literature review, *ii*) development of the Multi-objective Lichtenberg Algorithm, *iii*) application in structural design, and *iv*) application in Sensor Placement Optimization.

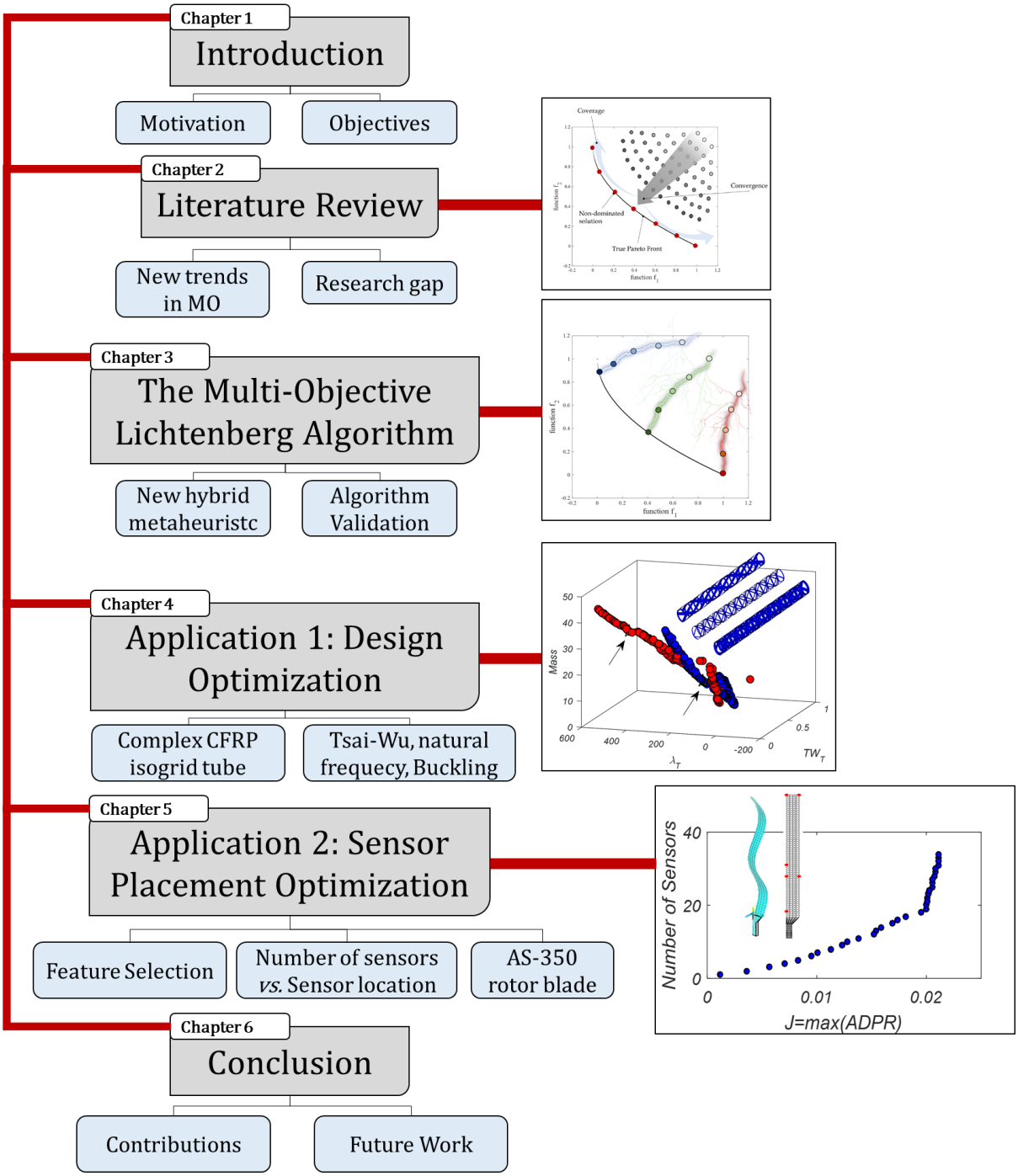

Figure 1.1 – Dissertation Flowchart

1.1 Research Objective

The main purposes of this Dissertation are: *i*) synthesize the main concepts, methods and algorithms of multi-objective optimization in mechanical engineering, pointing out the modern trends, *ii*) propose, develop, and validate the Multi-objective version of the Lichtenberg Algorithm, *iii*) apply it to complex multi-objective structural optimization problem, and *iv*) adapt and apply it in a complex and innovative sensor placement optimization method.

1.2 Dissertation Outline

The Dissertation is organized as follows:

- Chapter 2 presents a systematic literature review about multi-objective optimization in mechanical engineering: *i*) synthesize the main concepts of multi-objective optimization with examples and a critical discussion, and *ii*) situate which techniques and algorithms within this vast area have been applied to problems in mechanical engineering, pointing out modern and more efficient trends;
- Chapter 3 presents the development of the Multi-objective Lichtenberg Algorithm (MOLA): propose, develop, and validate the algorithm using complex test functions and constrained engineering problems with explicit equations;
- Chapter 4 presents the application of MOLA in the optimization of isogrid tubes made of CFRP.
- Chapter 5 presents the application of MOLA in the Sensor Placement Optimization of a real AS350 main helicopter rotor blade using feature selection.
- Chapter 6 concludes the dissertation with an overview of the main conclusions.
- Chapter 7 brings the publications and patents generated during this dissertation.

Chapter 2

A review of Multi-objective Optimization: Methods and Algorithms in Mechanical Engineering Problems

This Chapter summarizes the most cited applications of multi-objective optimization in mechanical engineering problems in the last five years and some others which, although not so recent, have great relevance. The main focus is to highlight the most modern and efficient trends in algorithms and decision-making techniques used, indicating precisely the decision variables and objective functions in real multi-objective optimization problems.

Some of the applications that can be found in this work are: *i*) problems in design optimization: meta-materials, functionally graded plates, airfoils, wind turbines, fan and pumps, security and support structures, suspensions, exchangers and expanders, beams, composites, etc. *ii*) problems in process engineering: welding, machining, and molding and *iii*) problems in structural health monitoring.

The Chapter is organized as follows: Section 2.1 presents a general theoretical background review about multi-objective optimization. Section 2.2 presents a systematic review of the literature on the main applications of multi-objective optimization in Mechanical Engineering, detailing

which algorithms, techniques, decision variables and objectives were used in each of the problems and Section 2.3 brings conclusions.

2.1 Theoretical Background

The optimization problems that must meet more than one objective are called Multi-objective Optimization Problems (MOPs) and present several optimal solutions (CHIANDUSSI *et al*., 2012). The solution is the determination of a vector of decision variables $\boldsymbol{X} = \{x_1, x_2, ..., x_n\}$ (variable decision space) that optimizes the vector of objective functions $F(\boldsymbol{X})=\{f_1(x), f_2(x), ..., f_n(x)\}$ (objective function space) within a feasible region of solutions subject to equality $h_i(x)$ or inequalities $g_i(x)$ constraints where x_{min} and x_{max} are the limits that determine the search space for each of the variables, or vector of variables (BARIL *et al*., 2011). As described in Equation (2.1) (GOMES, 2013; PAULA *et al*., 2019).

$$\begin{gathered} \min F(\boldsymbol{X})=\{f_1(\boldsymbol{x}), f_2(\boldsymbol{x}), ..., f_n(\boldsymbol{x})\} \\ \text{subject to: } h_i(\boldsymbol{x})=0,\ i=1, 2, ..., p \\ g_i(\boldsymbol{x}) \leq x\ 0,\ i=1, 2, ..., q \\ \boldsymbol{x}_{min} \leq \boldsymbol{x} \leq \boldsymbol{x}_{max} \end{gathered} \tag{2.1}$$

This leads to a set of solutions called Pareto-optimal, which according to Rao (2009) is a feasible region $\boldsymbol{X}$ so that there is no other feasible region $\boldsymbol{Y}$ such that $f_i(\boldsymbol{Y}) \leq f_i(\boldsymbol{X})$ *for* $i = 1, 2, ..., k$ with $f_j(\boldsymbol{Y}) \leq f_j(\boldsymbol{X})$ for at least one j. That is, there is no other feasible solution $\boldsymbol{Y}$ that would reduce some objective function without causing an increase in at least one other objective function at the same time. The method most commonly used to compare solutions is Pareto Dominance Relationship, which instead of determining a single optimal solution, leads to a set of optimal alternatives between the objectives. These solutions are also called non-dominated solutions or Pareto Front (PF) (JAIMES *et al*., 2009) and any of these solutions are optimal and it is up to the operator of the problem to choose the best one according to his preference. See the variable decision space and the objective or solution space with examples of non-dominated solutions in blue (PF) in Figure 2.1, where n is the number of design variables and k is the number of objective functions of the problem.

Possible solutions in variable decision space generate solutions in the objective space and dominance relations are analyzed to eliminate those that are not Pareto-optimal. As seen, this front is built through iterations and before having a final Pareto front, there are local Pareto fronts behind this. Each MOP has a characteristic PF, which can be continuous or discontinuous (disconnected) and convex or concave. A MOP will be considered convex if the viable set and the individual objective functions are convex (as in Figure 2.1) and this leads to a convex PF. If the viable set is not convex, or at least one of the functions is non-convex, the problem will be considered concave. In general, for non-convex MOP, PF can be concave and disconnected (DAS & DENNIS, 1998). Not every region of the objective space, including those above the PF, is a feasible region. There may be voids without solutions, which contribute to the discontinuity of the problem (BARIL *et al.*, 2011; COELLO *et al.*, 2007). Figure 2.2 illustrates this paragraph.

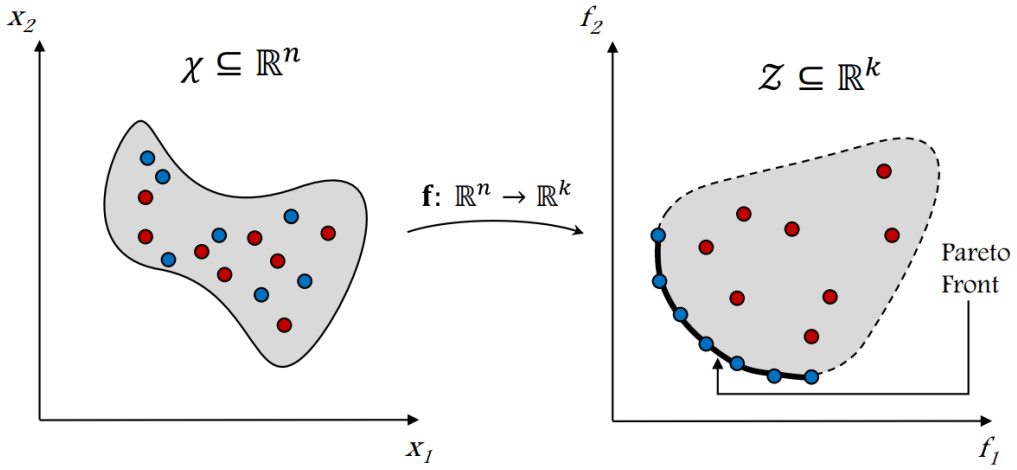

Figure 2.1 – Equivalences between the Search Space and the Objectives Space (GOMES *et al.*, 2018)

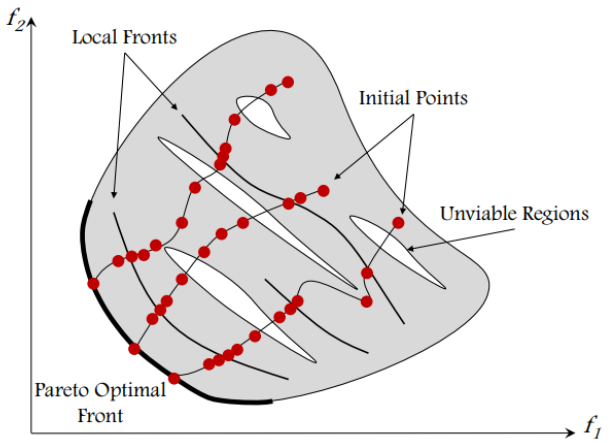

Figure 2.2 – Regions of a design problem with two-variable and two objective functions (GOMES *et al.*, 2018)

In mono-objective optimization, the specific parameters of each meta-heuristic must be correctly chosen for each problem to have the best exploration and exploitation response. This is respectively, being able to escape from local minimums and still being able to improve the precision of the solutions already found (OLORUNDA & ENGELBRECHT, 2008). In MOP, this alone is not enough. A good multi-objective optimization algorithm, when looking for a set of possible solutions forming the Pareto front, must be able to find a PF with precision (convergence) and good distribution of possible solutions throughout the solution space (coverage) (BRANKE *et al*., 2001; MIRJALILI *et al*., 2016b), as shown in Figure 2.3.

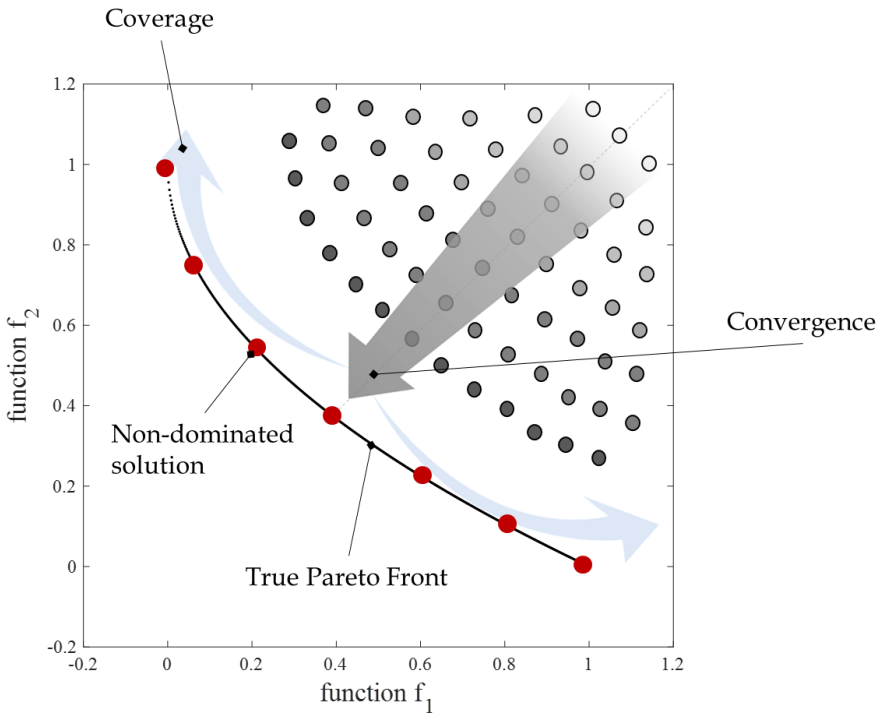

Figure 2.3 – Capabilities that a meta-heuristic must have to be successful in a MOP.

Accurately determine the set of non-dominated solutions to a problem is a hard task made possible by the development of better computers and new techniques and algorithms. Zitzler *et al.* (2000) interested in testing and comparing evolutionary multi-objective optimization algorithms has created six test functions that are still one of the most popular ones for testing new algorithms (MIRJALILI *et al*., 2016). The ZDT (Zitzler-Deb-Thiele) test functions are a set of problems with very diverse Pareto fronts in which the best algorithm is the one that has the Pareto front found closest to the true Pareto front. Figure 2.4 shows the true Pareto front for some of these functions.

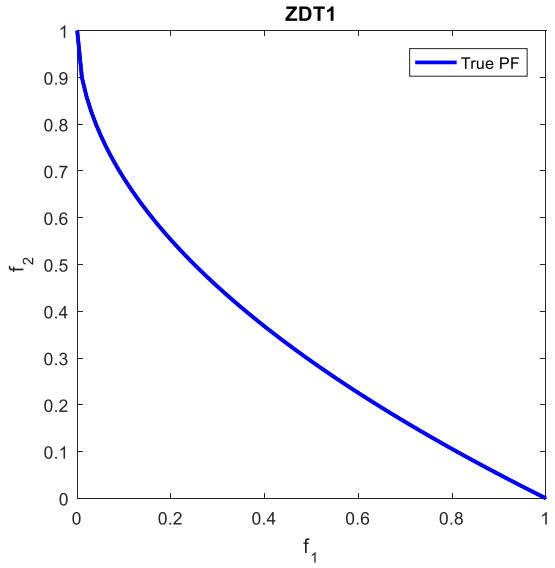

a) Convex PF

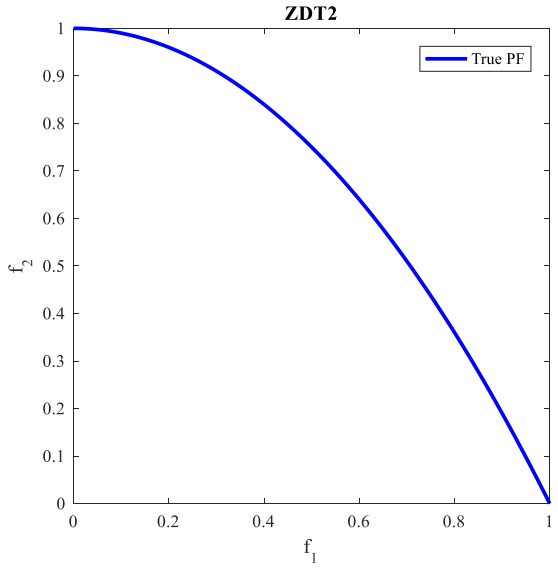

b) Concave PF

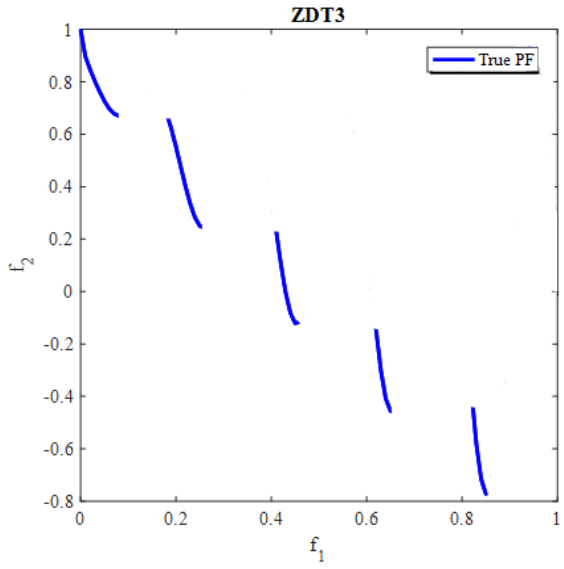

c) PF with several convex parts

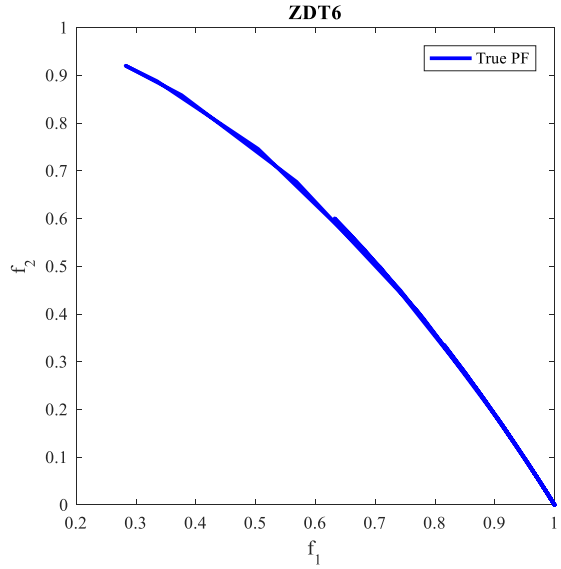

d) PF with two difficulties: no uniformity of search space and lowest density of the solutions near the true PF

Figure 2.4 – Main ZDT test functions for MOP

Note that the Pareto fronts of the ZDT1 (Figure 2.4a) and ZDT2 (Figure 2.4b) functions are continuous, however the first is convex and the second is concave. The ZDT3 (Figure 2.4c) represents the discreteness feature; its Pareto-optimal front consists of several noncontiguous convex parts and the ZDT4 (Figure 2.4d) contains 21^9 local Pareto-optimal fronts and, therefore, tests the algorithm´s ability to deal with multimodality. The first three ZDT functions have thirty design variables and the last, ten. Those functions that are well defined can check how well a new

algorithm has convergence and coverage capabilities. At the same time, it shows how diverse the Pareto fronts of a real engineering problem can be.

2.1.1 Main Methods to approach Multi-objective problems

There are several techniques for dealing with MOPs. In general, they are classified according to when the preferences of the problem operator (or decision maker, DM) are inserted in the problem: a *priori*, *interactive*, a *posteriori* methods or no preference method (COHON & MARKS, 1975).

2.1.1.1 No preference methods

In no preference methods the DM is not needed. Only one solution is computed and is usually as close as possible to the ideal point.

Global Criterion Method

The ideal point or ideal vector is the utopia solution that contains each individual optimal objective function value; see Equation (2.2) and Equation (2.3) (COELLO *et al*., 2007). The Nadir point is the exact opposite, is the vector that contains each separately maximum objective function value found.

$$f_i^0(x^{0i}) = \min f_i(x) \tag{2.2}$$

$$f^0 = \left[f_1^0, f_1^0, f_1^0, ..., f_k^0 \right]^T \tag{2.3}$$

Therefore, the best solution found in this method is seen in Equation (2.4) (MIETTINEN, 1998):

$$L_p = \min\left(\sum_{i=1}^{k} \left| f_i(x) - f_i^0 \right|\right)^{1/p} \tag{2.4}$$

where $f_i(x)$ is the objective function i evaluated for all x with i =1, 2, …, k the number of objectives and f_i^0 the minimum value found in the minimization separately of function i. The solution obtained depends greatly on the value chosen for p; widely used choices are 1, 2 or ∞. This is the function that provides the shortest distance between the PF and the ideal point. If p is one, there is a linear distance and if 2, a Euclidean distance (MIETTINEN, 1998).

The main drawback of these types of methods is to neglect all other solutions.

2.1.1.2 A priori preference articulation

In a *priori* methods the DM need to input its preference before optimization starts. This method have some difficulties: *i*) The DM, when initially taking its preferences, can neglect important aspects of the problem and consequently arrive at ineffective or even confusing results (THIELE *et al.*, 2009), *ii*) An algorithm like this should be run multiple times to determine the PF, and *iii*) some special PFs cannot be determined with this approach (DAS & DENNIS, 1998; MESSAC & MATTSON, 2002). The main drawbacks of these methods are that: *i*) an algorithm should be run multiple times to determine the Pareto optimal set, *ii*) there is a need to consult with an expert because an inexperienced DM can select bad regions for exploration and neglect better ones by inducing the optimization process in the wrong direction, and *iii*) some special Pareto optimal fronts cannot be determined with this approach (MIRJALILI, 2016).

Lexigraphic Method

In Lexigraphic method the DM must arrange the objective functions according to their absolute importance (best to worst). After, the most important objective function is minimized subject to the original constraints. If this problem has a unique solution, this is the solution of the whole MOP. Otherwise, the second most important objective function is minimized. Now, in addition to the original constraints, a new constraint is added to guarantee that the most important objective function preserves its optimal value. If this problem has a unique solution, this is the solution of the original problem. Otherwise, the process goes on as above (RAO, 1984)

Goal Programming

In this method, DM has to assign targets or a goal that is wished to be achieved for each objective. These values are incorporated into the problem as additional constraints and then the objective function tries to minimize the absolute deviations from the targets to the objectives. The simplest form of this method is in Equation (2.5) (COELLO *et al*. 2007, DUCKSTEIN 1984)

$$\min \sum_{i=1}^{k} \left| f_i(x) - T_i \right| \tag{2.5}$$

where T_i denotes the target or goal set by the DM for the *i*-th objective function $f_i(x)$.

Other less used a priori methods and references are: Min-Max Optimization (OSYCSKA, 1978; RAO, 1986); Multi-attribute Theory (NEUMANN & MORGENSTERN, 1944); ELECTRE

(elimination and choice translating algorithm) (BENAYOUN *et al.*, 1966) and its derivations; PROMETHEE (Preference Ranking Organization Method for Enrichment Evaluations) (BRANS *et al.*, 1986), among others.

2.1.1.3 An interactive preference articulation

In *Interactive* methods the DM can to articulate its preferences during the optimization process, usually based on the domain knowledge acquired during the optimization (FONSECA & FLEMING, 1993; JIM & SENDHOFF, 2002). These techniques normally operate in three stages: *i*) find a non-dominated solution, *ii*) get the reaction of the DM regarding this solution and modify the preferences of the objectives according to its need, and *iii*) repeat the two previous steps until the DM is satisfied (COHON & MARKS, 1975).

The main algorithms that use this technique are: *i*) Probabilistic Trade-Off Development Method (PROTRADE), *ii*) STEP Method, and *iii*) Sequential Multi-objective Problem Solving Method, *iv*) Interactive Surrogate Worth Trade-Off Method (ISWT), *v*) Geoffrion-Dyer-Feinberg Method (GDF), *vi*) Sequential Proxy Optimization Technique (SPOT), *vii*) Tchebycheff Method, *viii*) Reference Point Method, among others. (COHON, 1978; GOICOECHEA *et al.*, 1976; MONARCHI *et al.* 1973; MIETTINEN, 1998; and COELLO *et al.* 2007).

2.1.1.4 A *posteriori* preference articulation

In a *posteriori* methods, all possible non-dominated solutions are obtained and the DM can analyze the trade-off relationships between the objectives (COHON & MARKS, 1975). This method is the most used in the literature to solve real problems, since one of the advantages is to find PFs that no other method can find and with just one program run (MIRJALILI *et al.*, 2016).

Weighting Method

The idea is to associate each objective function with a weighting coefficient and minimize the weighted sum of the objectives. The multiple objective functions are transformed into a single objective function. The weights w_i are positive real numbers for all $i = 1, \ldots, k$ objective functions. The weights are normalized, that is, $\sum_{i=1}^{k} w_i = 1$. So, here is the Equation (2.6) (ZADEH, 1963):

$$\min \sum_{i=1}^{k} w_i f_i(x) \tag{2.6}$$

However, the main drawbacks of this approach are the need to run an algorithm multiple times to find multiple Pareto optimal solutions, dealing with all the challenges in every run, such as

the lack of information exchange between Pareto optimal solutions during optimization. This occurs cause the weights are always positive and therefore, concave PF can not be found. Still, it demands to consult with an expert to find the best weights (MIRJALILI, 2017). According to Miettinen (1998), this method can be an a priori method if the DM defines the weight it wants to transform a MOP into a mono-objective problem.

ϵ-Constraint Method

This method was introduced by Haimes *et al.* (1971) and only one of the objective functions is selected to be optimized and all other objective functions are converted into constraints by setting an upper bound to each of them. The problem to be solved has the form in Equation (2.7):

$$\begin{aligned} &\text{minimize} && f_l(x) \\ &\text{subject to} && f_j(x) \leq \varepsilon_j \end{aligned} \tag{2.7}$$

where for all $j=1, \ldots, k, j \neq l, l \in \{1, \ldots, k\}$.

Hybrid Method

This method combines the Weighting Method and the ϵ-Constraint Method (MIETTINEN, 1998).

Normal Boundary Intersection

The Normal Boundary Intersection (NBI) was proposed by Das & Dennis (1998) and according to the authors, the method is independent of the relative scales of the functions and is successful in producing an evenly distributed set of points in the Pareto set given an evenly distributed set of parameters, a property which the popular method of minimizing weighted combinations of objective functions lacks. However, according to Brito *et al*. (2016), this method is extremely sensitive to the presence of correlation between objective functions that are used in the construction of PF.

This method starts with the determination of the payoff matrix **[**Φ**]**. The vector of decision variables that minimizes the objective function $f_i\ (x)$ is represented by x_i^* and consequently the minimum value of $f_i\ (x)$ at this point is $f_i^*\ (x_i^*)$. When replacing the individual point x_i^* in the other functions, that is $f_i\ (x_i^*)$, this is a non-optimal value of this function. Repeating the algorithm for all *m* functions, is obtained the payoff matrix represented in Equation (2.8):

$$\Phi = \begin{bmatrix} f_1^*(x_1^*) & \cdots & f_1(x_i^*) & \cdots & f_1(x_m^*) \\ \vdots & \ddots & \vdots & \iddots & \vdots \\ f_i^*(x_1^*) & \cdots & f_i^*(x_i^*) & \cdots & f_i^*(x_m^*) \\ \vdots & \iddots & \vdots & \ddots & \vdots \\ f_m^*(x_1^*) & \cdots & f_m(x_i^*) & \cdots & f_m^*(x_m^*) \end{bmatrix} \tag{2.8}$$

Each line of **[**Φ**]** is composed of minimum and maximum values of $f_i\ (x)$. These sets of extreme points are used to normalize objective functions. Considering a set of weights w_i, the **[**Φ**]** × {w**}** will represent a point on the utopia line. Since η is a unit vector in the direction of origin and normal to the utopia line at points **[**Φ**]** × {w**}**, is obtained that **[**Φ**]** × {w**}** + **[**D**]** × {η**}** will represent the set of points in that normal. The point where the normal intersects the boundary of the viable region closest to the origin will be the point corresponding to the maximization of the distance between the utopia line and the PF (DAS & DENNIS, 1998; BRITO *et al.*, 2014). Therefore, the NBI method can be written as a constrained nonlinear maximization problem defined as in Equation (2.9):

$$\begin{aligned} &\text{Max}_{(x,t)}\ \text{D} \\ &\text{s.t. :}\ \ \textbf{[}\Phi\textbf{]}\times \{w\textbf{\}} + \textbf{[}\text{D}\textbf{]} \times \{\eta\textbf{\}}\ = F(x) \end{aligned} \tag{2.9}$$

This problem must be solved iteratively for different values of w to generate an equally spaced PF.

Technique for Order of Preference by Similarity to Ideal Solution

The Technique for the Order of Preference by Similarity to Ideal Solution (TOPSIS) was introduced by Hwang and Yoon (1981) and became a classic multiple attribute decision making method with more than 4500 citations (YOON & KIM, 2017). TOPSIS determines the positive ideal solution (A+) (Utopia point) as well as the negative ideal solution (A-) (Nadir Point) and normalizes each of the objectives and multiplies them by the weight assigned to each objective, being the sum of all weights w_i always one. Then it calculates the Euclidian distance of each solution (A_i) in the Pareto front to the utopia point (originating S_i^+) and to the Nadir point (originating S_i^-) and calculates the score P_i using Equation (2.10) (BYUN & LEE, 2005):

$$P_i = \frac{S_i^-}{S_i^+ + S_i^-} \tag{2.10}$$

If $P_i = 1$, A_i = A+ and if $P_i = 0$, A_i = A- (that is, the higher *Pi*, the better the solution). In few words, TOPSIS determines the best compromised solution, which was the closest to (A+) and the farthest from (A-) based on the Pareto set according to the objective weights and the normalization of these solutions. Note that with the Score P_i of each solution, it is possible to rank all solutions on the Pareto front from best to worst according to TOPSIS.

2.1.2 Main Algorithms to approach Multi-objective problems

Regardless of the way the DM approaches MOP, this is an optimization problem and must have some technique of general search that should lead to the maximization or minimization of the functions or their compositions. Just like optimizing a single objective, The MOP can be classified through three categories according to the applied search technique: enumerative, deterministic and stochastic.

Enumerative is the simplest search strategy where each possible solution is evaluated. However, this technique is inefficient or even unfeasible as search space becomes large, making the MOP solution extremelhighly computationally expensive (COELLO *et al.*, 2007). Deterministic methods are those based on gradient or derivatives and the most used in MOP are: *i*) Greedy, *ii*) Hill Climbing algorithms, *iii*) Branch and Bound, *iv*) Depth-First and *v*) Breadth-First, *vi*) best-first, and *vii*) calculations-based (BRASSARD & BRATLEY, 1988; GOLDEBERG, 1989; NEAPOLITAN & NAIMIPOUR, 1996). However according Parkinson *et al.* (2013) and Coello *et al*. (2007), deterministic algorithms have difficulty for optimization problems with: *i*) discrete-valued design variables; *ii*) large number of design variables; *iii*) multiple local minima, maxima, and saddle points (multimodal); *iv*) not differentiable objectives and constraints; and *vi*) discontinuities of functions or regions. Therefore, enumerative and deterministic search techniques are unsuitable in real-world and engineering MOPs. Therefore they will not be addressed in this paper.

Stochastic techniques have demonstrated great potential for the solution of complex MOPs and are increasingly gaining space with the increase in the speed and processing capacity of computers. Today these are the main techniques for engineers and designers and although there are several algorithms, the basis of all of them consists in the initialization of the optimization process with a set of random candidate solutions for a given problem and improve them over a pre-defined number of steps. To address the real-world issues, these algorithms should be equipped with different operators (MIRJALILI *et al*., 2017).

The literature shows that almost all stochastic algorithms used in multi-objective optimization were inspired by some optimal phenomena found in nature and are commonly called meta-heuristics. In general, there are four main groups that divide meta-heuristics according to the inspiration for their creation: *i*) based on evolution, *ii*) based on physical phenomena, *iii*) based on behaviors related to humans, and *iv*) based on swarms (HEIDARI *et al*., 2019). For Yang (2014), there is also a classification for meta-heuristic algorithms that can be based on trajectories or population.

In the literature, an immense variety of meta-heuristics can be found that are capable of solving mono-objective optimization problems, but the number of algorithms capable of solving a MOP is much lesser.

2.1.2.1 Evolutionary Algorithms

Evolutionary algorithms were the first meta-heuristics created to deal with multi-objective optimization problems and they drastically broke with most of the classic methods presented earlier. They deal simultaneously with a set of possible solutions (the so-called population). This allows finding several members of the Pareto optimal set in a single run of the algorithm and are less susceptible to the shape or continuity of the PF (COELLO *et al*., 2007).

In short, they use paradigms from natural evolution, such as selection, recombination, and mutation to lead a population (set) of individuals (decision vectors) towards optimal or near-optimal solutions (BACK, 1996). The first meta-heuristic created in this sense was by Holland (1975), it dealt with mono-objective problems and is called Genetic Algorithm (GA). The first to be developed to deal with MOP´S is now called multi-objective evolutionary algorithm (MOEA) or Vector Evaluation Genetic Algorithm (VEGA) (SCHAFFER, 1985). VEGA was mainly aimed for solving problems in machine learning (COELLO *et al*., 2007).

After this, many other derivations with attempts at improvement came. The main ones are: *i*) VEGA, *ii*) Lexigraphic Ordering GA (LOGA- a *priori* preference) (FOURMAN, 1991), *iii*) Vector Optimized Evolution Strategy (VOES) (KURSAWE, 1991), *vi*) Weight-Based GA (WBGA) (HAJELA & LEE, 1992), *v*) Multiple Objective GA (MOGA) (FONSECA & FLEMING, 1993), *vi*) Niched Pareto GA (NPGA, NPGA 2) (HORN & NAFPLIOTS, 1993; HORN *et al.*, 1994), *vii*) Non-dominated Sorting GA (NSGA, NSGA II) (SRINIVAS & DEB, 1994; DEB *et al*., 2000), *viii*) Strength Pareto Evolutionary Algorithm (SPEA, SPEA II) (ZITZLER & THIELE, 1999; ZITZLER *et al.*, 2001), *ix*) Multi-objective Evolutionary algorithm Based on Decomposition (ZHANG & LI,

2007), *x*) Pareto Archived Evolution Strategy (PAES) (KNOWLES & CORNE, 2000), among others.

With some exceptions, the distinction among all evolutionary multi-objective algorithms is mainly due to the differences in the paradigms used to define the selection operators, whereas the choice of the variation operators is generic and dependent on the problem. As example, one of the most popular is the NSGA II which can be applied to continuous search spaces as well as to combinatorial search spaces, whereas the selection operators stay the same, the variations operators (mutation and combination) must be adapted to the representations of solutions in the decision space (EMMERICH & DEUTZ, 2018). All population-based multi-objective algorithms are similar. They start the optimization process with multiple candidate solutions and such solutions are compared using the Pareto dominance operator. The most well regarded ones are: SPEA, NSGA-II, MOEA/D, and PAES (MIRJALILI *et al.*, 2016)

Although most of these algorithms are divided between a *priori*, *interactive* or a *posteriori* methods, most of them are like the latter. All are stochastic. According to the no-free-lunch theorem, none of them can be excellent at solving any type of problem. Zitzler *et al.* (2000) applied several evolutionary algorithms to identify the PF of the ZDT3 function shown in Figure 2.4c. Figure 2.5 has the result for each of these algorithms and also that of a rand search. As evidenced, any evolutionary algorithm can be better than a rand, but there are significant differences between them and these differences can vary from problem to problem.

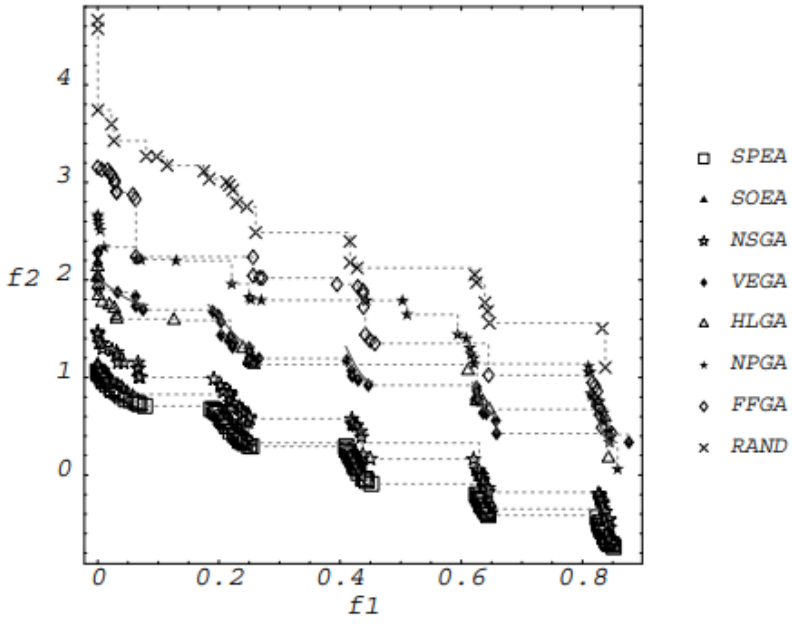

Figure 2.5 – Performance of the main evolutionary algorithms in the ZDT3 function (adapted from Zitzler *et al.* (2000))

2.1.2.2 Others Meta-heuristics

Although there are good evolutionary algorithms for certain types of problems, that its inspiration is natural evolution, it has been shown that there is still room for improvement for specific problems. Based on this, other important multi-objective optimization algorithms found in the literature are: *i*) Simulated Annealing for Multi-objective Optimization (SAMO) (SERAFINI, 1994); *ii*) Multi-objective Tabu Search (MOTS) (GANDIBLEUX *et al*., 1997); *iii*) Multi-objective Ant-Q (MOAQ) (MARIANO & MORALES, 1999); *iv*) Vector Evaluated Particle Swarm (VEPSO) (PARSOPOULOS *et al.*, 2002); *v*) MOPSO (MOSTAGHIM & TEICH, 2003); *vi*) Adaptive Weighted Particle Swarm Optimization (AWPSO) (MAHFOUF *et al.*, 2004); *vii*) Artificial Immune Systems (AIS) (COELLO COELLO & CORTEZ , 2005); *viii*) Multi-objective Water Cycle Algorithm (MOWCA) (SADOLLAH *et al*., 2015); *ix*) Multi-Objective Grey Wolf Optimizer (MOGWO) (MIRJALILI *et al*., 2016); *x*) Multi-objective Imperialist Competitive Algorithm (MOICA) (BILEL *et al.*, 2016); *xi*) Self-adaptive Multi-objective Brain Storm Optimization (SMOBSO) (GUO *et al.*, 2015); *xii*) Multi-objective Ant Lion Optimization (MOALO) (MIRJALILI *et al*., 2016b); *xiii*) MOGOA (Mirjalili *et al*., 2017), *xiv*) Multi-objective Sine-Cosine algorithm (MO-SCA) (TAWHID & SAVSANI, 2017), *xv*) Multi-objective Stochastic Fractal Search (MOSFS) (KHALILPOURAZARY, *et al*., 2019), *xvi*) Multi-objective Seagull Optimization Algorithm (MOSOA) (DHIMAN *et al*., 2020), *xvii*) Evolutionary MOSOA (EMOSOA) (DHIMAN et al., 2020b), *xviii*) Differential Evolution-Crossover Quantum Particle Swarm Optimization (DE-CQPSO) (XING-GANG *et al*., 2020) *xix*) Multi-objective Sunflower Optimization (FRANCISCO *et al*., 2021), etc. As well as the evolutionary algorithms, all of them have their internal parameters that regulate their search according to their inspiration and then, these solutions are compared using a Pareto dominance operator. All are stochastic algorithms and most of them has a *posteriori* preference.

It is possible to observe a huge variety of stochastic algorithms found in the literature. For Yang (2014), there are no good or bad algorithms, but one more appropriate for a given optimization problem. It is a difficult task for a single algorithm to face any type of MOP with good balance of exploration, exploitation, convergence, coverage, and low computational cost at the same time. This fact suggests that there is always an opening for the development of new meta-heuristics.

2.2 Literature Review

Multi-objective optimization has been improved and developed for some decades as it faces several problems that may be encountered. The number of applications has been growing in Mechanical Engineering and the following are those that are considered most relevant or recent, divided into the subareas where multi-objective optimization is present: design optimization, manufacturing, and structural health monitoring.

2.2.1 Multi-objective Problems in Design Optimization

Undoubtedly one of the greatest applications in mechanical engineering is in determining the geometry of structures to obtain the best possible performances. Generally related to weight, stiffness, aerodynamics and/or modal parameters. The more objectives that must be met at the same time, the more complex MOP becomes. Relevant applications are cited in the text and the objective functions, decision variables, and algorithm employed are in Table 2.1.

Grachi *et al.* (2020) found a design for a meta-material with the highest vibration attenuation in a low-frequency range. Meta-materials are composites that are geometrically engineered to have unnatural mechanical properties.

Schlieter & Dlugosz (2020) optimized the design of an airfoil by proposing a new optimization methodology and obtaining many optimal Pareto solutions for a large number of decision variables. Li *et al*. (2020) proposed a new method for optimizing the design of wind turbine blades that surpassed traditional methods, since in addition to optimizing structural strength and stiffness of the blade also considers the noise and power generation efficiency. Wang *et al.* (2017) also studied multi-objective wind turbine blade design proposing a novel gradient-based multi-objective evolution algorithm based on both uniform decomposition and differential evolution (MODE/D), which according to the author, performed better than NSGA-II mainly when the number of objectives is increased.

Fan *et al.* (2020) designed a new mixed flow flan improving a currently standard model. The author increased the efficiency by 11.71% and the pressure raised by 50.15% using Orthogonal Method (OM). The purpose of this method is to test the influence of a particular factor over the whole outcome, with the view of obtaining optimal configuration in terms of the performance levels (ZHANG *et al.,* 2011). Zhang *et al.* (2019) also applied multi-objective optimization using OM in design of Axial Flow Pump where the new design's head and efficiency increased by 17.8% and 4.26%, whilst the shaft power and the pressure pulsation coefficient reduced by 1.22% and 11%, respectively. Wang & Huo (2018) used the same approach to improve the hydraulic performance of

a centrifugal pump. Karimi *et al.* (2016) proposed a design optimization approach for floating offshore wind turbine support structures, where the authors found the locus of platform cost minima and wind performance maxima for a given environmental condition and sea state spectrum modifying the geometry of the structure (multi-objective constrained problem).

Moleiro *et al.* (2020) studied metal-ceramic functionally graded (FG) plates, which are composed of a main functionally graded material layer and may include metal and/or ceramic faces under thermo-mechanical loadings. Other authors who also studied this type of structure with a pit in multi-objective optimization were: Ashjari & Khoshravan (2017) and Franco Correia *et al.* (2018 & 2019). Both considered constraints on the problem.

Multi-objective optimization is widely found in the design of colliding structures. Asanjarani *et al.* (2017) presented a crashworthiness optimization of the tapered thin-walled square tube with indentations using one and multi-objective approach, where the authors found an optimized collision geometry. Zhang *et al.* (2019a) developed a hybrid multi-objective optimization approach for absorbing structures in train collisions that brought good results using multi-objective artificial bee colony. Peng *et al.* (2016) also studied structures for collision using NSGA-II with an approach using finite element methods and design of experiments (DOE).

Ebrahimi-Nejad *et al.* (2020) tried to find the best design of a sports car suspension system using simplified quarter-car models and TOPSIS. Other authors who studied suspension designs using a multi-objective approach were: *i*) Zhang *et al.* (2019b) performed the multi-objective suspension system optimization for an in-wheel-motor driven electric vehicle, *ii*) Zhang & Wang (2019c) conducted a parametric study to optimize a half-vehicle suspension system model, *iii*) Fossati *et al.* (2019) used NSGA-II and numerical computational studies comprising the multi-objective optimization of a full-vehicle suspension, *iv*) Jiang & Wang (2015, 2016) used TOPSIS to optimize the suspension system of a truck and also to optimize handling stability and ride comfort.

Panagant *et al.* (2021) conducted a research using 14 types of meta-heuristics in 8 types of classical trusses subject to bound and stress constraints and compared the results of each one, concluding that the algorithm proposed by them was the one that had the best performance, the Success History-based Adaptive Multi-objective Differential Evolution (SHAMODE-WO). Panagant *et al.* (2019) also used 14 meta-heuristics, this time in an automotive floor-frame. The authors concluded that the meta-heuristic proposed in their work was one of the best algorithms, the Real-code Population-Based Incremental Learning hybridized with Adaptive Differential evolution (RPBILADE).

In the thermal area some designs can be found. Rao *et al.* (2017) applied single and multi-objective optimization in design of plate-fin heat exchangers, whose design involves a number of geometric and physical parameters with high complexity. The general approaches are based and trial and error and few studies before it used multi-objective optimization. One of these is by Ahmadi *et al.* (2011) who used NSGA-II. However, Rao compared this study to his and concluded that Jaya algorithm had a better result. Bahadormanesh *et al.* (2017) applied multi-objective optimization in improvement design of radial expanders of Organic Rankine Cycles (ORC) using firefly algorithm, where it was possible to pre-select better parameters for the construction of these rotors. Wang *et al.* (2013) also applied multi-objective optimization in ORC, but aiming to improve aspects thermodynamics and economics using NSGA-II.

Studies in the field of composite materials can also be found. Vo-duy *et al*. (2017) optimized a beam structure made of laminated composite using finite element method. Ghasemi & Hajmohammad (2016) applied multi-objective optimization in design of laminated composite cylindrical shell under external hydrostatic pressure for minimum cost and maximum buckling pressure. Other authors who also worked with the optimization of carbon fiber structures using a multi-objective approach were: Arian Nik *et al.* (2012), Lee *et al.* (2012), Omkar *et al.* (2012), Kalantari *et al.* (2016), Ikeya *et al.* (2016), and Diniz *et al*. (2021).

(Intentionally left blank)

Table 2.1 – Multi-objective Optimization System in Design Problems

Authors	Objective Functions	Decision Variables	Optimization Method	Structure
Panagant *et al*. (2021)	Structural Mass and Compliance	Several variables related to the size and number of trusses	fourteen meta-heuristics	Truss
Panagant *et al*. (2019)	Strucutural mass, welding cost, and compliance	Topology, shape, and size	fourteen meta-heuristics	floor-flame
Grachi *et al.* (2020)	Metamaterial inertia and Bragg scattering effect	Layer thickness and number of layers	MO based on GA	Metamaterial
Schlieter & Dlugosz (2020)	Equivalent stress, displacement, frequency, mass	24 design variables (geometry)	MO based on DE	airfoil
Moleiro *et al.* (2020)	Mass, displacement, and Tsai-Hill failure criteria	Thickness, power-low distribution, the thickness of metal	Direct MultiSearch (DMS)	FG blades
Ashjari, Khoshravan (2017)	Mass and deflection	FG core volume fractions and thickness of the face sheets	NSGA II	FG blades
Franco Correia *et al*. (2018 and 2019)	Mass, cost, natural frequency	Index of the power-law of volume fractions, thickness of FGM layer, and face sheets	DMS	FG blades
Li *et al.* (2020)	Structural strength, stiffness, noise reduction and, aerodynamic performance	Chord length and twist angle (for each cross section)	MOPSO and finite volume method	Wind turbine blade
Wang *et al.* (2017)	Energy production, blade mass, root thrust, cost	30 related to design	MODE/D	Wind tubine blade
Fan *et al.* (2020)	Efficiency and Pressure	Hub angle of impeller (and wrap) and diffuser	Orthogonal Method	Mixed Flow Fan
Zhang *et al.* (2019d)	Head, efficiency, shaft power, and pressure pulsation	Number of blades, blade setting angle, hub ratio, distance between the blade, and the guide vane	Orthogonal Method	Axial Flow Pump
Wang & Huo (2018)	Indexes head, efficiency, shaft power, and pump net positive suction head	Impeller outlet width, blade inlet angle, blade outlet angle, and cape angle	Orthogonal Method	Centrifugal Pump
Karimi *et al.* (2016)	Cost model and wind turbine performance metric	Nine geometric variables of multi-body platform	NSGA-II	offshore support
Asanjarani *et al.* (2017)	Specific energy absorption, ratio between average, and maximum crushing forces	Cross section, thickness, taper angle, number and radius of indentations	RSM, NSGA-II, and desirability function	tapered thin-walled square tube
Zhang *et al.* (2019a)	Capability of absorbing impact and energy	Side length and wall thickness of hexagonal tube	MOABC	train collision piece
Ebrahimi-Nejad *et al.* (2020)	unsprung and sprung mass accelerations, displacement and suspension travel	Stiffness and damping	TOPSIS	Sports car suspension
Zhang *et al.* (2019b)	Sensitive of the front double pivot and the rear double wishbone suspensions	Eighteen parameters related to stiffness and damping coefficients	NSGA-II	Suspension system
Fossati *et al.* (2019)	Three objective functions related to comfort and safety	Six parameters being stiffness and damping coefficients of each suspension	NSGA-II	full-vehicle suspension
Rao *et al.* (2017)	Total surface area, total annual cost, total pressure drop, and effectiveness	Seven design variables related to geometry	Jaya Algorithm	plate-fin heat Exchangers
Bahadormanesh *et al.* (2017)	Thermal efficiency and size parameter	different organic working fluids, mass flow rate, evaporator temperature, maximum pressure	Multi-objective firefly algorithm	radial expanders
Vo-duy *et al*. (2017)	Weight, natural frequency	Volume fractions, thickness, and fiber orientation angles	NSGA-II	beam structure
Ghasemi (2016)	Mass/cost, buckling	Cylinder thickness, radius, and lenght	NSGA-II	composite cilidrical
Arian Nik *et al*. (2012)	Rigidity, buckling	Fiber orientation	NSGA-II	Composite plate
Lee *et al.* (2012)	Weight, deformation	Stacking sequence, thickness, material	MOGA	Composite plate
Omkar *et al.* (2012)	Weight, cost	Fiber orientation	VEPSO	Composite plate
Kalantari *et al.* (2016)	Weight, cost	Thickness, fiber, and resin	NSGA-II	Composite plate
Ikeya *et al.* (2016)	Mass, compliance	Volume fraction, thickness	GA	Composite plate

2.2.2 Multi-objective Problems in Manufacturing

Processing engineering is an extensive area in Mechanical Engineering, the largest areas of which are Welding, Machining, and Molding.

2.2.2.1 Welding

Welding is one of the most important areas of engineering and there are currently many types of processes. Some of these processes can have a large number of decision variables controlling the process, with high complexity of correlation or analytical solutions. Still, there can be numerous objectives to be optimized simultaneously. Some of them are to increase productivity, decrease costs, reduce the thermally affected zone, increase the reinforcement, decrease (or increase) the hardness, decrease the emission of toxic gases, decrease the consumption of electric energy, increase the impact strength, increase the tensile strength, increase elongation in the weld area, reduce noise pollution, among others. As seen, the use of Meta-heuristics has collaborated a lot to deal with this extensive area. The most relevant applications are cited in the text and the objective functions, decision variables and algorithm are in Table 2.2.

Ahmad *et al.* (2019) studied Submerge Arc Welding (SAW) looking for optimal parameters to achieve productivity and weld quality. SAW is a versatile welding process widely used in fabrication and manufacturing of marine and pressure vessels, pipelines, and offshore structures. Other authors who also studied the SAW process aiming at multi-objective optimization, generally as weld quality, strength, hardness and/or productivity, were: Choudhary *et al.* (2019), Ahire *et al.* (2018), Sailender *et al.* (2018), Silva *et al.* (2018), Rao *et al.* (2017), Al Dawood *et al*. (2017), Yifei *et al.* (2018) (welding robot parameters), Torres *et al.* (2020), among others.

Sowrirajan *et al.* (2018) applied multi-objective optimization to find the optimum clad layer dimensions in pressure vessels using stainless steel that maximize clad height and width, and minimize depth of penetration in a FCAW (Flux Cored Arc Welding) process. Paula *et al*. (2019) and Almeida *et al.* (2020) also studied the optimization of the parameters of this process.

Shao *et al.* (2017) studied the optimization of gas metal arc welding (GMAW) parameters and sequences for low-carbon steel (Q345D) T-joint using FEM and DOE concluding that the welding residual deformation and stress always have opposite behavior and are very influenced by the process parameters. Lorza *et al.* (2018) also studied the optimization of welded joints in GMAW using FEM, but another algorithm, the NSGA II. Like the previous one, this work approached a methodology to reduce the error between the FEM and a real case. Both seek the selection of optimal process parameters.

Another welding process that many authors approached to optimize their parameters was the friction stir welding (FSW). Gupta *et al.* (2016a & 2016b) studied this process for joining different alloys in two works with different approaches, but the same materials. In both studies, the optimal parameters found were the same. Shanjeevi *et al.* (2014) studied for AISI 304l austenitic stainless steel and copper points. Wakchaure *et al.* (2018) for Alloy 6082 using Taguchi-GRA and artificial neural network (ANN) and Senthil *et al.* (2020) for AA6063-T6 pipes using Analysis of Variance (ANOVA) and RSM.

Saha & Mondal (2017) studied the optimization of manual metal arc welding (MMAW) process parameters for nanostructured hardfacing material using hybrid approach with Taguchi, TOPSIS, and PCA (Principal Component Analysis) identifying the optimal process parameters. The study of the optimization of welding parameters by a multi-objective approach was found less frequently in other processes because they are not so common or are recent: *i*) Laser-magnetic hybrid welding (LMW) by Yang *et al.* (2018a), *ii*) hot wire laser welding (HLW) by Yang *et al.* (2018b) *iii*) Hybrid laser-arc welding (HLAW) by Gao *et al.* (2016), *vi*) laser welding process (LW) by Jiang *et al.* (2016) using FEM, Kriging (a meta-model), and NSGA-II, *v*) Micro resistance spot welding (MRSW) by Chen *et al.* (2018), and *vi*) Laser beam machining by Belinato *et al*. (2018).

Another type of multi-objective problem related to welding is the local scheduling. Lu *et al.* (2018) studied an approach to welding shop scheduling that, according to the authors, should simultaneously consider economic, environmental, and social impacts. In this way, the authors proposed a multi-objective approach using a novel hybrid multi-objective grey wolf optimizer (HMOGWO) for makespan (total sum time of each process), energy consumption, and noise pollution (ignores in previous studies). The same authors in Lu *et al.* (2017) applied the same algorithm for dynamic scheduling in a real-world welding industry. In both cases the authors concluded that the algorithm used outperforms known EA´s.

2.2.2.2 Machining

Another major area of manufacturing engineering is machining. As with welding, machining has a wide range of processes like milling, turning, drilling or cutting and each can have a great number of decision variables that control the processes. Some of the conflicting objectives to be optimized simultaneously are minimizing roughness, minimizing cost, minimizing cutting force, increasing productivity, increasing material removal, decreasing process variability, reducing residual stress, among others. The most relevant applications are cited in the text and the objective functions, decision variables, and algorithm employed are in Table 2.3.

Rao *et al.* (2016) applied multi-objective optimization using Non-dominated sorting Teaching-Learning Based algorithm (NSTLBO) in three machining process (turning, wire-eletric-discharge machining, and laser cutting) and two micro-machining processes (ion beam micro-milling and micro wire-electric-discharge machining) looking for the best process parameters. The authors compared this algorithm with NSGA-II and others algorithms.

Lin *et al.* (2016) studied machining parameters in multi-pass turning operations for low carbon manufacturing considering reducing machine cost, energy consumption and environmental impacts using a multi-objective teaching-learning-based optimization algorithm (MOTLBO) in dry and wet cut. Sahu & Andhare (2018) applied multi-objective optimization to improve the machinability of Titanium alloy in cryogenic turning process using Teaching-Learning Based Optimization (TLBO), JAYA, GA, and RSM. Mia *et al.* (2018) also studied cryogenic turning of a Titanium alloy. Sivaiah & Chakradhar (2018) improved the cryogenic turning process during machining of hardened stainless steel.

Gaudêncio *et al*. (2019) proposed a model for machining quality in the AISI 12L14 steel turning process using fuzzy multivariate mean square error, that is, the objectives are decrease roughness to minimize the roughness and its own variability (Multivariate mean square error – MMSE). Almeida *et al*. (2018) used the same steel and mean and standard deviation roughness objectives to optimize parameters in turning. Park *et al.* (2016) studied turning process of hardened material aiming to resolve environmental issues reducing the consumed energy and improving energy efficiency. The energy decreased 16% and the efficiency could be improved 11% compared to the non-optimized system. Warsi *et al.* (2018) studied a sustainable turning of Al 6061 T6 where the proposed parameters resulted in reduction of specific cutting energy by 5% and improvement of 33% in material removal rate while surface roughness remained unaffected.

Another machining process is milling. Qu *et al.* (2016) applied multi-objective optimization to select optimum parameters in milling thin-walled plates. Montalvo-Urquizo *et al.* (2018) also studied milling creating a numerical model with FEM in which the accuracy of the method compares very well with experimental data.

Other machining processes can be found in the literature that have gained more space and multi-objective approaches, but even less common, such as: *i*) powder mixed electric discharge (PMEDM) – studied by Prakash *et al.* (2016)(first in this process to use NSGA-II) and Tripathy & Tripathy (2017); *ii*) electrical discharge machine – studied by Abidi *et al.* (2018) and Prakash *et al.* (2018), and *iii*) Abrasive Water jet Machine (AWJM) – studied by Dumbhare *et al.* (2018) and Rao *et al.* (2017).

2.2.2.3 Molding

Molding is another area in which multi-objective optimization is not yet fully explored. It also has a significant number of decision variables that control the process and many objectives to be optimizing simultaneously. Among the analyzed processes, this process had the least number of studies. Most were in the injection process and aimed at reducing the warpage, minimizing the cycle time or reducing costs, materials or energy used. The most relevant applications are cited in the text and the objective functions, decision variables and algorithm employed are in Table 2.4.

Li *et al.* (2018b) proposed an approach to optimize the fiber-reinforced composite injection molding process. Kitayama *et al.* (2016) proposed another methodology to multi-objective optimization of injection parameters for short cycle time and warpage reduction using conformal cooling channel. The same author in Kitayama *et al.* (2017) used the same methodology to find the optimal parameters in plastic injection molding for minimizing warpage and cycle time. Zhang *et al.* (2015) studied the optimization of the injection molding process parameters for a diesel engine oil cooler. Okabe *et al.* (2017) proposed a new multi-objective optimization approach for resin transfer molding process using FEM, MOGA, self-organizing map, and scatter plot matrix.

Li *et al.* (2017) applied multi-objective optimization in a biodegradable polymer stent structure and stent microinjection molding process using FEM, DOE, and Kriging surrogate method. The authors improved the expansion performance and the microinjection molding process of the biresorbable polymeric stent with tiny struts.

(Intentionally left blank)

Table 2.2 – Multi-objective Optimization System in Welding Process

Authors	Objective Functions	Decision Variables	Optimization Method	Process
Choudhary *et al*. (2019)	Bead width, reinforcement, and penetration	Voltage, feed, speed, nozzle to plate distance, flux condition, and plate distance	GA, JAYA Algorithm, and desirability function	SAW
Ahmad *et al*. (2019)	UTS, Hardness, deposition rate, reinforcement height, and bead width	Current, voltage, speed, and heat input	Taguchi-desirability function	SAW
Ahire *et al.* (2018)	Welding strength, welding deposition rate	Current, speed, root gap, and electrode angle	Response Surface and GA	SAW
Sailender *et al.* (2018)	UTS and Hardness	Voltage, feed, speed, and nozzle to plate distance	Taguchi	SAW
Silva *et al.* (2018)	Dilution, reinforcement, and bead width radio	Voltage, feed, and nozzle to plate distance	ANOVA	SAW
Rao *et al.* (2017)	Bead width, weld reinforcement, weld penetration, tensile strength, and weld hardness	Current, speed, and feed	JAYA, GA, PSO, and Imperialist Competitive Algorithm	SAW
Al Dawood *et al*. (2017)	UTS and hardness	Current, voltage, speed	Taguchi-fuzzy interference system	SAW
Yifei *et al.* (2018)	Productivity and cost	Welding path	GA, Particle Swarm Optimization	SAW
Torres *et al.* (2020)	Joint dimensions and dilution	Voltage, speed, wire feed rate, contact distance	Generalized reduced gradient (GRG)	SAW
Rivas *et al.* (2020)	Carbon dioxide emissions, slag, wastes, electric power, material, labor, and energy cost	Current, voltage, welding speed	NSGA II, MOEA/D, MOPSO, SPEA II, and PESA II	SAW
Sowrirajan *et al.* (2018)	Clad height, clad width, and depth of penetration	Open circuit voltage, wire feed rate, welding speed, distance, and electrode angle.	RSM and NSGA-II	FCAW
Shao *et al.* (2017)	Welding stress and deformation	Current, voltage, speed, sequence, and direction	DOE and MOPSO	GMAW
Lorza *et al.* (2018)	Temperature field and angular distortion	Current and voltage	NSGA II	GMAW
Gupta *et al.* (2016a)	Tensile strength, average hardness, and average grain size at weld nugget zone	Rotational speed, welding speed, shoulder, and pin diameter	Grey Relational Analysis coupled with PCA and Taguchi	FSW
Gupta *et al.* (2016b)	Tensile strength, micro-hardness, and grain size	Idem Gupta *et al.* (2016a)	Artificial Intelligence and NSGA II	FSW
Shanjeevi *et al.* (2014)	Tensile strength, metal loss, and weld time	Friction and upset pressure, rotational speed	TOPSIS and Taguchi	FSW
Wakchaure *et al.* (2018)	Tensile strength and impact strength	Tool rotation speed, welding speed, and tilt angle	ANN, GRA, and Taguchi	FSW
Senthil *et al.* (2020)	Yield, tensile strength, and elongation	Rotational and weld speed	ANOVA and RSM	FSW
Saha & Mondal (2017)	Weld bead width, reinforcement, and bead hardness	Current, voltage, and welding speed	TOPSIS-PCA	MMAW
Yang *et al.* (2018a)	Macro-weld profile, microstructure, and hardness	Magnetic flux density, laser power, welding speed	NSGA II and Taguchi	LMW
Yang *et al.* (2018b)	Welding depth and reinforcement and strength	Laser power, welding speed, hot-wire current	Meta-models and NSGA II	HLW
Chen *et al.* (2018)	Tensile-shear, weld nugget size, failure energy	Ramp time, welding time, current, and force	NSGA-II	MRSW
Gao *et al.* (2016)	Depth of penetration, bead width, and bead reinforcement	Laser power, current, distance between laser, and arc and travelling speed	NSGA II and Taguchi	HLAW
Jiang *et al.* (2016)	Bead width and depth of penetration	Laser power and position and welding speed	Kriging and NSGA-II	LW
Lu *et al.* (2018)	Makespan, total penalty of machine load, and instability	Permutation of tasks, actual quantify of the welders, and the starting time	HMOGWO	-
Lu *et al.* (2017)	Makespan, noise pollution, energy consumption	Actual, start and finish processing time	HMOGWO	-

Table 2.3 – Multi-objective Optimization System in Machining Process

Authors	Objective Functions	Decision Variables	Optimization Method	Process
Rao *et al.* (2016)	Tool flank wear and surface roughness	Cutting speed, feed, and depth of cut	NSTLBO and NSGA II	5 different machining process -txt
Lin *et al.* (2016)	Carbon emissions, operation time, and cost	Velocity, feed rate, dept of cut and spindle speed of machine tools	MOTLBO	turning
Sahu & Andhare (2018)	Roughness and force of cutting	Speed of cutting, feed rate, and depth of cut	TLBO, JAYA, GA and RSM	turning
Sivaiah & Chakradhar (2018)	roughness, flank wear and remove rate	Speed of cutting, feed rate, and depth of cut	Taguchi and TOPSIS	Cryogenic turning
Mia *et al.* (2018)	Cutting force, specific energy, temperature, surface roughness, material removal	Cutting speed, feed rate, and number of jets	Gray-Taguchi	Cryogenic turning
Gaudêncio et al. (2019)	Roughness and MMSE	Cutting speed, cutting feed, machining depth	RSM, GRG, and NBI	turning
Almeida *et al.* (2018)	Mean and deviation of roughness	Cutting speed, feed, and depth of cut	RSM	
Park *et al.* (2016)	Cutting energy and energy efficiency	Cutting speed, feed rate, nose radius, edge radius, rake, and relief angles	RSM, NSGA-II, and TOPSIS	turning
Warsi *et al.* (2018)	Cutting energy, material removal, and roughness	Cutting speed, feed, and depth of cut	Gray-RSM	turning
Qu *et al.* (2016)	Cutting force, roughness, milling efficiency	Spindle speed, feed per tooth, axial depth of cut	NSGA-II	milling
Montalvo-Urquizo *et al.* (2018)	Deformation, stress, shape error, and tool wear	Cutting velocity and axial cutting depth	Simulation-based multi-objective optimization	milling
Niu *et al.* (2017)	Residual stress, material removal rate, roughness, and surface hardness	Milling speed, feed per tooth, width of cut, depth of cut, and amplitude ultrasonic	NSGA II	milling
Prakash *et al.* (2016)	Surface roughness and micro-hardness	Peak current, pulse duration, duty cycle, and silicon powder concentration	Taguchi, RSM, and NSGA-II	PMEDM
Tripathy & Tripathy (2017)	Material removal rate, tool wear rate, electrode wear ratio, and surface roughness	Powder concentration, peak current, pulse on time, duty cycle, and gap voltage	ANOVA, GRA, and TOPSIS	PMEDM
Abidi *et al.* (2018)	Material removal rate, roughness, and tool wear rate	Capacitance, electrode material, and discharge	MOGA II	EDM
Prakash *et al.* (2018)	Material removal rate and surface roughness	Peak current, pulse-on, duty cycle, and powder concentration	MOPSO	Mixed-EDM
Dumbhare *et al.* (2018)	Surface roughness and kerf taper angle	Abrasive flow rate, standoff distance, and transverse speed	ANOVA and RSM	AWJM
Rao *et al.* (2017)	Surface roughness and kerf taper angle	Transverse speed, pressure, stand-off distance, tilt angle, surface speed, and abrasive flow rate	MO-Jaya and PROMETHEE	AWJM

Table 2.4 – Multi-objective Optimization System in Molding Process

Authors	Objective Functions	Decision Variables	Optimization Method	Process
Li *et al.* (2018b)	Warpage, volumetric shrinkage, and residual stress	Fiber content, fiber aspect ratio, melt temperature, injection pressure, and cooling time	Taguchi, RSM and NSGA-II	Injection (fiber-reinforce composite)
Kitayama *et al.* (2016)	Cycle time and warpage	Melt temperature, injection time, packing pressure, packing time, cooling time, cooling temperature	Sequential approximate optimization and radial basis function	Injection (plastic)
Kitayama *et al.* (2017)	Packing pressure profile and warpage	Packing pressure profile, melt temperature, injection time, cooling temperature of coolant and cooling time	Sequential approximate optimization and radial basis function	Injection (plastic)
Zhang *et al.* (2015)	Warpage and clamping force	Gate open time, molding temperature, melt temperature, injection time, packing pressure and time, cooling time	Neural network and MOPSO	Injection (plastic)
Li *et al.* (2017)	Stent expansion in a stenotic artery and molding quality	Length, thickness, and outer diameter	Kriging Surrogate	Microinjection
Okabe *et al.* (2017)	Fill time, dry spot, weld line, and wasted resin	Injection points	MOGA	Resin-transfer

2.2.3 Multi-objective Problems in Structural Health Monitoring

Structural Health Monitoring (SHM) is a structural inspection methodology that allows an early diagnosis of structural health through non-destructive techniques, algorithms and the use of sensors in real time. The application of multi-objective optimization can be in the numerical analysis of the collected data and also in the optimization of the reading of the structure through, for example, positioning of the sensors (GOMES *et al*., 2018). The most relevant applications are cited in the text and the objective functions, decision variables and algorithm employed are in Table 2.5.

The study of the positioning of the sensors aims cost reduction by minimizing the number of sensors by improving the efficiency of data reading. In the literature some cases can be found considering multi-objective optimization. In highlight are: *i*) Ferentinos & Tsiligiridis (2007) (wireless sensors subject to the connectivity and spatial density constraints), *ii*) GOMES *et al*. (2018) (composite plates), *iii*) Lin *et al*. (2018) (truss structure – 3D), *iv*) Zhou *et al.* (2021) (wireless sensors), and *v*) Li *et al.* (2018) also studied composite plates and used wavelet decomposition.

With positioned sensors, the numerical approach to the treatment of these data considering inverse methods can have a multi-objective approach. It is important to note that these data can be acquired directly in the structure and/or through finite element (FE) model updating procedure, as can be seen in Alexandrino *et al.* (2019), where the authors proposed a robust method of identifying ellipses and circular holes in composite plates. The ellipse having one of its axes much larger than the other could be considered in the authors' work as a crack.

Figure 2.6 shows a summary of a standard methodology applied in SHM when using a multi-objective approach. First, the structure to be analyzed is defined. Then, a study of the strategy to be adopted in relation to the sensors is made. Finally, an iterative process takes place using an optimization algorithm, usually a meta-heuristic, until some convergence criterion is reached (number of iterations or stipulated difference).

Perera & Ruiz (2008) successfully applied a methodology to large structures such as bridges through a two-step methodology. The first stage is to detect the occurrence of damage and the location of damaged zones by FE model updating using damage functions (TEUGLHS *et al*., 2002). The use of damage functions avoids adjusting the possible damage values of all the elements separately. This results in a reduced number of parameters to be determine, which contributes to avoiding optimization numerical problems and makes its application to large-scale structures easier. In the second stage, refined location of damage and estimation of severity, a standard FE model updating technology with independent adjustment of the design variables is applied, but in this case,

the number of variables is much reduced because only the elements belonging to the zones identified previously as damaged are now assumed to be damaged.

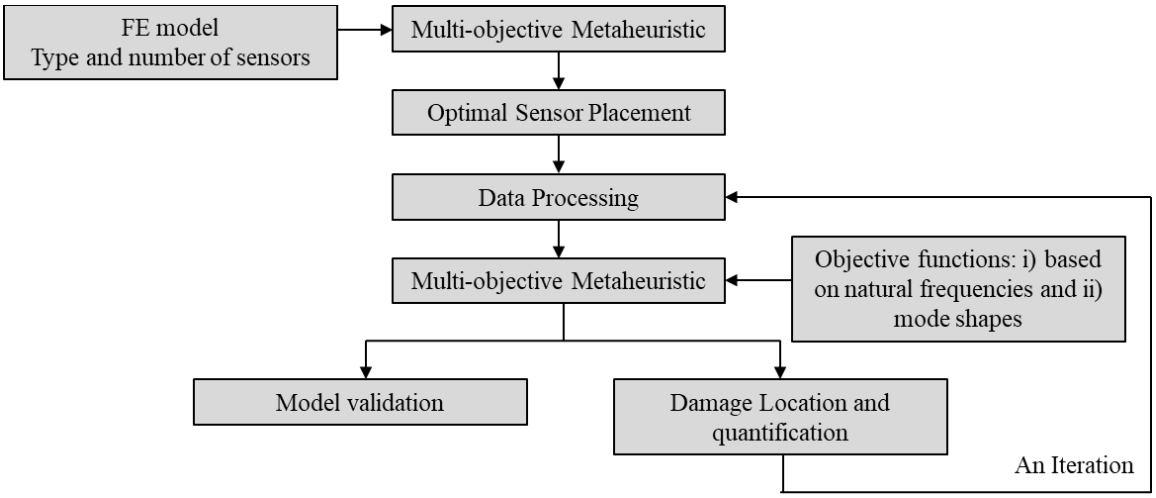

Figure 2.6 – Framework for SHM in a multi-objective approach

Kim & Park (2004) made a very interesting study of identifying a crack on a rectangular plate where they addressed the multi-objective problem in two ways: comparing the two objectives into one using the weighting sum method and without composing them. They reported that the proposed multi-objective EA was more efficient than the single objective EA.

Some authors have analyzed three-dimensional steel structures: *i*) Cha & Buyukozturk (2015) showed a methodology that could be used effectively for detecting minor local damage, although real-world validation using experimental data is still needed; *ii*) Alkayem *et al.* (2017) studied 3D steel structures through two algorithms applying them in their mono and multi-objective versions and concluded that in this case PSO and MOPSO had more accurate results and less computational cost; *iii*) Wang *et al.* (2012) compared FE model updating using NSGA-II, differential evolution for multi-objectives (DEMO) and multi-objective particle swarm optimization (MOPSO) and noted that DEMO outperformed NSGA-II and MOPSO for all damage patterns, and *iv*) Nizar *et al.* (2018) used a methodology that uses at the same time two meta-heuristics and the TOPSIS getting good results even with bad conditions or with incomplete date.

Slipping away from the application of multi-objective optimization in the positioning of sensors or in the identification of damage itself, a relevant article was found on the planning application of the SHM methodology: Kim & Frangopol (2016) proposed a probabilistic optimum SHM planning based on the probabilistic fatigue damage assessment which aimed to determine the

cost important parameters and their weights in order to have the best possible planning of methodology.

(Intentionally left Blank)

Table 2.5 – Multi-objective Optimization System in Structural Health Monitoring

Authors	Objective Functions	Decision Variables	Optimization Method	Object
Ferentinos & Tsiligiridis (2007)	Total energy related to parameters and sensing points uniformity	Uniformity of sensors points, number of sensors, operational energy consumption battery energy consumption.	GA (mono-objective) with weighted sum method	composite plates
Gomes *et al.* (2018)	Fisher Information Matrix and difference module of mode shapes	Location and number of sensors	NSGA	composite plates
Lin *et al*. (2018)	Response covariance sensitivity and correlation analysis	Location and number of sensors	NSGA-II	truss structure
Zhou *et al.* (2021)	Information effectiveness (mode shapes) and network performance (standard deviation of total energy)	Location and number of sensors	MO discrete firefly algorithm based on neighboring information (MDFA/NS) and NSGA II	composite plates
Li *et al.* (2018)	Number of sensors and vibration response	Location and number of sensors	NSGA-II and Wavelet decomposition	composite plates
Alexandrino *et al.* (2019)	Differences in the mean stress and variance	x, y, r (circular hole) x, y, a, b, θ (elliptical hole)	NSGA II, neural networking, and fuzzy decision making	composite plates
Kim & Park (2004)	Difference module of the natural frequencies and Modal Assurance Criterion (MAC) – related to mode shapes	Element position and stiffness reduction factor in this element.	GA with sum method and MOGA	composite plates
Perera & Ruiz (2008)	Modal frequencies and mode shapes	Element location and damage index	SPGA	truss structure
Cha & Buyukozturk (2015)	Modal Strain Energy and mode shapes	Structural element and Young´s modulus reduction	Implicit Redundant Representation GA and NSGA-II	truss structure
Wang *et al.* (2012)	Natural Frequencies and accumulative MAC	Truss element and reduction ration	MOPSO, NSGA-II, and MODE	truss structure
Alkayem *et al.* (2017)	Difference module of the natural frequencies and MAC	Truss element and Young´s modulus reduction	GA, MOGA, PSO, and MOPSO	truss structure
Nizar *et al.* (2018)	Modal strain energy and mode shape	Truss element and Young´s modulus reduction	MOPSO and Lévy flights	truss structure
Kim & Frangopol (2016)	Expected damage detection delay, expected maintenance delay, damage detection time-based reliability index, expected total life extension, and expected life cycle cost	Uncertainties of fatigue damage, maintenance delay, damage detection delay, effects if maintenance actions, service life and costs, maintenance, and structural failure	Multi-objective probabilistic optimization process (MOPOP)	-

According to Alkayem *et al.* (2017), some of the studies in Table 2.5 have effectively demonstrated the advantage of multi-objective functions rather than conversion into single-objective functions using the weighted sum method. This is because when using a combination between a single-objective optimization algorithm (such EA) and the weighting sum method to solve multiple objectives, the outcome is a sub-set of total Pareto optimal solutions, while a powerful multi-objective meta-heuristic algorithm can generate the whole Pareto optimal solutions or at least the majority of them.

2.2.4 General Discussion

All recent or relevant publications found for multi-objective optimization in mechanical engineering in this work are in Tables 2.1, 2.2, 2.3, 2.4, and 2.5, where it contains the decision variables, the objective functions, the algorithms, and the structure or process to be optimized. In total, 90 researches were detailed from the point of view of the multi-objective approach.

Of these works, 23 different algorithms were used and since in some works more than one is used, it totaled 102 applications. NSGA-II was the most used, appearing in 32 researches, just behind came MOPSO with 11 appearances, MOGA with 5, Jaya with 5, MODE with 3, and Ortoghonal Method with 3. The other algorithms found in the Table appeared less than twice and this includes the only gradient-based method in the list: the GRG. Note that of the 23 algorithms found, 18 appeared less than twice.

A widely used methodology was that of RSM, where the authors performed analysis using DOE or Taguchi and found polynomial regression curves that were optimized using desirability functions or other algorithms. In all, 18 studies followed this methodology. Of those which used and detailed the decision-making technique adopted, TOPSIS was the most present, being in 6 of the works found.

2.3 Chapter Conclusion

Multi-objective optimization is an area that has been highly developed in the last decades and several methodologies, algorithms and decision techniques have been created. However, the amount of information in the literature can make the choice of a methodology to address a problem and this work aimed to show through a systematic and detailed review of the literature what are the most used algorithms, techniques, decision variables and objective functions employed in ninety different research papers in mechanical engineering.

It can be seen that classic optimization methods, such as gradient-based methods, that had their importance in the past lost space to new algorithms that emerged with the advancement of computing, more able to deal with a greater number of variables, multiple objectives and nonlinearities. Meta-heuristics are the most suitable to deal with multi-objective optimization problems, being evolutionary algorithms the most used in the literature, mainly the NSGA-II. Next comes a swarm algorithm, MOPSO. Even the evolutionary and swarm algorithms are being challenged by new and more powerful meta-heuristics with more appropriate routines for specific problems, such as the Jaya algorithm, Multi-objective Grey Wolf Optimizer, Success History-based Adaptive Multi-objective Differential Evolution, Real-code Population-Based Incremental Learning hybridized with Adaptive Differential evolution or Non-dominated sorting Teaching-Learning Based algorithm. Since most of these algorithms use the Pareto dominance relationship to find non-dominated solutions, the overwhelming majority of recent problems use a *posteriori* decision-making technique, where the decision maker tries to come up with all possible optimal solutions to the problem before choosing the best one. A widely used a posteriori decision-making technique is TOPSIS.

Even so, it was possible to verify that these powerful tools of multi-objective optimization are still little used in mechanical engineering and those who made their use, obtained great improvement in the object in which they work.

(Intentionally left Blank)

Chapter 3

Multi-objective Lichtenberg Algorithm: A Hybrid Physics-based Metaheuristic for Solving Engineering Problems

This Chapter presents all the details of creating the Multi-Objective Lichtenberg Algorithm (MOLA). It will be tested via several test functions, of which three are from the group known as the Zitzler-Deb-Thiele test functions (ZDT) (Zitzler *et al*., 2000), some of the most used test functions in literature, while the other ten tests are from the test function group known as CEC2009 (Zhang *et al*., 2008), which is considered to be the most challenging function group contained in literature on multi-objective optimization algorithms (MIRJALILI *et al*., 2016).

Still in the validation process, the optimizer will be tested on three constrained real engineering problems. During the algorithm testing process, MOLA will be compared against NSGA-II (DEB *et al*., 2000), MOPSO (MOSTAGHIM & TEICH, 2003). It will also be compared with the MOEA/D (Zhang & Li, 2007), MOGWO (Mirjalili *et al*., 2016), and the MOGOA (Mirjalili, *et al*., 2017). Inverted Generational Distance (IGD), Spacing (SP), and Maximum Spread (MS) will be considered to assess the convergence and coverage of these algorithms.

The Chapter is organized as follows: Section 3.1 presents the development of the MOLA in detail. Section 3.2 presents the validation methodologies, results, and discussion. Section 3.3 draws the conclusions.

3.1 Multi-objective Lichtenberg Algorithm

A new meta-heuristic inspired by lightning storms and Lichtenberg Figures was recently created in a mono-objective version. Pereira *et al*. (2021) presents all the details surrounding the creation of the Lichtenberg Algorithm (LA). The optimizer has been successfully applied in damage identification, and to identify cracks and delaminations in composites, and in design applications like isogrid lowers limb prosthetics (PEREIRA *et al*., 2020b; PEREIRA *et al*., 2021; FRANCISCO *et al*., 2020). The algorithm creates a Lichtenberg Figure (LF) that is put into the search space. Points of its structure are taken as candidates to evaluate the objective function(s). Below is a brief summary of how this figure is constructed and how the algorithm works.

Lichtenberg (1777) was the first to study the phenomenon of the propagation of electric discharges in dielectric (insulating) material, which makes a figure to branch out and bend. According to Merrill (1939), it is impossible to determine the resistances at each point while also knowing the heterogeneities of the material, thus resulting in the random growth of the figure in each case, even on the same material and under the same electrostatic conditions.

This random growth has unspeakable physical and mathematical indeterminations that until today, and probably for a long time, will be incalculable. The direction of lightning depends on the air temperature, density, pressure, and humidity of the dielectric medium, the type of soil below the cloud, the density of the cloud, the speed of the particles within it, and what types of particles are present, whether there are oxides or not. Needless to say, there are a wide array of variables leading to a single result, a stochastic event that spreads in the direction of least resistance. Turner (2019), suggested that a LF can be built using a random growth process with many particles, forming a cluster. Due to its stochastic model, each execution of the algorithm can generate different figures. Therefore, the construction of a Lichtenberg Figure is completely numerical.

Among the main growth models that can be found in the literature, the Diffusion Limited Aggregation (DLA) theory was chosen, proposed by Witten & Sander (1981) and (1983). A binary matrix (0 and 1) is built like a map, and a particle, represented by the number one, is fixed in the center. The cluster is built using values of a matrix equal to one, while the empty spaces are equal to zero. Each matrix element with a value equal to one is a particle in the cluster, and the number of them (N_p) in the cluster is defined at the beginning of the program. This matrix can be represented by a Bitmap figure (black and white). The space for building the figure is defined by creating a radius (R_c), and from this radius the matrix is generated with lines and columns equal to two times the R_c (diameter).

Particles are randomly released across the matrix, and if they reach the cluster that, in the beginning was only one particle in the center, they have an *S* probability of staying fixed, also called the stickiness coefficient. This parameter controls the density of the cluster. The closer to 0, the denser the cluster. The particle walks are plotted randomly, radially, and as if they were on a Cartesian plane starting from the center and settling down anywhere on the map, rounding off the position to a matrix element with a line and column. At this point a particle can be added only if there is another particle next, confirmed by a lateral check. If a particle reaches a radius slightly larger than R_c, it is exterminated and another one starts the random walk again. This happens until all the particles determined at the entrance N_p are contained in the cluster, or until the cluster reaches the creation radius. The number of points in LF is not always equal to N_p for this reason.

Each particle in the cluster can be transformed into locations on a Cartesian plane and the LF can be plotted at any size, slope, or starting point. The extracted figure is then plotted in the exact size of the search space in the center. This figure can be plotted with different sizes and rotations, selected at random at each iteration. This is done as a measure to improve the exploration and exploitation capabilities of the algorithm, in addition to preventing a flawed reading of the search space.

Another parameter of the optimizer is the refinement (*ref*), an input constant parameter that can be from 0 to 1 and creates a second LF (red) every iteration from 0 to 100% of the size of the main LF (blue) - See Figure 3.2. This smaller scale figure improves the local search. If *ref* = 0, only one LF acts on the global optimizer at every iteration (blue).

Not all LF points are used to compute the objective function(s). The number of points used for this purpose or population (*pop*) is defined at the beginning of the algorithm, and is usually 10 times the number of design variables of the problem. The LF points that will represent the population are chosen throughout the LF structure, which is modified at each iteration, and are represented graphically by black dots, all of which are always within the search space by means of a check. This shape means that the LA is a hybrid algorithm since it merges two types of algorithms found in literature i.e., population and trajectory. This hybrid routine, which was not found among any of the meta-heuristics, has brought great capacity for exploitation and exploration to the mono-objective version of the algorithm, revealing great potential for the multi-objective version.

The sixth parameter is the switching factor (*M*), a parameter that changes the LF in the optimizer input data. This parameter can be set to zero, one, or two. If set to 1, a figure is generated when starting the program, and the same figure is used in all of the iterations during execution. If

set to 2, a new figure is generated at each iteration. If *M* is set to 0, a previously saved figure is used in the optimizer, i.e., no figure is generated.

This algorithm is used to construct plane (2D) and spatial (3D) Lichtenberg figures, which means that the algorithm can be used for problems with two or three decision variables. Since the algorithm needs a physical space to be built, when dealing with more variables, a projection (or mirroring) of these figures is made for *n* variables. Finally, the number of iterations (N_{iter}) is also defined as an initial configuration parameter of the MOLA algorithm, which is equal to 100 iterations, a very common number for many algorithms found in literature.

All points evaluated in the search space generate solutions in the objective space and these solutions are compared using the Pareto dominance relationship, where the non-dominated solutions are kept in the solution space and the non-dominated ones are excluded. The set of non-dominated solutions for each iteration forms the current Pareto front of the problem, which tends to approach the real one through the iterations. The Multi-objective Lichtenberg Algorithm (MOLA) works considering all points of the current Pareto front as candidate points to plot LFs . At each iteration, one of these points is selected at random to plot a LF, generating a forced search in the regions in the variable space that have better values for objective functions (Figure 3.1).

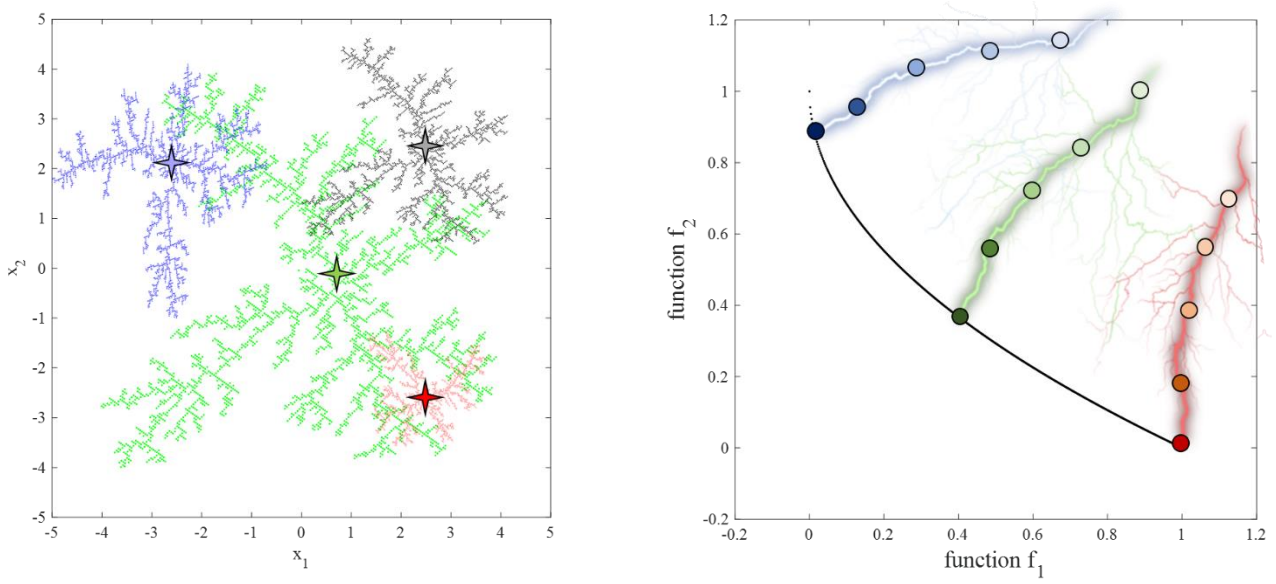

(a) (b)

Figure 3.1 - Basic search strategy of MOLA in the design and objective space.

Figure 3.2 shows MOLA acting in the variable space for a two-variable problem, and Table 3.1 shows some recommendations for the parameter ranges that can be used. As was explained

earlier, there are parameters for flat and spatial Lichtenberg figures according to the dimension of the problem. Table 3.2 summarizes the algorithm using a pseudo code.

Table 3.1 - Recommended LA Control Parameters

R_c	$50 \leq R_c \leq 250$
N_p	$10^3 \leq N_p \leq 10^6$
S	$0 \leq S \leq 1$
Pop	$10*d \leq Pop \leq 40*d$
ref	$0 \leq ref \leq 1$
M	0, 1 or 2
N_{iter}	$10^3 \leq N_{iter} \leq 10^6$

Given the information contained in Tables 3.1 and 3.2, a user can easily use the MOLA. After defining the objective functions and the lower and upper boundaries (LB and UB), the user must set the parameters R_c , N_p , S , Pop , ref , M , and N_{iter}. The basis of the algorithm is the LF, and the creation process is well explained above and depends on the R_c, N_p, and S. Initially the LF is programmed to fill the entire search space based on the LB and the UB definitions.

The LF creation process can take about two minutes. If M = 0, no LF is created during the optimization process, but rather one that was previously saved is loaded with R_c = 200, N_p = 10^6, and S = 1. These Values were found after analyzing the Design of Experiments (DOE) and the Analysis of Variance (ANOVA) using weighted least-squares. If M = 1, only one LF is created and used in all iterations. If M = 2, which is not recommended, a LF is created at each iteration. Note that if M = 1 or 2, the parameters R_c, N_p, and S lose their functionality. To get an idea of the influence of M on simulation times, if M = 0 in the mono-objective version the algorithm takes less than a second to give the answer. If M = 1 it takes about 2 minutes, and if M = 2 it takes 3h.

The LF is composed of many points and is put into the search space at each iteration with different rotations and sizes independent of M (Fully random, large scales improve exploration and small scales improve exploitation), during N_{iter} iterations. To improve exploitation, a second LF, smaller than the main LF, can be created with a rate *ref*. Only *Pop* points from the structure are evaluated in the objective function and each point evaluated in search space is plotted in the objective space. Then the Pareto dominance relationship is evaluated and a current Pareto front is created. At each iteration, in addition to the LF being plotted in different sizes and rotations, the LF is fired through a central point, which in the single-objective version is the best point from the previous iteration, and in the multi-objective version it is a random point in the current Pareto front.

Table 3.2 – Pseudo-code of the Multi-objective Lichtenberg Algorithm

Algorithm 1 - Main

Set objective functions and search space – J_i, upper and lower bounds
Set number of iterations and population – N_{iter}, *Pop* (common to all optimizers)
Set Refinement and Parameter for changing the LF – *Ref*, *M* (LA routine parameters)
Set LF Parameters – R_c, N_p, *S*
if *M* = 0, load LF, **end if**
if *M* = 1, Create a LF, **end if**
while (iter < N_{iter}) **do**
if *M* = 2, Create a LF, **end if**
$X_{trigger}$ = search space center (trigger point of the first LF)
if *ref* = 0
Apply random scale and rotation
Initialize random population through LF, X_i (i = 1, 2, … , *Pop*)
else
copy LF to create a second LF of size ref * LF (Local)
Apply the same random scale and rotation to both
Initialize global random population through LF, $Xglobal_i$ (i = 1, 2, … , 0.4**Pop*)
Initialize local random population through LF, $Xlocal_j$ (j = 1, 2, … , 0.6**Pop*)
$X_i = Xglobal_i + Xlocal_j$
end if
Calculate J_i for each X_i of the problem
Find dominated and non-dominated solutions analyzing J_i
Build the current Pareto front with non-dominated solutions
Save non-dominated solutions through iterations
Delete all dominated solutions
Randomly select one of the non-dominated solution and your decision vector (X_{ND})
$X_{trigger} = X_{ND}$
iter = iter +1
end while
return Pareto front

Algorithm 2 – Creation of LF

Create an matrix of R_c - sized zeros
Place a unitary particle in its center
While ($i < N_p$) **do**
Randomly place a unitary particle in the matrix
if the plotted unitary particle t is next to another unitary particle
if rand < *S*
This new unitary particle is placed in the matrix
$i = i + 1$
else
The plotted unitary particle is eliminated
end if
end if
if the cluster of unitary particles reaches R_c
The simulation is finished
end if
end while
X = coordinates of all unitary particles for Cartesian space in the size of the search space.

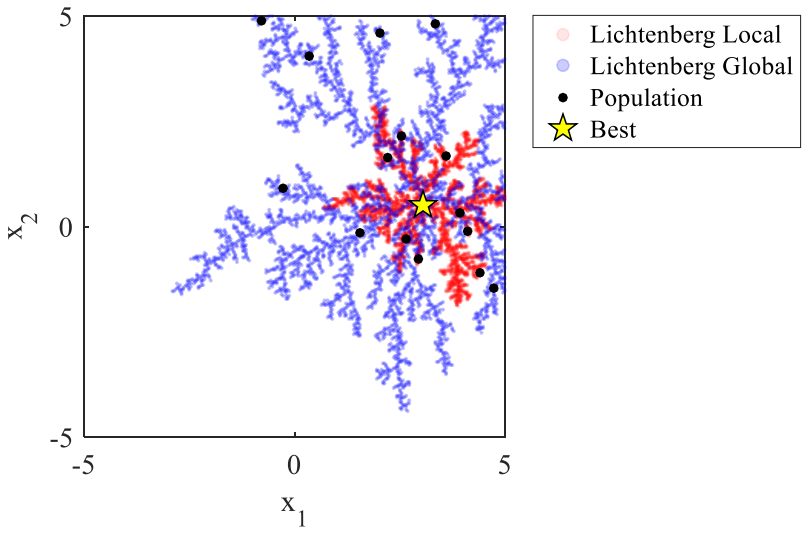

Figure 3.2 - Population distribution in the Lichtenberg Figures (*pop* = 15 and *ref* = 0.4)

3.2 Validation and Discussion

The Multi-objective Optimization Lichtenberg Algorithm will be tested via a set of test functions and in real optimization problems.

3.2.1 Test functions

Initially, some of the test functions proposed by Zitzler *et al.* (2000), known as the ZDT test functions, will be chosen so that the MOLA is tested and compared with the two of the most widely used meta-heuristics in multi-objective optimization problems in recent years, the NSGA-II and the MOPSO, the former representing evolutionary algorithms, and the latter swarm algorithms. The chosen functions are shown in Table A.1 (Appendix A). The ZDT1 has a convex Pareto front, the ZDT2 a concave front, and the ZDT3 is made up of many disconnected convex parts.

For these functions, 50 search agents and 100 iterations were defined for all the algorithms. These values are used to compare the results of the MOPSO and the NSGA-II found in a study by Mirjalili *et al.* (2016). The parameters of the MOLA for these applications are $Pop = 50$, $N_{iter} = 100$, $R_c = 200$, $N_p = 10^6$, $S = 1$, $ref = 0.4$, and $M = 0$. The chosen values were found after an analysis of the Design of Experiments (DOE) and the Analysis of Variance (ANOVA), using weighted least-

squares and considering 10 complex functions. The Model Indicator fit (R^2) of the analysis was more than 90%. The parameters of the other algorithms are:

i) MOPSO:

$\varphi_1 = \varphi_2 = 2.05$;

$\varphi = \varphi_2 + \varphi_1$; $\chi = 2/(\varphi\text{-}2+(\varphi^2\text{-}4\varphi)^{(1/2)})$ (inertia weight);

$c_1 = \chi\, \varphi_1$ (personal coefficient);

$c_2 = \chi\, \varphi_2$ (social coefficient);

$\alpha = 0.1$ (grid inflation parameter);

$\beta = 4$ *(leader selection pressure parameter);*

nGrid =10 (number of grids per each dimension); and

ii) *NSGA-II:*

$P_c = 0.8$ *(cross over probability); and*

$P_m = 0.1$ *(mutation probability).*

These MOPSO and NSGA-II parameters are excellent and widely used in literature (Mirjalili *et al*., 2017). Figure 3.3 shows the best Pareto front found after 10 runs of the three algorithms.

The chosen ZDT functions were very diverse, and were convex, concave, and discontinuous. Figure 3.3 shows that the MOLA obtained Pareto fronts with excellent convergence and coverage. The non-dominated solutions found basically coincide with the real solution in the three cases. Furthermore, can behighlighted that the MOLA rapidly converges to the region of the true Pareto front. Figure 3.4 shows this convergence for the ZDT1 function and Figure 3.5 for the ZDT3.

(Intentionally left Blank)

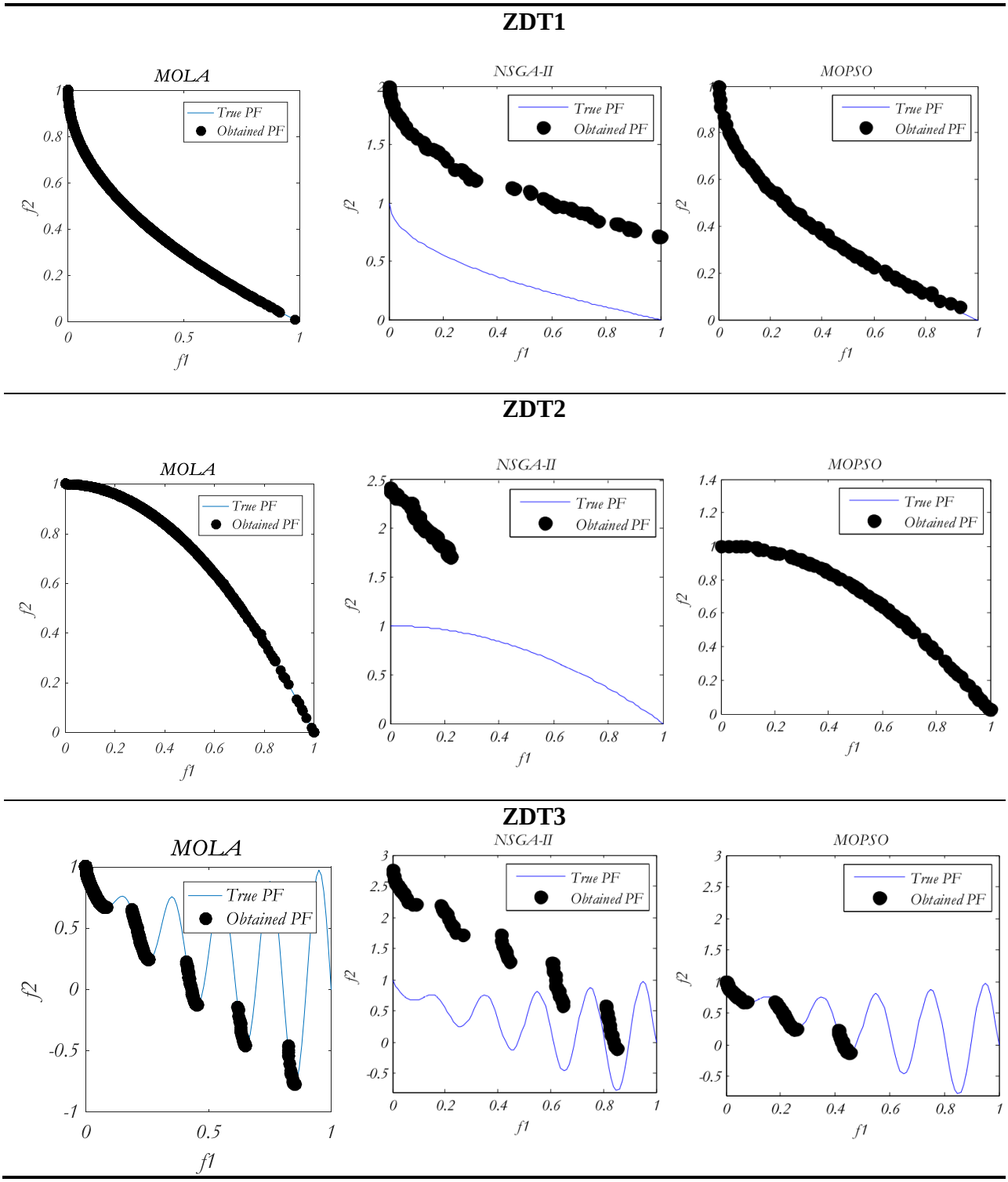

Figure 3.3 – Pareto front found by MOLA, NSGA-II, and MOPSO in the ZDT test functions

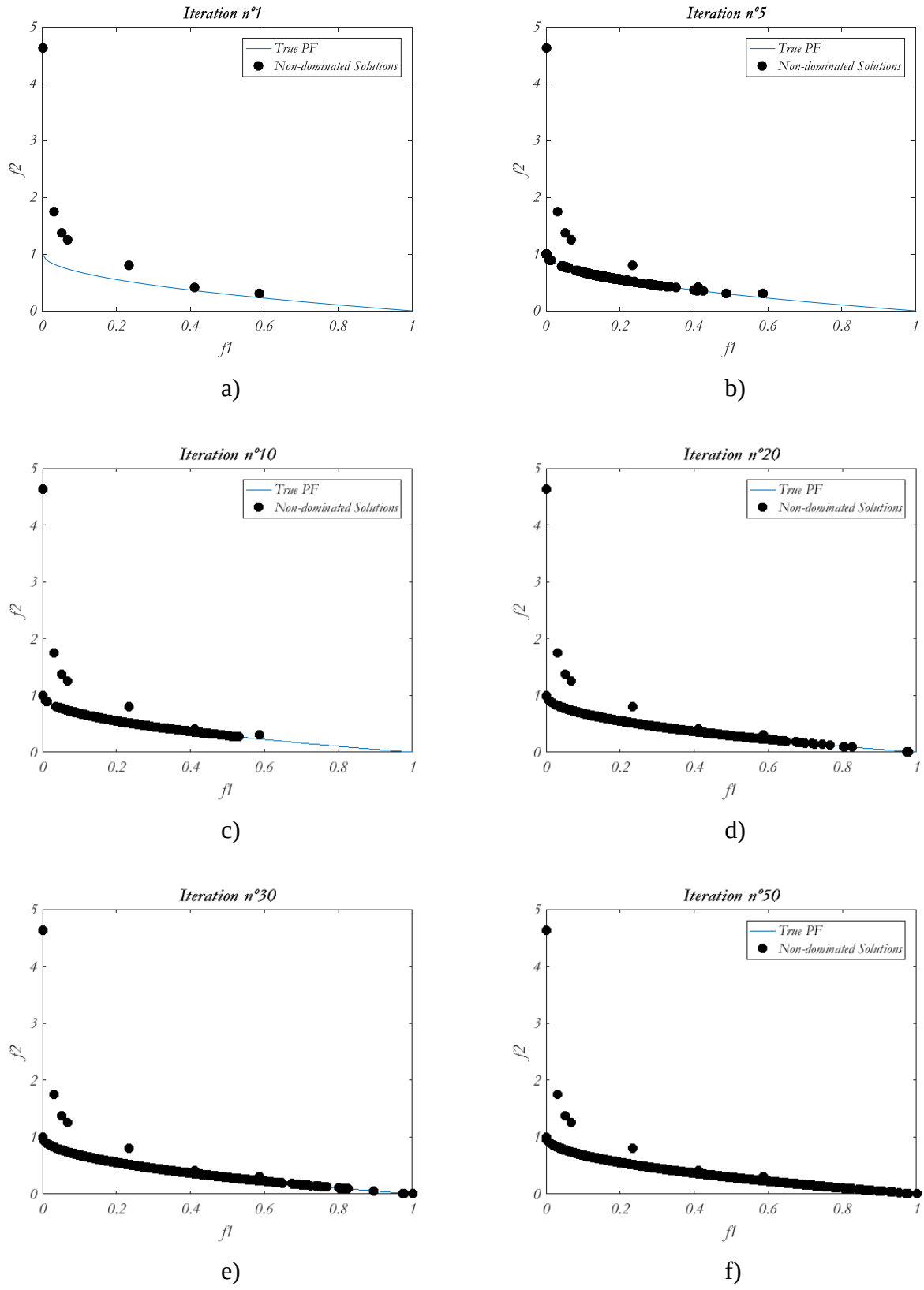

Figure 3.4 – Convergence results for the first 50 iterations of the MOLA for a convex function

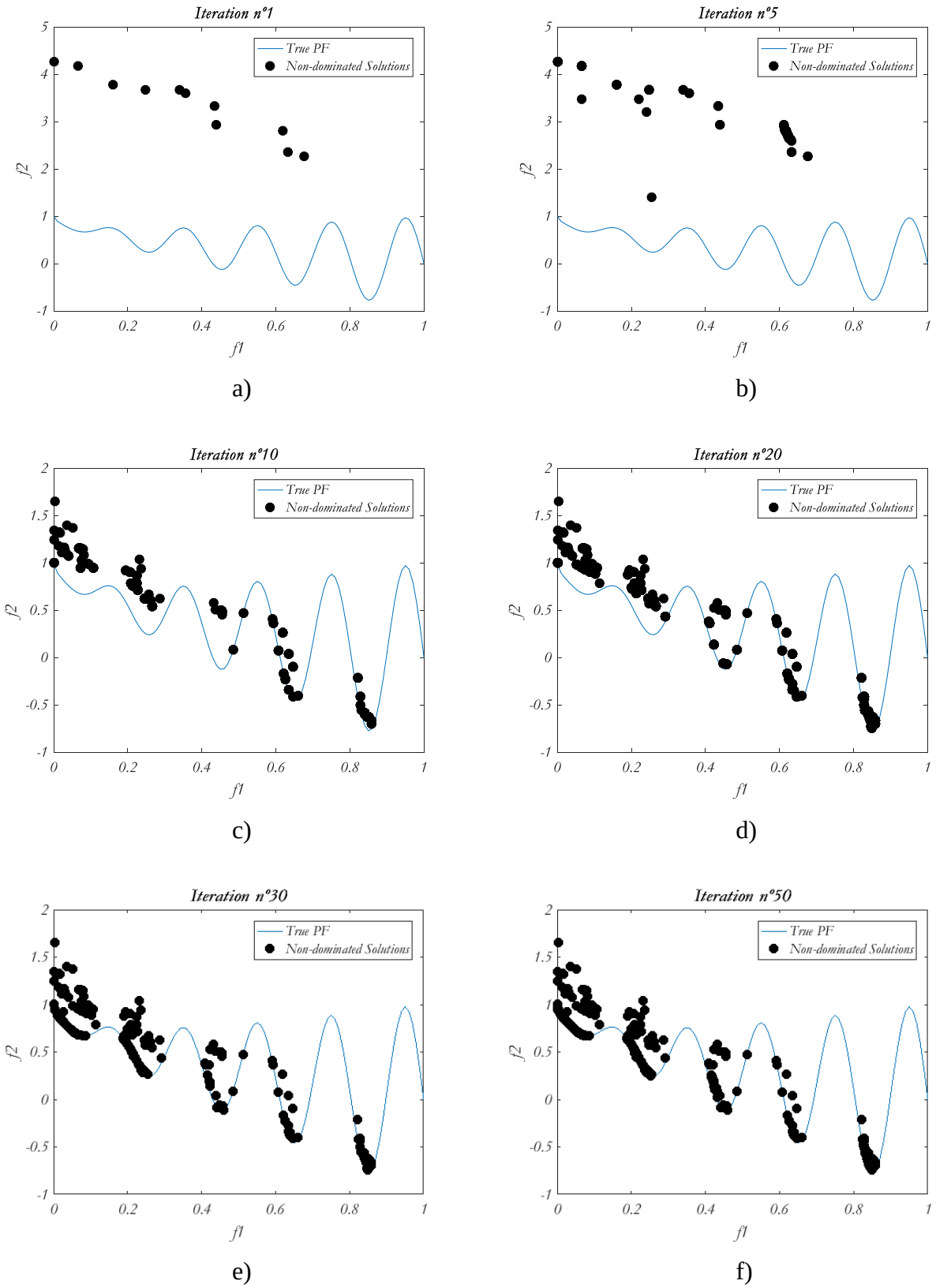

Figure 3.5 – Convergence results for the first 50 iterations of the MOLA for a complex disconnected function.

In addition to the figures at the Pareto front, a metric that quantifies the convergence of algorithms will be used to measure how close the obtained Pareto optimal solutions are to the true Pareto front. The Inverted Generational Distance (IGD) is expressed in Equation (3.1) (SIERRA & COELLO, 2005):

$$IGD = \sqrt{\sum_{I=1}^{nt} (d'_i)^2} \Big/ n \tag{3.1}$$

where:

nt is the number of true Pareto optimal solutions; and

d'_i indicates the Euclidean distance between the *i-th* true Pareto optimal solution and the closest Pareto optimal solution obtained in the reference set.

If the IGD is null, the solutions obtained are equal to the true Pareto front. In Figure 3.6, the algorithm was run a few times with the same parameters and the best Pareto front found was chosen. Now, the algorithms will be run 10 times for comparison with Mirjalili *et al*. (2017), and to obtain the average, standard deviation, and the worst and best IGD value for each one. Table 3.3 shows these results.

Table 3.3 – Evaluation of the MOLA convergence (using IGD) for the ZDT test functions.

Function	Algorithm	Average	SD	Best	Worst
	MOLA	0.00658	0.004777	**0.0011**	0.0197
ZDT1	NSGA-II	0.05988	0.005436	0.0546	0.0702
	MOPSO	**0.00422**	0.003103	0.0015	0.0101
	MOLA	0.00393	0.00510	**0.0008**	0.0017
ZDT2	NSGA-II	0.13972	0.02626	0.1148	0.1834
	MOPSO	**0.00156**	0.00017	0.0013	0.0017
	MOLA	0.03877	0.007270	**0.0302**	0.0508
ZDT3	NSGA-II	0.04166	0.008073	0.0315	0.0557
	MOPSO	**0.03782**	0.006297	0.0308	0.0497

From Table 3.3, can be stated that the MOLA surpasses the most widely used algorithm today in literature, in every aspects relative to the convergence using the IGD metric, as it had the lower average, standard deviation, and still the best result found within the simulations for all test functions. This last achievement also outperforms the MOPSO. However, the results from Figure 3.3, where the MOLA was the only algorithm to find all segments of the Pareto Front in the ZDT 3 function, in terms of convergence, show that MOPSO was slightly better. Now, a comparison with more complex functions and other algorithms will be made to further validate the algorithm.

MOLA, MOPSO, MOGWO, MOGOA, and MOEA/D will be compared using the CEC2009 (ZHANG *et al*., 2008) test functions with multimodal, convex, discrete, and non-convex optimal Pareto fronts. These functions are the most difficult test functions in literature for multi-objective optimization (MIRJALILI *et al.*, 2017). Table A.2 (Appendix A) shows these functions. The parameters of MOLA and MOPSO are the same as when applying the ZDT functions, however, for comparison's sake with Mirjalili *et al.* (2016), and (2017), the number of search agents is 100 and the number of iterations is 3000. *The other parameters for each algorithm are:*

i) *MOGWO (algorithm similar to MOPSO):*

α = 0.1 (grid inflation parameter);

β *= 4 (leader selection pressure parameter); and*

nGrid = 10 (number of grids per dimension),

ii) *MOGOA:*

c_{max} *= 1; and*

c_{min} *= 0.0001 (c is* a decreasing coefficient that regulates grasshoppers); *and*

iii) *MOEA/D:*

N = 100 (subproblems);

T = 10 (neighbors);

n_r *= 1 (maximal copies of a new child in the update);*

δ = 0.9 (probability of selecting parents from the neighborhood);

F = 0.5 (mutation rates); and

η = 30 (distribution index).

The MOGWO and MOGOA parameters were the same as those used by Mirjalili *et al.* (2017), and (2016), in the studies that presented these algorithms, which are considered to be the best. The MOEA/D parameters are the same as those used by these authors for comparison's sake. Figure 3.6 shows the best Pareto front found for some of the algorithms after 10 individual runs.

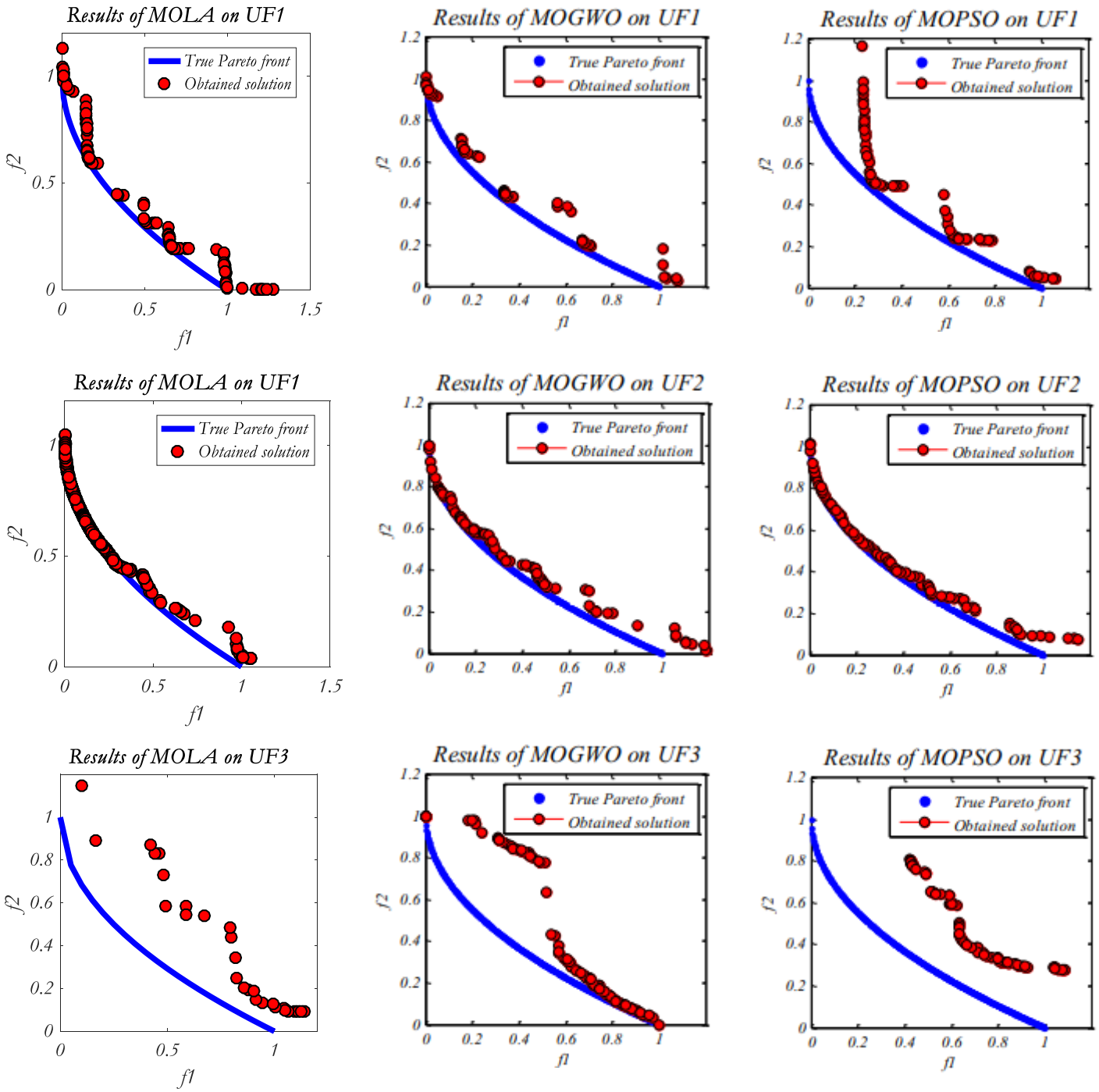

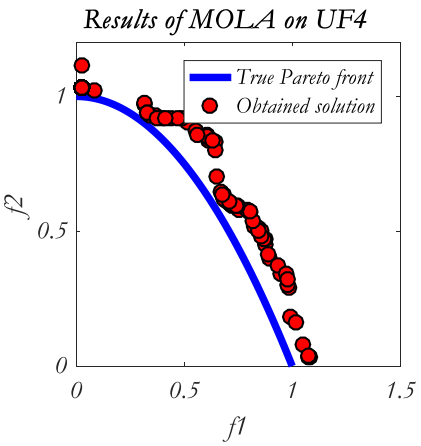
Results of MOLA on UF4
True Pareto front
Obtained solution
f2
f1

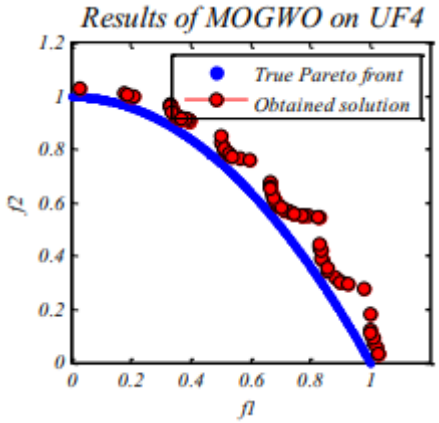
Results of MOGWO on UF4
True Pareto front
Obtained solution
f2
f1

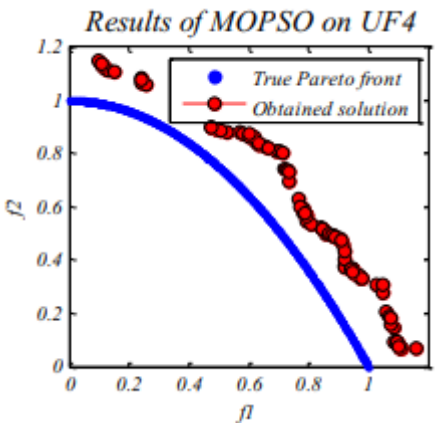
Results of MOPSO on UF4
True Pareto front
Obtained solution
f2
f1

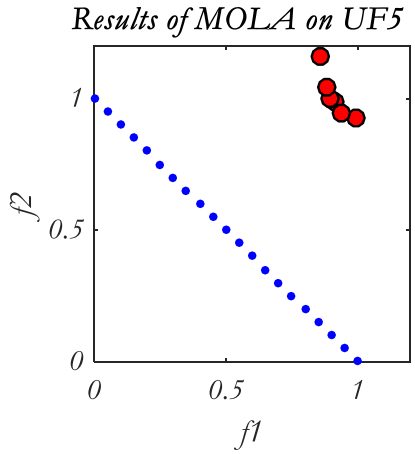
Results of MOLA on UF5
f2
f1

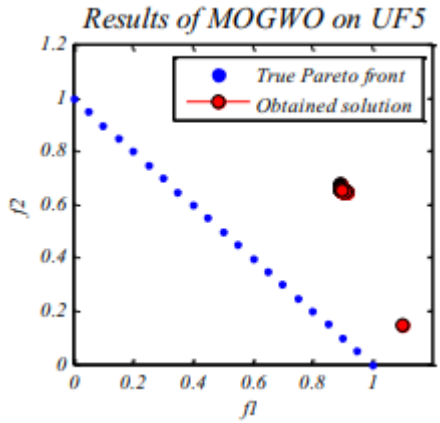
Results of MOGWO on UF5
True Pareto front
Obtained solution
f2
f1

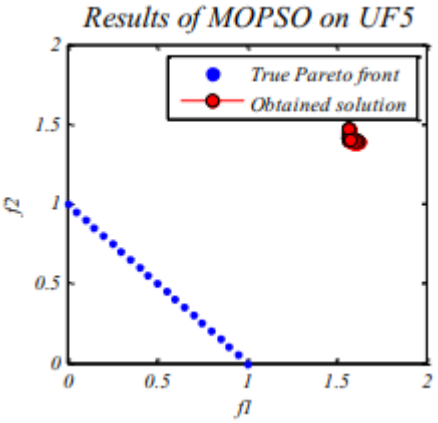
Results of MOPSO on UF5
True Pareto front
Obtained solution
f2
f1

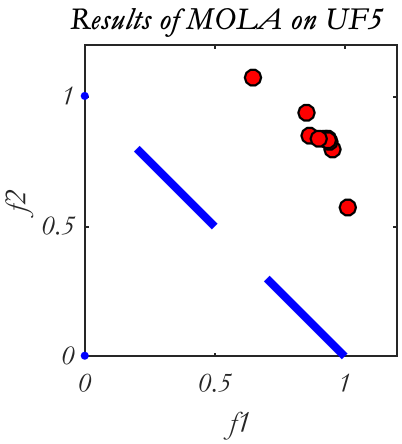
Results of MOLA on UF5
f2
f1

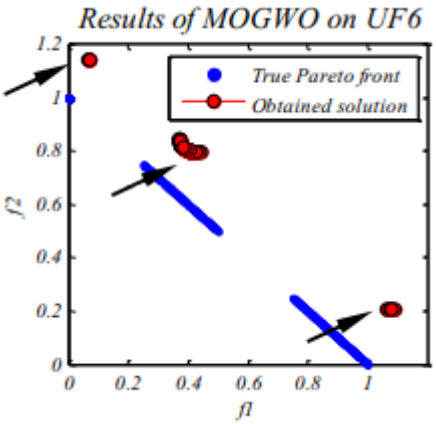
Results of MOGWO on UF6
True Pareto front
Obtained solution
f2
f1

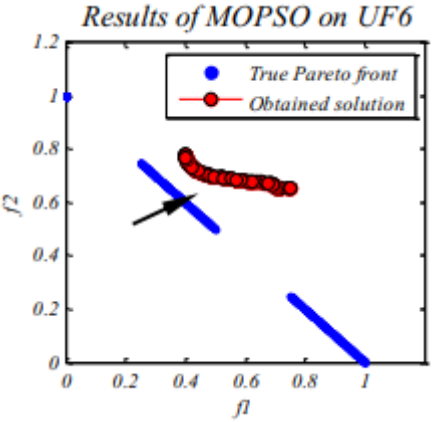
Results of MOPSO on UF6
True Pareto front
Obtained solution
f2
f1

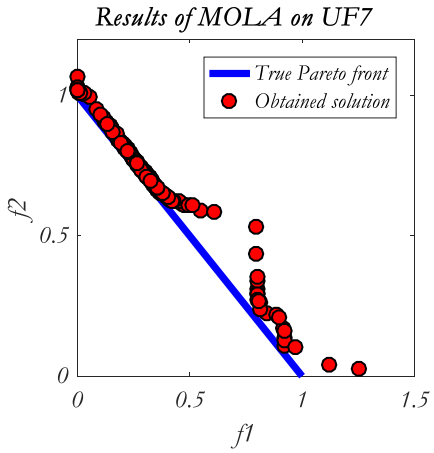
Results of MOLA on UF7
True Pareto front
Obtained solution
f2
f1

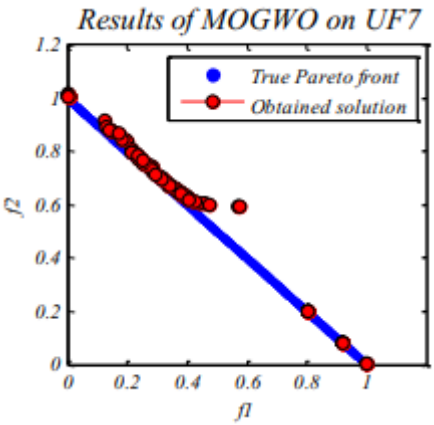
Results of MOGWO on UF7
True Pareto front
Obtained solution
f2
f1

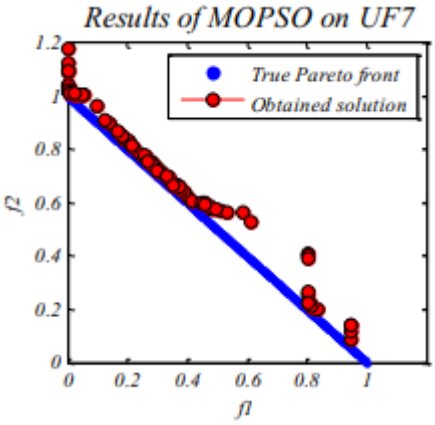
Results of MOPSO on UF7
True Pareto front
Obtained solution
f2
f1

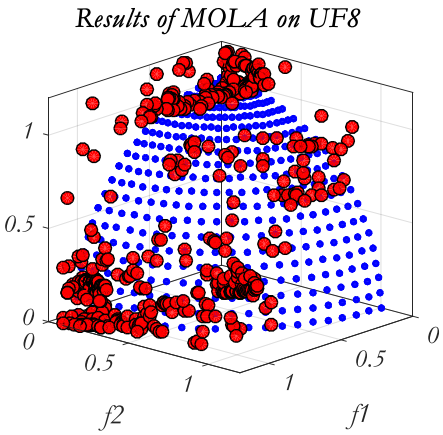
Results of MOLA on UF8
f2
f1

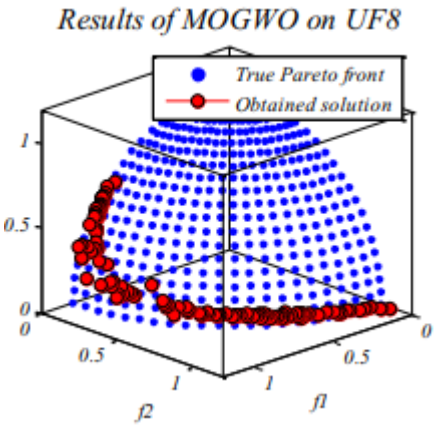
Results of MOGWO on UF8
True Pareto front
Obtained solution
f2
f1

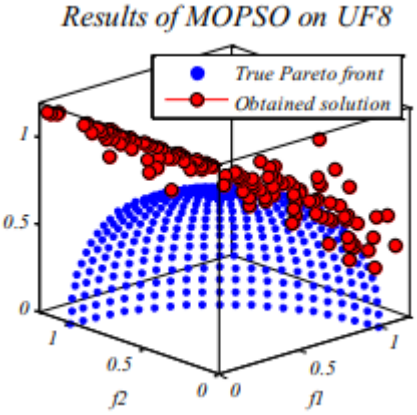
Results of MOPSO on UF8
True Pareto front
Obtained solution
f2
f1

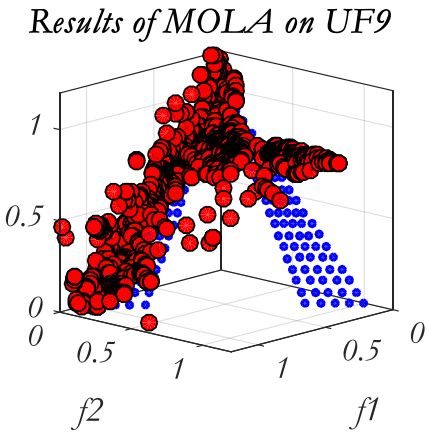
Results of MOLA on UF9
f2
f1

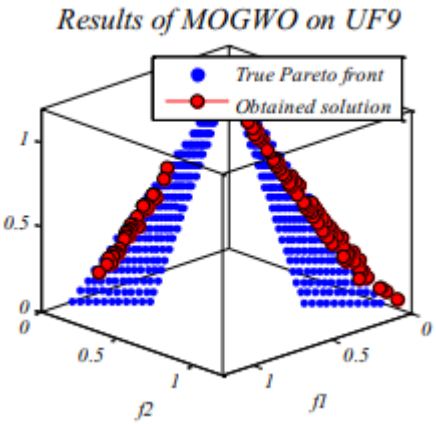
Results of MOGWO on UF9
True Pareto front
Obtained solution
f2
f1

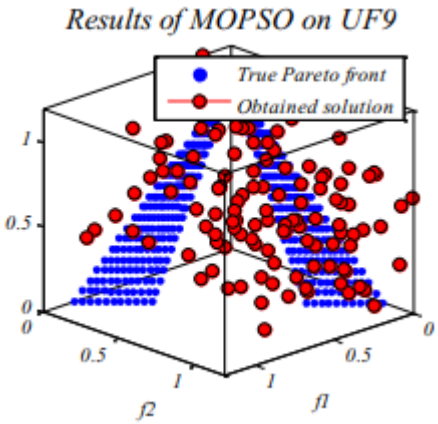
Results of MOPSO on UF9
True Pareto front
Obtained solution
f2
f1

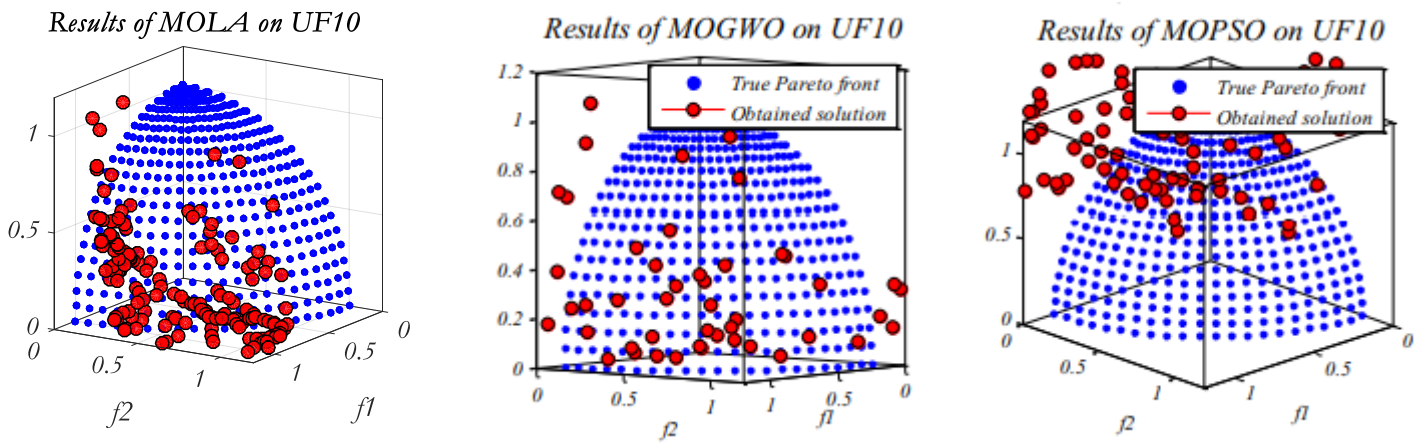

Figure 3.6 – Pareto front found by MOLA, MOGWO, and MOPSO in the CEC2009 test functions

Only convergence was analyzed in the ZDT functions. Now, two other parameters will be calculated to better compare the algorithms and discuss MOLA's capacity in multi-objective optimization problems. To measure the coverage and quantitatively compare the algorithms, the spacing (SP) (Coello *et al.*, 2004; Schott, 1995), and maximum spread (MS) (Zitzler, 1999), measures are employed. SP and MS are given in Equation (3.2) and (3.3), respectively.

$$SP = \sqrt{\frac{1}{n-1}\sum_{I=1}^{n}(\bar{d} - d_i)^2} \tag{3.2}$$

where $\bar{d}$ is the average of all d_i; n is the number of Pareto optimal solutions obtained; and

$d_i = (|f_1^i(\vec{x}) - f_1^j(\vec{x})| + |f_2^i(\vec{x}) - f_2^j(\vec{x})|)$ for all $i, j = 1, 2, 3, \ldots, n$.

$$MS = \sqrt{\sum_{i=1}^{o}\max(d(a_i, b_i))} \tag{3.3}$$

where d is a function to calculate the Euclidean distance; a_i is the maximum value in the *i-th* objective; b_i is the minimum in the *i-th* objective; and o is the number of objectives.

Note that for IGD and SP, lower values mean better results. However, for the MS, higher values shows a better algorithm with higher coverage. The algorithms will be run 30 times to obtain the average, standard deviation, the worst and best IGD, and the SP and MS values for

each one. Tables 3.4, 3.5 and, 3.6 show these results. In fact, these test functions are more complex. It can be noted a higher processing time required for obtaining the Pareto fronts relative to the ZDT functions, and in most functions all algorithms had difficulty matching the real Pareto front. The difficulty was even greater for three objective functions.

Certainly, one of the most important comparison parameters is the IGD, which measures how much the algorithm converged or approached the minimum of the functions. In less complex ZDT functions, MOLA had the best overall IGD results for all functions, but lagged behind MOPSO in the averages for this metric. In more complex CEC functions, MOLA surpassed MOPSO in the IGD average in all tested functions. The same goes for MOEA/D, although this algorithm has not been used in tri-objective functions (UF8, UF9, and UF10), since there is no MATLAB® version. Thus, MOLA proves to be a more convergent algorithm than the most traditional algorithms used in literature today, i.e., NSGA-II, MOPSO, and MOEA/D.

This achievement becomes even more solid when is observed that MOLA had the lowest standard deviation for the same metric. Considering some modern algorithms, like the MOGWO and MOGOA, can be observed that MOLA had a better average result in 6 of the 10 CEC functions (UF1, UF2, UF3, UF5, UF7, and UF10) in terms of convergence. But MOLA came in second losing to MOGWO in UF4 and UF6, and to MOGOA in UF8. MOLA outperforms or is competitive with all compared algorithms in terms of convergence.

Although a study on processing time has not been carried out, it is important to highlight that MOLA has one of the best simulation times of all algorithms.

(Intentionally left Blank)

Table 3.4 –IGD Results of Algorithms in the CEC 2009 Test Functions

UF	Algorithm	Average	SD	Worst	Best	UF	Average	SD	Worst	Best
1	**MOLA**	**0.07304**	0.01400	0.09315	**0.04784**	2	**0.04557**	0.00765	0.06010	**0.03491**
	MOGWO	0.11442	0.01954	0.15774	0.08023		0.05825	0.00739	0.07322	0.04980
	MOPSO	0.13700	0.04407	0.22786	0.08990		0.06040	0.02762	0.13051	0.03699
	MOGOA	0.18110	0.02500	0.21000	0.14300		0.09590	0.03860	0.16810	0.04880
	MOEA/D	0.18710	0.05070	0.24640	0.12650		0.12230	0.01070	0.14370	0.10490
3	**MOLA**	**0.17880**	0.05750	0.3721	**0.10771**	4	0.06132	0.00623	0.07139	**0.05228**
	MOGWO	0.25569	0.08070	0.36786	0.12950		**0.05867**	0.00048	0.05936	0.05797
	MOPSO	0.31399	0.04473	0.37773	0.25648		0.13504	0.00739	0.15189	0.12733
	MOGOA	0.23800	0.06620	0.36900	0.16820		0.07020	0.00480	0.07880	0.06390
	MOEA/D	0.28865	0.01592	0.31294	0.26342		0.06810	0.00210	0.07040	0.06470
5	**MOLA**	**0.78494**	0.26541	1.21239	0.47988	6	0.34200	0.09133	0.39322	0.26973
	MOGWO	0.79707	0.37857	1.73857	0.46795		**0.27937**	0.10448	0.55036	**0.19338**
	MOPSO	2.20237	0.55304	3.03836	1.46479		0.64752	0.26612	1.24281	0.37933
	MOGOA	1.15590	0.16610	1.41740	**0.89780**		0.77710	0.27690	1.32880	0.49390
	MOEA/D	1.29145	0.13489	1.46746	1.12306		0.68812	0.05533	0.74011	0.55235
7	**MOLA**	**0.05854**	0.03822	0.16631	0.03653	8	0.43293	0.17948	0.72459	0.33272
	MOGWO	0.16036	0.13911	0.40142	0.06275		2.05777	1.14552	3.87888	0.46131
	MOPSO	0.35395	0.20442	0.61512	0.05402		0.53671	0.18257	0.79637	0.24530
	MOGOA	0.17260	0.06330	0.33200	0.11500		**0.28050**	0.07490	0.45320	**0.21540**
	MOEA/D	0.45520	0.18980	0.67700	**0.02900**		-	-	-	-
9	**MOLA**	0.23834	0.11350	0.52398	**0.10456**	10	**0.87980**	0.16891	1.31631	0.72061
	MOGWO	**0.19174**	0.09250	0.44794	0.12910		3.59453	3.48829	12.9564	1.04314
	MOPSO	0.48850	0.14449	0.72210	0.33355		1.63719	0.29879	2.16220	1.22008
	MOGOA	0.44270	0.06090	0.56620	0.37420		0.90430	0.18480	1.22850	**0.64320**
	MOEA/D	-	-	-	-		-	-	-	-

Table 3.5 –SP Results of Algorithms in the CEC 2009 Test Functions

UF	Algorithm	Average	SD	Worst	Best	UF	Average	SD	Worst	Best
1	**MOLA**	0.01087	0.00763	0.03173	0.00640	2	0.00637	0.00408	0.01690	0.00322
	MOGWO	0.01237	0.01462	0.04641	0.00081		0.01108	0.00362	0.01816	0.00758
	MOPSO	0.00898	0.00247	0.01464	0.00670		0.00829	0.00168	0.01245	0.00624
	MOGOA	**0.00120**	0.00110	0.00310	**0.00000**		**0.00070**	0.00110	0.00310	**0.00000**
	MOEA/D	0.00380	0.00150	0.00670	0.00210		0.00880	0.00080	0.01040	0.00800
3	**MOLA**	0.00560	0.00940	0.02870	0.00480	4	0.00374	0.00112	0.00467	0.00231
	MOGWO	0.04590	0.01453	0.07050	0.01549		0.00969	0.00390	0.01722	0.00583
	MOPSO	0.00699	0.00170	0.01007	0.00476		0.00666	0.00091	0.00809	0.00546
	MOGOA	**0.00190**	0.00240	0.00550	**0.00000**		**0.00010**	0.00020	0.00060	**0.00000**
	MOEA/D	0.02680	0.02064	0.06256	0.00078		0.00730	0.00060	0.00840	0.00610
5	**MOLA**	0.12475	0.10415	0.36924	0.03238	6	0.02052	0.01315	0.08814	0.00022
	MOGWO	0.15231	0.16247	0.51247	0.00843		0.01446	0.01246	0.04112	0.00191
	MOPSO	0.00479	0.00408	0.01206	0.00006		0.02084	0.03258	0.11140	0.00215
	MOGOA	**0.00070**	0.00050	0.00140	0.00010		**0.00030**	0.00040	0.00110	**0.00000**
	MOEA/D	0.00278	0.00553	0.01615	**0.00000**		0.00630	0.01267	0.03030	**0.00000**
7	**MOLA**	0.00440	0.00324	0.00991	0.00133	8	**0.00573**	0.00243	0.01278	**0.00325**
	MOGWO	0.00824	0.00856	0.03106	0.00031		0.00687	0.00474	0.01879	0.00365
	MOPSO	0.00670	0.00285	0.01240	0.00325		0.02682	0.00827	0.04473	0.01531
	MOGOA	**0.00010**	0.00010	0.00020	**0.00000**		0.01750	0.00850	0.03200	0.00690
	MOEA/D	0.00540	0.00300	0.01170	0.00080		-	-	-	-
9	**MOLA**	0.01413	0.01769	0.10395	0.00395	10	0.02441	0.01709	0.06476	0.00975
	MOGWO	0.01743	0.00633	0.02856	0.00653		0.02523	0.01500	0.05384	**0.00000**
	MOPSO	0.02343	0.00405	0.03087	0.01716		0.01994	0.00348	0.02665	0.01536
	MOGOA	**0.01390**	0.01010	0.03200	**0.00000**		**0.00670**	0.00410	0.01230	**0.00000**
	MOEA/D	-	-	-	-		-	-	-	-

A good algorithm must also have its coverage analyzed. The SP is a metric that tries to quantify the spacing between each solution. In this sense, MOGOA proved to be an efficient algorithm, since it had the lowest average results for all functions, with the exception of UF8, where MOLA showed the best result. MOLA was second for all other functions, with the exception of UF1, UF5, and UF6.

The MS, which is also a measure of coverage, tries to determine the greatest breadth of results coming from the algorithms. Using this metric, MOLA showed expressive results in all functions, proving itself to be an algorithm comparable to those that found the most extreme solutions. This can also be seen in Figure 3.6.

Figure 3.7 shows an analysis of the IGD variability of each algorithm, in a boxplot, when run 30 times, to obtain the data for Table 3.4. One can see that MOLA had the lowest variability in the UF6, UF7, UF8, and UF10 functions. With the exception of UF9, the algorithm obtained significant consistency in the results when compared to the other algorithms, which increases its reliability.

Table 3.6 –MS Results of Algorithms in the CEC 2009 Test Functions

UF	Algorithm	Average	SD	Worst	Best	UF	Average	SD	Worst	Best
	MOLA	**2.12802**	0.96854	1.48799	**4.73259**		**2.21718**	0.77078	1.37998	**3.86729**
	MOGWO	0.92680	0.06884	0.81797	0.99711		0.90972	0.02867	0.84695	0.94792
1	MOPSO	0.64538	0.19292	0.26592	0.95226	2	0.91205	0.02560	0.86654	0.95301
	MOGOA	0.72700	0.15070	0.48990	0.91200		0.88450	0.03530	0.81500	0.93600
	MOEA/D	0.51770	0.16610	0.3149	0.73130		0.87200	0.00560	0.85990	0.87790
	MOLA	**2.0424**	1.5921	1.2870	**5.2903**		**1.52025**	0.02114	1.49272	**1.53831**
	MOGWO	0.94982	0.08777	0.76809	1.0000		0.94242	0.00093	0.94095	0.94327
3	MOPSO	0.61030	0.10575	0.38172	0.77145	4	0.81275	0.01367	0.79441	0.83449
	MOGOA	0.60510	0.11000	0.40260	0.70600		0.90500	0.01390	0.88340	0.93100
	MOEA/D	0.23994	0.12129	0.08975	0.47863		0.88320	0.01810	0.85320	0.91390
	MOLA	**0.59653**	0.25660	0.25490	**1.01712**		**1.75957**	0.88565	0.57262	**2.47410**
	MOGWO	0.39503	0.17494	0.03006	0.61042		0.67360	0.12323	0.38838	0.81492
5	MOPSO	0.27926	0.09575	0.15574	0.43827	6	0.27435	0.11285	0.15436	0.52516
	MOGOA	0.23790	0.11310	0.11500	0.48940		0.25250	0.12940	0.06950	0.46000
	MOEA/D	0.29215	0.03470	0.23834	0.34380		0.09677	0.20715	0.00000	0.59484
	MOLA	**1.92767**	0.74624	1.42452	**3.75726**		**1.31140**	0.47951	0.85379	**1.41560**
	MOGWO	0.80126	0.30865	0.02252	0.98746		0.44573	0.18574	0.18863	0.86376
7	MOPSO	0.42928	0.27553	0.14458	0.87714	8	0.50810	0.16136	0.22723	0.71476
	MOGOA	0.84600	0.07920	0.70290	0.95700		0.44170	0.15860	0.16610	0.63420
	MOEA/D	0.56320	0.24210	0.14960	0.99150		-	-	-	-
	MOLA	**0.97184**	0.56386	0.38240	**2.04713**		**0.62378**	0.37834	0.22583	1.21162
	MOGWO	0.83991	0.19759	0.28750	0.93753		0.29721	0.34651	0.03194	0.92828
9	MOPSO	0.19816	0.16351	0.06771	0.64242	10	0.13015	0.06263	0.06489	0.25404
	MOGOA	0.19380	0.07300	0.11750	0.29400		0.32330	0.12370	0.17040	0.52900
	MOEA/D	-	-	-	-		-	-	-	-

The Multi-objective Lichtenberg Algorithm proved capable when applied in multi-objective optimization problems, since it had equivalent results which were even superior in some aspects in the tested functions relative to important recent and commonly used meta-heuristics.

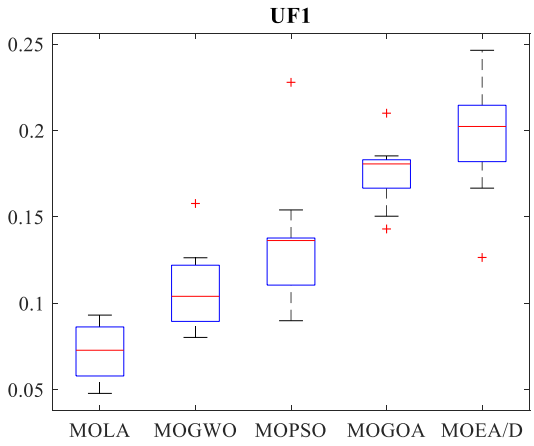

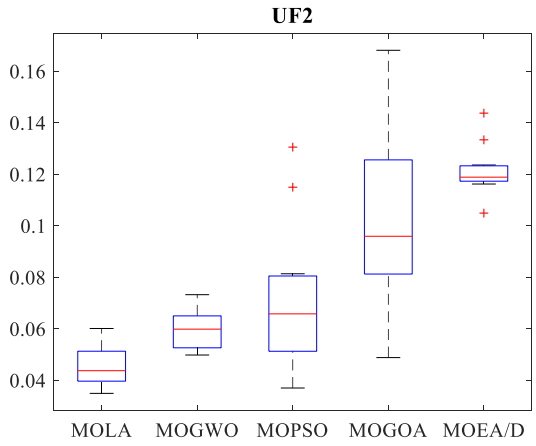

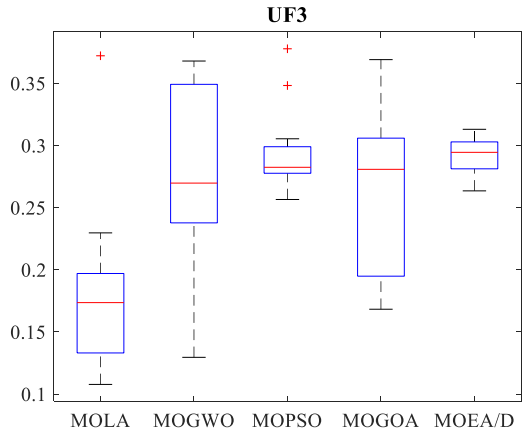

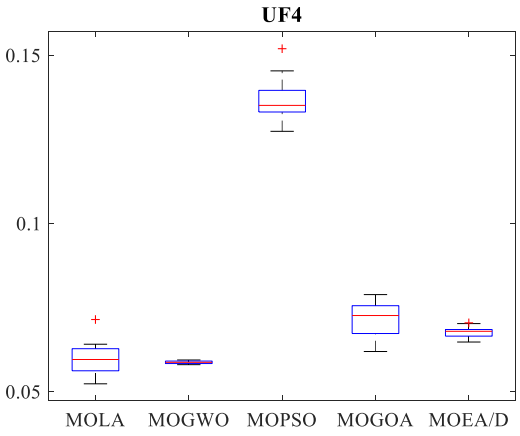

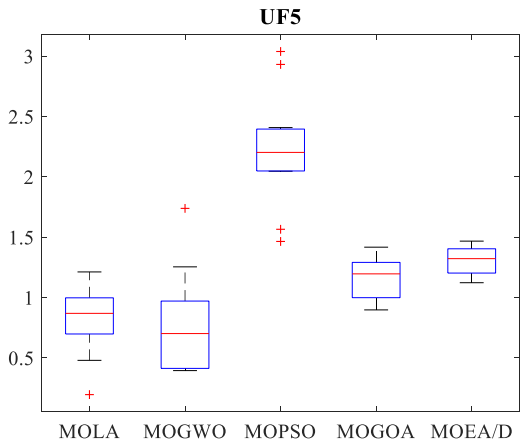

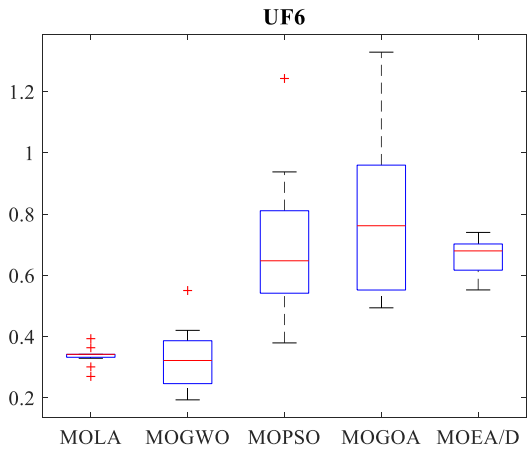

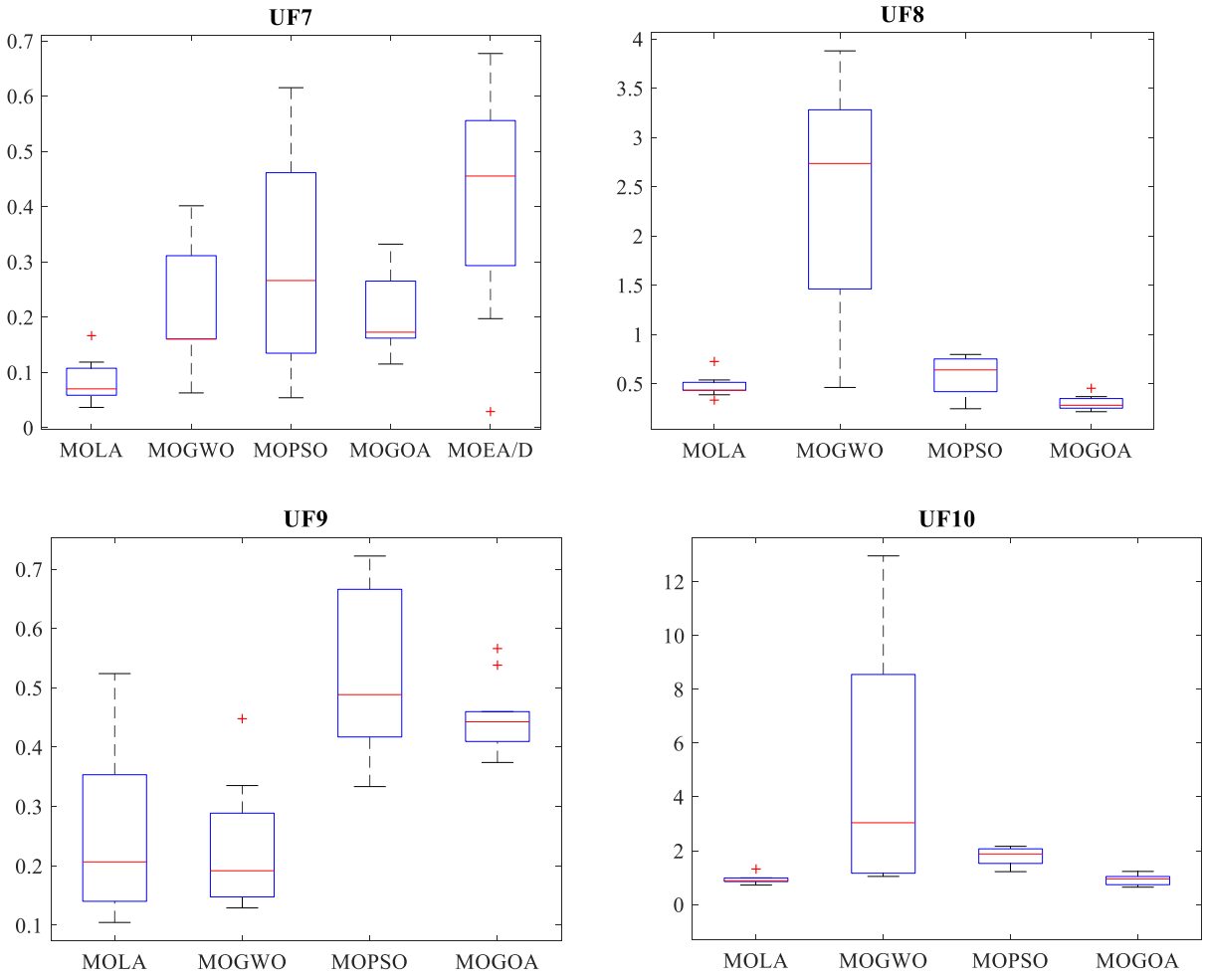

Figure 3.7 – Analysis of the sensitivity of algorithms in CEC 2009 functions.

3.2.2 Constrained Engineering Problems

To solve constrained problems, the MOLA was equipped with a constraint handling technique. The “penalty” function penalizes search agents that violate any of the constraints at any level (COELLO, 2000), causing the objective function to gain exurbitant values. Three constrained engineering problems were selected to further prove the efficiency of the algorithm, a welded beam design, a four-bar-truss design, and a disc brake design. These three problems can be found in Ray & Liew (2002), and the representative figures of these problems are shown in Figure 3.8.

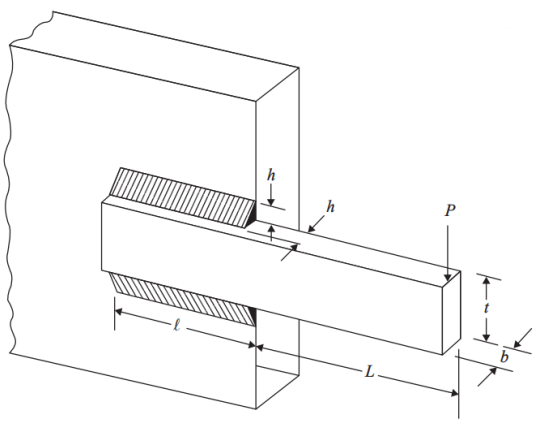

a) Welded Beam Design (Rao, 2009)

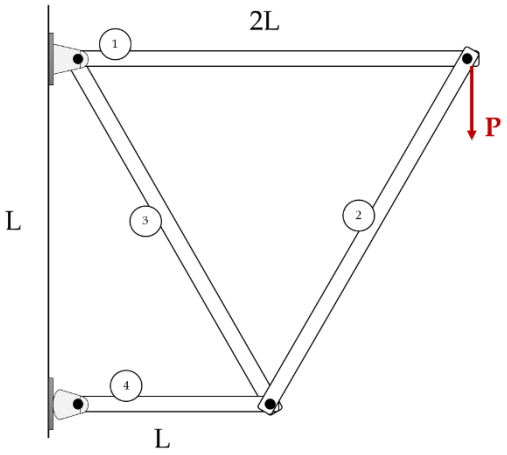

b) Four bar truss design

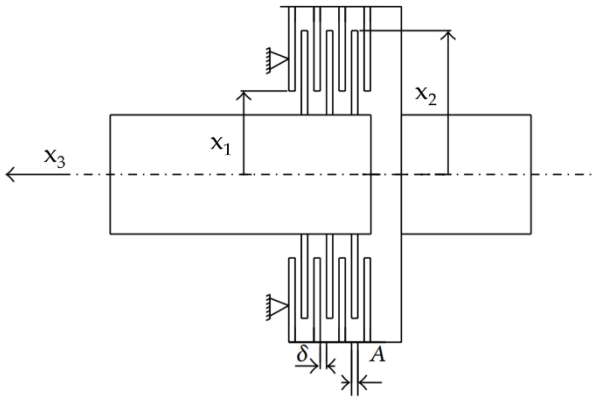

c) Disk Brake Design

Figure 3.8 – Multi-objective Optimization in Mechanical Designs

The welded beam design works with four variables, the width (x_1=h), the length (x_2=l) of the welded area, the depth (x_3=t), and the thickness (x_4=b) of the beam. The objectives are to minimize the total manufacturing costs (f_1) (Equation 3.4), and the deflection of the beam (f_2) (Equation 3.5), under the appropriate constraints (Equations 3.6 to 3.9), and the search space (Equation 3.10).

$$\min f_1(x) = 1.1047 x_1^2 x_2 + 0.04811 x_3 x_4 (14 + x_2) \quad (3.4)$$

$$\min f_2(x) = 2.1952 / x_3^3 x_4 \quad (3.5)$$

$$g_1(X) = \tau(X) - 13600 \leq 0 \quad (3.6)$$

$$g_2(X) = \sigma(X) - 30000 \leq 0 \quad (3.7)$$

$$g_3(X) = x_1 - x_4 \leq 0 \quad (3.8)$$

$$g_4(X) = 6000 - P_C(X) \leq 0 \quad (3.9)$$

$$0.125 \le x_i \le 5, i = 1,4;\ 0.125 \le x_i \le 10.0, i = 2,3 \tag{3.10}$$

where:

$$\tau(X) = \sqrt{(\tau')^2 + 2\tau''\tau'\frac{x_2}{2R} + (\tau'')^2};\ \tau'(X) = \frac{P}{\sqrt{2}x_1x_2};\ \tau''(X) = \frac{MR}{J};\ M = P(L + \frac{x_2}{2});$$

$$R = \sqrt{\frac{{x_2}^2}{4} + (\frac{x_1 + x_3}{2})^2};\ J = 2\left\{\frac{x_1x_2}{\sqrt{2}}\left[\frac{{x_2}^2}{12} + (\frac{x_1 + x_3}{2})^2\right]\right\};\ \sigma(X) = \frac{504000}{x_4{x_3}^2};\ \delta(X) = \frac{4PL^3}{E{x_3}^3x_4};$$

$$P_C(x) = \frac{4.013}{L^2}\left(1 - \frac{x_3}{2L}\sqrt{\frac{E}{4G}}\right)\sqrt{(\frac{EG{x_3}^2{x_4}^6}{36})}$$

P = 6000 lb;
L = 14 in;
$E = 30 \times 10^6$ psi;
and $G = 12 \times 10^6$ psi.

The 4-bar truss design problem is a well-known problem in the structural optimization field (COELLO & PULIDO, 2005), wherein the structural volume (f_1) (Equation 3.11), and the displacement (f_2) (Equation 3.12) of a 4-bar truss should be minimized, subjected to only the search space (Equations 3.13 and 3.14). There are four design variables related to the cross sectional area of members 1, 2, 3, and 4.

$$\min f_1(x) = 200(2x_1 + \sqrt{2x_2} + \sqrt{x_3} + x_4) \tag{3.11}$$

$$\min f_2(x) = 0.01((2/x_1) + (2\sqrt{2}/x_2) - (2\sqrt{2}/x_3) + (2/x_4)) \tag{3.12}$$

$$1 \le x_i \le 5, i = 1,4 \tag{3.13}$$

$$1.4142 \le x_i \le 3, i = 2,3 \tag{3.14}$$

The disk brake design has two objectives, to minimize the stopping time (f_1) (Equation 3.15), and the mass of a brake (f_2) (Equation 3.16). There are four design variables, the inner radius of the disk (x_1), the outer radius of the disk (x_2), the engaging force (area between the brake disc and the brake blocks) (x_3), and the number of friction surfaces (x_4), and it has five constraints (Equations 3.17 to 3.21), and a search space given in Equation 3.22.

$$\min f_1(x) = 4,9(10^{-5})(x_2^2 - x_1^2)(x_4 - 1) \tag{3.15}$$

$$\min f_2(x) = (9,82(10^6)(x_2^2 - x_1^2))/((x_2^3 - x_1^3)x_4x_3) \tag{3.16}$$

$$g_1(X) = 20 + x_1 - x_2 \tag{3.17}$$

$$g_2(X) = 2,5(x_4 + 1) - 30 \tag{3.18}$$

$$g_3(X) = \frac{x_3}{(3{,}14(x_2^2 - x_1^2)^2)} - 0{,}4 \tag{3.19}$$

$$g_4(X) = \frac{2{,}22(10^{-3})(x_3)(x_2^3 - x_1^3)}{(x_2^2 - x_1^2)^{2-1}} \tag{3.20}$$

$$g_5(X) = 900 - (2{,}66(10^{-2})x_3x_4(x_2^3 - x_1^3)) / ((x_2^2 - x_1^2)) \tag{3.21}$$

$$55 \le x_1 \le 80;\ 75 \le x_2 \le 110;\ 1000 \le x_3 \le 3000;\ 2 \le x_4 \le 20 \tag{3.22}$$

The parameters used in MOLA in these problems are the same as in the ZDT functions. The set of non-dominated solutions found for each of these problems is shown in Figure 3.9, together with the true Pareto front. There are no other solutions that, when modified, do not negatively impact the other solutions. It is up to the decision maker to choose the point that represents the values of the objectives, and consequently the design variables according to their choice criteria. This chapter does not pose to discuss decision-making techniques. Once again, a substantial result can be seen from MOLA. It can be seen the power of MOLA in constrained optimization.

(Intentionally left Blank)

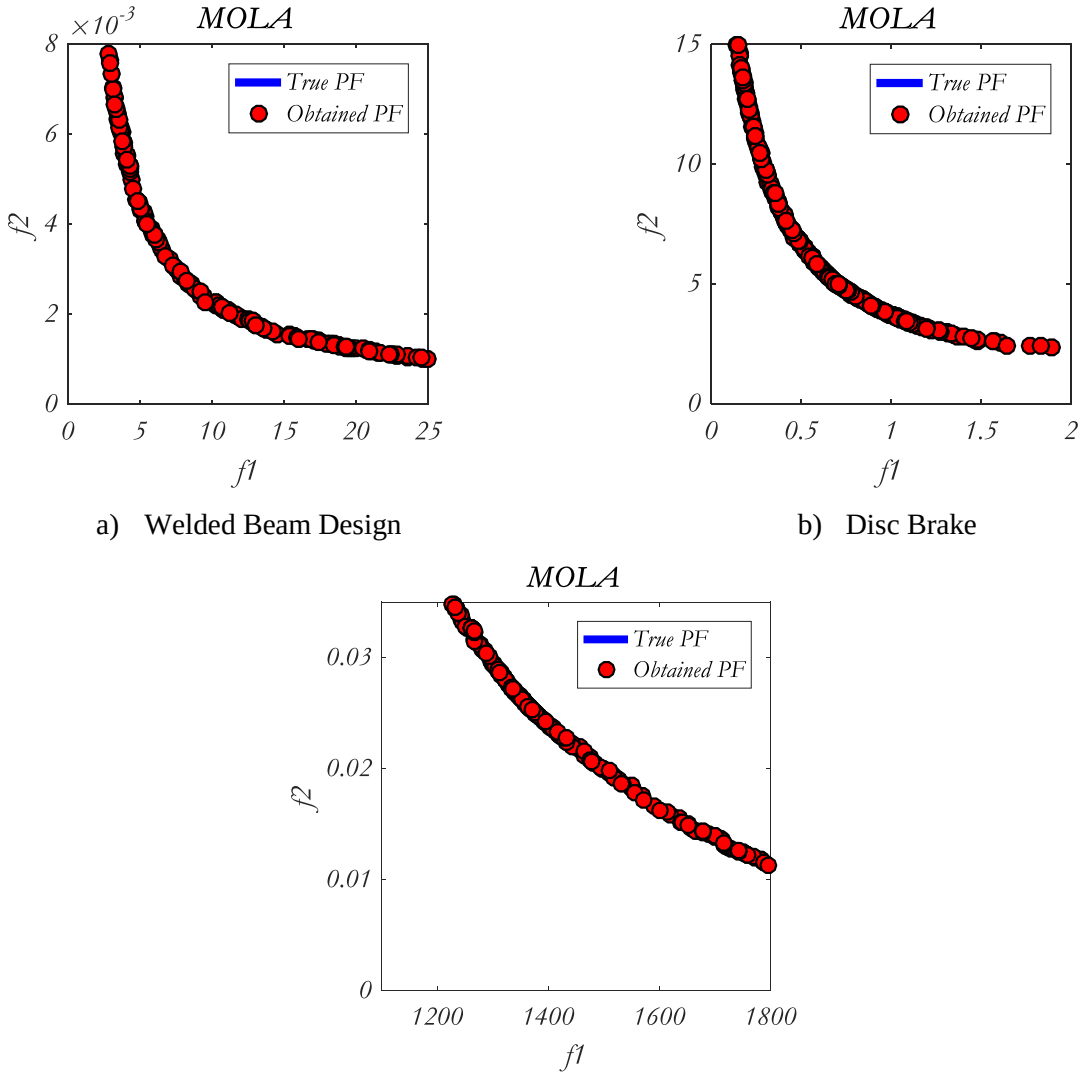

a) Welded Beam Design

b) Disc Brake

c) 4-bar-truss

Figure 3.9 – Pareto front found for the constrained problems

3.3 Chapter Conclusion

The first multi-objective meta-heuristic inspired by the physical phenomenon of lightning and Lichtenberg's Figures was created. Since this is based on the theory of Diffusion Limited Aggregation, a numerical algorithm does not require internal sub-calculations present in most other traditional or recent meta-heuristics.

The proposed MOLA was compared with NSGA-II, MOPSO, MOEA/D, MOGWO, and MOGOA in the ZDT and CEC 2009 test suites. The IGD, SP, and MS were used to measure the

convergence and coverage of the results. The MOLA proved to be a promising algorithm, resulting in the best mean MS value for all 13 test functions used, with the best mean IGD value at 6, and came in second in other tests, still showing competitive SP values. Visually, the MOLA found many non-dominated-solutions, with a great distance between extreme solutions (high MS).

The validated algorithm paying homage to Christoph Lichtenberg was applied to three real multi-objective constrained optimization problems where the non-dominated solutions found practically overlapped the real (analytical) ones.

(Intentionally left Blank)

Chapter 4

Deep Multi-objective Design optimization of CFRP Isogrid Tubes using Lichtenberg Algorithm

Isogrid structures, hollow structures composed of circular and helical ribs forming triangular micro-structures, were initially developed for the aeronautical industry, considerably reducing the mass without significantly compromising the rigidity of structures. The advance of additive manufacturing technology contributed to the development of these complex structures, facilitating their applications in other sectors, such as the development of human prostheses. Since then, the subject has gained more visibility in the literature.

Junqueira *et al*. (2019) studied the isogrid performance under compression and torsion efforts. Using numerical and experimental approach, the authors proved that the model has better performance than conventional tubes applied as prosthetic tubes. Equally important, Li *et al.* (2019) used the additive technique to build hierarchical isogrid and evaluated its buckling resistance and plastic performance. In the same way, Forcellese *et al*. (2020) used the 3D printing process to develop a lattice panels in polyamide reinforced with short carbon fiber. The

authors studied how the geometric parameter affect the compressive strength and buckling performance.

Likewise, Akl *et al*. (2008) developed numerical methods to describe the performance of plates with isogrid stiffeners and optimized both the static and dynamic characteristics of the model. Similarly, Jadhav and Mantena (2007) carried out an optimization study to find the geometric parameters that maximize the specific energy absorption and Rao (2013) studied the optimal design of laminate composite isogrid with dynamically reconfigurable quantum PSO.

Recently, Francisco *et al*. (2020) carried out design optimization studies for carbon fiber reinforced polymer isogrid with lower limb prosthesis applications. The authors performed all the optimizations using particle swarm optimization (PSO) and Lichtenberg algorithm (LA). The authors used the Response Surface Methodology to find the set of equations that represent the complex structural behavior of isogrid structures and then used LA and PSO to optimize the model.

Nevertheless, according to the best of the authors' knowledge, very few efforts have been devoted to the development of isogrid optimization aiming several responses simultaneously. Francisco *et al.* (2021) were one of the first to consider the optimization of CFRP isogrid structures considering more responses, but used metamodeling resulting from the Response Surface Methodology (RSM) and substantial results were found.

In this Chapter, MOLA will be applied to optimize an isogrid Tube made by CFRP considering six different structural responses, i.e., mass, Tsai-Wu failure index, instability coefficient (under compression and torsion efforts), and natural frequency. As with all previous studies, the multi-objective optimization will be performed using metamodels from a RSM design, which generates second order polynomial equations that represent the model with a certain level of confidence (LA-RSM methodology).

However, the use of this methodology can lead to the generation of simplified Pareto fronts that can hide the true behavior of these structures when optimized. Therefore, it will be applied for the first time in the literature the multi-objective optimization of isogrid tubes considering the direct responses of the Finite Element Method (FEM) software, interacting with the MOLA during the optimization process (LA-FEM methodology). In this way, there is no error between the solutions generated by the algorithm and the simulation in the FEM, in addition to opening possibilities to find the true nature of the Pareto fronts of these types of structures, that is, to evaluate their convexity, continuity, feasible regions, etc.

The optimization objectives will be distributed and compared with other results in the literature through three cases: Torsion, Compression and Modal performance. The Pareto fronts of the two methodologies will be compared using IGD, SP, and MS to assess which of the two has more convergence and coverage. The best PF according to these metrics will be chosen to discuss the non-dominated solutions and obtain the decision variables for the optimized Carbon Fiber-Reinforced Polymer (CFRP) isogrid tube.

Therefore, the Chapter is organized as follows: Section 4.1 brings the Theoretical Background, which presents a summary of the knowledge needed for the work. Section 4.2 shows the Methodology. Section 4.3 brings the results and discussions and finally, Section 4.5 draws the conclusion.

4.1 Theoretical Background

According to Fan *et al.* (2019), the meet point of helical and circular ribs is called nodes. It is created triangular (or another geometric figure) between these points to provide structural stability (SORRENTINO *et al.*, 2017; ZHENG *et al.*, 2015). There are two theories in the literature about the word "isogrid". Some authors believe that structures formed just by equilateral triangless can be called isogrid and "iso" refers to isotropy of the structure (KANOU *et al.*, 2013). On the other hand, some authors agree that all lattice structure (even those there are not isotropic) must be called isogrids (HUYBRECHTS *et al.*, 1999; AKL *et al.*, 2008).

Isogrid structures can be just the rigid ribs or can be the rigid ribs cover with a coating, the first model is used in this paper and is called open and the second is called close. Eight variables can be used to describe the structure, they are: angle between helical ribs (φ), width of circular (δ_c) and helical (δ_h) ribs, thickness (h), length (L), diameter (D), distance of circular (α_c), and helical (α_h) sleepers from the axis of the structure. The first three are the main ones in the design of the isogrid tube and that is why they are the decision variables in this study and are represented in Figure 4.1.

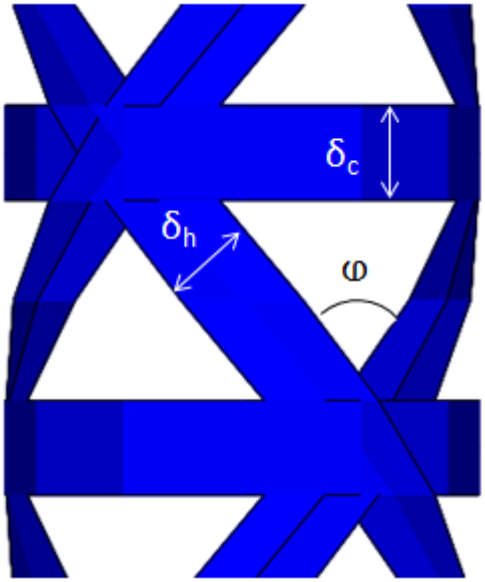

Figure 4.1 – Geometric parameters of the isogrid tube

Two main researchers studied the optimization of isogrid structures. Totaro *et al*. (2004) used the geometric parameters of an isogrid as variables in an optimization problem focused in minimize safety factors. The author evaluated a structure subjected to axial load and found the optimal parameters. Another procedure was used by Vaziliev and Razin (2006) and will be described here. An optimization based on load normalization factor (p) given by Equation 4.1 was proposed. The author compares p with the parameters p_s (Equation 4.2) and p_o (Equation 4.3). These can be resulted into the three cases shown in Table 4.1.

$$p = \frac{4P}{\pi D^2} \tag{4.1}$$

$$p_s = \frac{48\bar{\sigma}^2}{\pi E_h}\sqrt{\frac{\bar{\sigma}p}{kE_c}} \tag{4.2}$$

$$p_o = p_s\sqrt{\frac{1}{2}\sqrt{\frac{2E_h\bar{p}}{E_c} + \sqrt{\frac{2E_h\bar{p}}{E_c} - 1}}} \tag{4.3}$$

Table 4.1 – Optimum results for three different cases in isogrid (adapted from VASILIEV & RAZIN, 2006)

Case 1 ($p \leq p_s$)	Case 2 ($p_s \leq p \leq p_o$)	Case 3 ($p_o \leq p$)
$\bar{h} = \frac{1}{4}(\frac{48\pi^4 k^2 \bar{p}^3}{E_h E_c^3} p^4)^{1/10}$	$\bar{h} = \frac{1}{4}(\frac{\pi^2 k \bar{p}}{E_c \bar{\sigma}} p^2)^{1/4}$	$\bar{h} = \frac{\pi p}{16\bar{\sigma}} \sqrt{\frac{k E_h p_s}{3\bar{\sigma} p_o}}$
$tg\varphi = \frac{1}{2}$	$tg^2\varphi = \frac{p_s}{4p}$	$tg^2\varphi = \frac{p_s}{4p_o}$
$\bar{\delta}_h = \frac{5}{4\pi}(\frac{108\pi^2 E_c p^2}{E_h^3 k^4 \bar{p}})^{1/10}$	$\bar{\delta}_h = \frac{2}{\pi sin2\varphi} \sqrt{\frac{3\bar{\sigma}}{k E_h}}$	$\bar{\delta}_h = \frac{2}{\pi sin2\varphi} \sqrt{\frac{3\bar{\sigma}}{k E_h}}$
$\bar{\delta}_c = \frac{\bar{\delta}_h}{2\bar{p}}$	$\bar{\delta}_c = \frac{p_s \bar{\delta}_h}{2p\bar{p}}$	$\bar{\delta}_c = \frac{p_s p_o \bar{\delta}_h}{\bar{p} p^2}(\frac{p_o^2}{p^2} - \frac{1}{2})$

The variables shown in Table 4.1 to calculate the parameters are the ultimate stress of helical ribs under compression efforts ($\bar{\sigma}$) , the Young's modulus (E), the mass density (ρ) and the local buckling coefficient (*k*). It implies axisymmetric global buckling when $p \leq p_s$ or $p_s \leq p \leq p_o$ and no axisymmetric global buckling when $p_o \leq p$. The author found the optimized mass is given by Equation 4.4.

$$M = \pi D L h \rho_h \left(2\bar{\delta}_h + \bar{\rho}\bar{\delta}_c\right) \tag{4.4}$$

Finally, the use of isogrid structure is due its high mechanical performance and low weight. In this way, in this work, CFRP will be used as it is a material that helps in minimizing mass and has high mechanical resistance.

4.1.1 Response Surface Method

The formulation of explicit equations for the behavior of CFRP isogrid tubes is complex and varies greatly depending on both the loading and boundary conditions. However, with the physical structure for experimental evaluation or a finite element software where the structure can be modeled, mathematical and statistical methods can be applied to obtain equations that

(significantly) represent the model. That is, that allows obtaining metamodels. One of these methods is the Response Surface Method (RSM).

Through the elaboration of an experimental matrix using Design of Experiments (DoE), the responses can be used to create equations based on the fit of a second order model as shown in Equation 4.5 (MONTGOMERY, 2003):

$$Y = \beta_0 + \sum_{i=1}^{k} \beta_i x_i + \sum_{i=1}^{k} \beta_{ii} x_i^2 + \sum_{i<j} \sum \beta_{ij} x_i x_j + \varepsilon \tag{4.5}$$

where *k* is the number of decision variables of the problem.

The central composite design (CCD) is used in RSM to generate a complete quadratic model using all decision variables, being 2^k factorial points, 2k axial points, and a central point. According to Montgomery (2003), the *Y* metamodel can have a good representation of the real problem within the experimental region if the operator of the problem has good knowledge in the estimation of this region.

The adjustment of the models is given through the coefficient of determination (R^2), which represents the percentage of variation in the response that is explained by the conceptual model. However, a high value of R^2 does not necessarily imply a good model, as adding variables to the model will always increase such coefficient of determination, regardless of the variable added whether (or not) statistically significant. Due to this fact, most of the time, it is chosen to use the R^2 coefficient adjusted (R^2_{adj}), which does not increase whenever a variable is added to the template; if an unnecessary term is added, the value of R^2_{adj} decreases. With the response surface model adjusted, one can proceed to the process optimization and results validation (MONTGOMERY, 2017).

4.2 Methodology

The optimization of the isogrid structure depends on the acquisition of output responses from the decision variable inputs. In this study, Mechanical ANSYS APDL® is used. A reduced number of experiments can be done to build the metamodel through RSM, which is performed in MINITAB® Software, or the optimizer can be linked directly into FEM for a deep optimization.

4.2.1 Numerical Modelling using Finite Element Mehod

Francisco *et al.* (2020) studied an isogrid numerical model and made comparisons with experimental tests. The results found by the authors showed that the numerical approach is in accordance with the experiments. In this way, in this work will be used the same shell element with 8 nodes and six degrees of freedom used in that study.

The isogrid model proposed is made with CFRP T300/epoxy. This material was analyzed by Madhavi (2009). The author carried out experimental test for characterization of this material and the parameters are shown in Table 4.2. This data was used by Francisco *et al*. (2020 & 2021) for numerical analysis of a prosthetic tube.

Table 4.2 – Properties of T300 Carbon Fiber/Epoxy Resin (Adapted from Madhavi, 2009).

Propriety	Unit	Value	Standard
E_1	GPa	144	ASTM D3039
E_2	GPa	6.5	ASTM D3039
G_{12}	GPa	5.6	ASTM D3518
S_{12}	MPa	40	ASTM D3518
σ_1^T	MPa	1200	ASTM D3039
σ_2^T	MPa	17	ASTM D3039
σ_1^C	MPa	600	ASTM D3410
σ_2^C	MPa	80	ASTM D3410
ILSS	MPa	42	ASTM D2344
ρ	g/cm³	1.35	ASTM D3039
υ_{12}	--	0.21	ASTM D3039

The isogrid is formed by 7 sheets of 0.2mm each, i.e., the total thickness of the model is equal to 1.4mm. This value was adopted by Junqueira *et al.* (2019) and shows excellent results in experimental tests. In addition, it is important to highlight that the orientation of the carbon fibers is shown in Figure 4.2. For the numerical analysis, the force and the moment were applied at the end of the structure while the other side is locked as shown in Figure 4.3. The loads used in numerical model are according to the standard that have the norms to structural testing of lower limb prosthesis (NBR ISO 10328: 2002). The adopted loads are 4480 N for compression test and 7.1 N·m for torsion tests.

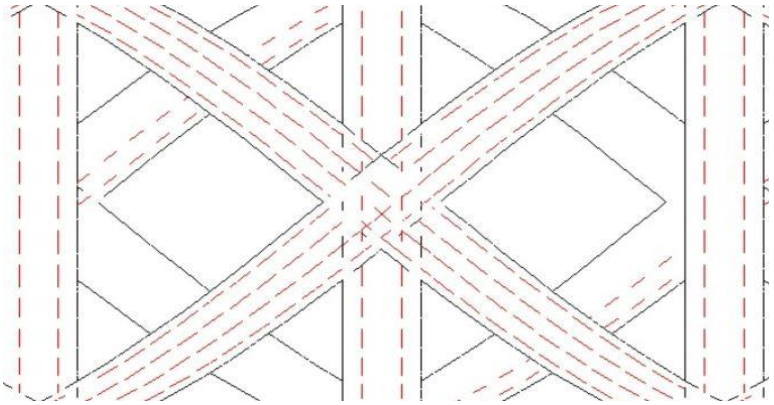

Figure 4.2 – Fiber orientation used to build the isogrid (FRANCISCO *et al.*, 2021)

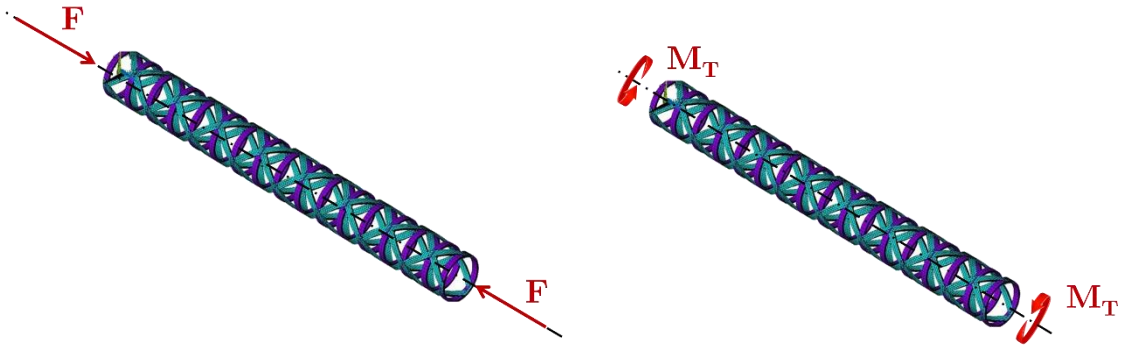

(a) (b)

Figure 4.3 – Boundary conditions applied to the model for (a) compression test and (b) torsion cases.

Having the structure modeled, the main objectives to be analyzed will be the Mass, natural frequency, Tsai-Wu and critical buckling load in the isogrid tube torsional, and compression scenarios.

The Tsai-Wu failure criterion (TW) was used in this work to determine the safety factor of the composite orthotropic shells. This criterion takes into consideration the total effort energy to predict failure, i.e., the failure will occur when the index is greater or equal to the unit. Therefore, it is necessary to minimize it and this criterion can be modeled as shown in Equation 4.6.

$$F = F_1\sigma_1 + F_{11}\sigma_1^2 + F_2\sigma_2 + F_{22}\sigma_2^2 + 2F_{12}\,\sigma_1\sigma_2 + F_{66}\tau_{12}^2 \quad (4.6)$$

where:

$$F_1 = \frac{1}{X_{1T}} - \frac{1}{Y_{1C}};\ F_2 = \frac{1}{X_{2T}} - \frac{1}{Y_{2C}};\ F_{11} = \frac{1}{X_{1T}Y_{1C}};\ F_{22} = \frac{1}{X_{2T}Y_{2C}};\ F_{66} = \frac{1}{S_{12}^2} \quad (4.7)$$

$$F_{12} = \frac{1}{2P^2}\left[1 - P\left(\frac{1}{X_{1T}} - \frac{1}{Y_{1C}} + \frac{1}{X_{2T}} - \frac{1}{Y_{2C}}\right) - P^2\left(\frac{1}{X_{1T}Y_{1C}} + \frac{1}{X_{2T}Y_{2C}}\right)\right] \quad (4.8)$$

where σ_1 ,σ_2 , τ_{12}^2 are the principal stress; $X_{1T,}$ X_{2T} are the tensile strength in fiber direction and transversal fiber direction, respectively; Y_{1C}, Y_{2C} are the compressive strength in fiber direction and transversal fiber direction, respectively; S_{12} is the shear strength of material.

The critical buckling load (C_{cr}) is another response analyzed in this work with the intention of maximization. It can be associated with an eigenvalue (λ) and the stiffness matrix of the structure as shown by equations 4.9 and 4.10 below.

$$([K] - \lambda[K_G])\{\theta\} = 0 \quad (4.9)$$

$$C_{cr} = \lambda \cdot F_i \quad (4.10)$$

where [K] is the global stiffness matrix and $[K_G]$ is the global geometric stiffness matrix of the isogrid tube. So, the lambda is a multiplier greater than one that shows how many times the structure can support the initial load without buckling.

4.2.2 Response Surface Design

More than 8 input variables can be used in the isogrid structure code in FEM, however, the main ones that control the others and are continuous are: *i*) the angle between helical ribs (φ), ranging from 20 to 50°, *ii*) width of the helical crossbeams (δ_h), ranging from 2 to 6 mm, and *iii*) width of the circular crossbars (δ_c), ranging from 2 to 6 mm. These intervals are recommendations found in Francisco *et al*. (2021) and Junqueira *et al*. (2019).

Using the CCD with 3 decision variables, 8 factorial, 6 axial, and 1 central experiments are generated. Adding 5 central points to assess the variability of the problem, there are the 20 experiments in Table 4.3. The objectives are: Mass (M), natural frequency (ω_n), eigenvalues associated with the critical buckling load for compression (λ_C) and torsion (λ_T) and Tsai-Wu criteria for compression (TW_C) and torsion (TW_T).

Table 4.3 – Experimental matrix of the CFRP isogrid tube metamodeling

		Input Parameters		
	Simulation	φ (°)	δ_c (mm)	δ_h (mm)
Factorial points	#1	20	2	2
	#2	50	2	2
	#3	20	6	2
	#4	50	6	2
	#5	20	2	6
	#6	50	2	6
	#7	20	6	6
	#8	50	6	6
Axial points	#9	20	4	4
	#10	50	4	4
	#11	35	2	4
	#12	35	6	4
	#13	35	4	2
	#14	35	4	6
Center points	#15	35	4	4
	#16	35	4	4
	#17	35	4	4
	#18	35	4	4
	#19	35	4	4
	#20	35	4	4

4.2.3 Multi-objective Optimization of Isogrid Tubes

For the construction of a visible Pareto front, 3 case studies will be developed. Each of these cases will be performed with the two methodologies (LA-FEM and LA-RSM) and the generated Pareto fronts will be compared. The one that presents the best result for the three metrics used will be chosen for the discussion of the optimization of the isogrid tube in that case.

Case I is a torsion case and aims to minimize the mass and Tsai-Wu and maximize the critical buckling load. The optimization problem can be seen in Equation 4.11. Note that the minus sign can be associated with the objective one want to maximize.

$$\begin{aligned} &\min F(X)=\{M(X), -\lambda_T(X), TW_T(X)\} \\ &\textit{subject to:} \\ &\quad 20 \leq \varphi \leq 50\ [°] \\ &\quad 2 \leq \delta_h \leq 6\ [mm] \\ &\quad 2 \leq \delta_c \leq 6 [mm] \end{aligned} \tag{4.11}$$

Case II is a case of Compression. The optimization problem modeling is similar to the previous one and is expressed in Equation 4.12:

$$\begin{aligned} &\min F(X)=\{M(X), -\lambda_C(X), TW_C(X)\} \\ &\textit{subject to:} \\ &\quad 20 \leq \varphi \leq 50\ [°] \\ &\quad 2 \leq \delta_h \leq 6\ [mm] \\ &\quad 2 \leq \delta_c \leq 6 [mm] \end{aligned} \tag{4.12}$$

Case III is about modal performance and is composed of two objectives. It aims to minimize mass and maximize the first natural frequency. The optimization problem is expressed in Equation 4.13.

$$\begin{aligned} &\min F(X)=\{M(X), -\omega_n(X)\} \\ &\textit{subject to:} \\ &\quad 20 \leq \varphi \leq 50\ [°] \\ &\quad 2 \leq \delta_h \leq 6\ [mm] \\ &\quad 2 \leq \delta_c \leq 6 [mm] \end{aligned} \tag{4.13}$$

Case IV unites all the six studied objectives for the first time in literature. The optimization problem is expressed in Equation 4.14.

$$\begin{aligned} &\min F(X)=\{M(X), -\lambda_C(X), TW_C(X), -\lambda_T(X), \\ &\qquad TW_T(X), -\omega_n(X)\ )\} \\ &\textit{subject to:} \\ &\quad 20 \leq \varphi \leq 50\ [°] \\ &\quad 2 \leq \delta_h \leq 6\ [mm] \\ &\quad 2 \leq \delta_c \leq 6 [mm] \end{aligned} \tag{4.14}$$

The MOLA parameters for the multi-objective optimization of Equations 4.11 to 4.14 will be, for the two methodologies: $Pop = 100$; $N_{iter} = 100$; $R_c = 200$; $N_p = 10^6$; $S = 1$; $ref = 0.4$; and $M = 0$.

The Pareto fronts generated for each cases using the two methodologies will be compared using the IGD, SP, and MS. These metrics need a Pareto front of reference, often called true Pareto front (TPF) to evaluate the methodology or algorithm. As this problem is

complex and there is no real Pareto front in the literature to use as a reference, a Pareto front resulting from all solutions of all methodologies for each case will be used.

4.3 Results and Discussion

4.3.1 Metamodeling

Applying the simulations in Table 4.3, output variables are shown in Table 4.4.

Table 4.4 – Results of the Experimental Matrix of the Isogrid Tube

Decision Variables			**Objectives**					
φ (°)	δ_c (mm)	δ_h (mm)	TW_C	λ_C	TW_T	λ_T	*Mass(g)*	ω_n *(Hz)*
20	2	2	1.180	1.29	0.177	4.71	10.09	2270.37
50	2	2	1.799	3.12	0.169	28.69	14.94	3266.82
20	6	2	0.552	2.35	0.419	8.81	15.79	1867.83
50	6	2	1.660	4.73	0.136	55.85	27.05	2463.69
20	2	6	0.445	15.79	0.211	58.82	24.56	2513.03
50	2	6	2.239	17.36	0.055	272.25	32.68	3810.46
20	6	6	0.304	23.33	0.191	88.57	30.26	2346.92
50	6	6	0.848	19.26	0.084	391.47	44.79	3309.55
20	4	4	0.428	8.54	0.164	32.09	20.18	2312.34
50	4	4	0.997	12.03	0.100	157.54	29.87	3286.47
35	2	4	0.792	10.33	0.097	62.85	19.98	3268.24
35	6	4	0.550	15.69	0.212	103.89	28.53	2787.73
35	4	2	1.162	3.42	0.224	21.35	16.41	2583.91
35	4	6	1.494	23.05	0.139	178.52	32.10	3183.51
35	4	4	0.562	13.45	0.100	82.15	24.26	2993.60
35	4	4	0.682	14.49	0.110	102.84	26.19	3071.66
35	4	4	0.636	13.96	0.103	88.79	25.13	2993.76
35	4	4	0.531	13.07	0.140	76.25	24.10	2906.92
35	4	4	0.509	12.71	0.153	71.09	23.48	2891.44
35	4	4	0.543	14.46	0.090	95.91	25.30	3077.11

All metamodels found had an adjusted fit greater than 80%, being considered reasonable. These results are shown in Table 4.5. The generated metamodels that will be used in the LA-RSM methodology are in Table 4.6.

Table 4.5 – Table for fit regression model

Objective	R^2 (adj)
M	99.33
TW_T	81.02
λ_T	99.09
TW_C	80.69
λ_C	94.24
ω_n	97.36

Table 4.6 – Coefficients of Metamodels generated by the Response Surface Method

Objective	β_1	β_2	β_3	β_1^2	β_2^2	β_3^2	β_{12}	β_{13}	β_{23}	β_0
M	0.323	2.209	4.005	0.000	0.000	0.000	0.000	0.000	0.000	-11.38
TW_T	-0.006	0.061	-0.146	0.000	0.000	0.014	-0.001	0.001	-0.006	0.492
λ_T	-9.070	32.300	-19.600	0.132	0.000	0.000	-0.606	1.804	0.000	21.2
TW_C	0.031	-0.127	-0.726	0.000	0.000	0.083	0.000	0.000	0.000	1.725
λ_C	0.035	1.260	4.194	0.000	0.000	0.000	0.000	0.000	0.000	-10.91
ω_n	55.700	-68.800	175.000	-0.459	0.000	-20.160	-1.397	3.480	0.000	1172

4.3.2 Multi-objective optimization

The Pareto fronts generated for the optimization problems of Equations 4.11 to 4.14 are shown in Figure 4.4. It is possible to see the non-dominated solutions and the best solution found using the Technique for Order of Preference by Similarity to ideal Solution (TOPSIS) (BYUN & LEE, 2005) for the LA-FEM and LA-RSM methodologies in the performance cases of Torsion, Compression and Modal. The TOPSIS selects the solution in front of Pareto that is both closest to the ideal and farthest from the worst.

The main motivation for using the two methodologies for each case is to compare the accuracy of the results. In terms of computational cost, each simulation using FEM takes about 40s. In the LA-RSM methodology, there are 20 experiments, which generates a simulation time of 13 minutes. In the LA-FEM, there are $40 \times Pop \times N_{iter}$ experiments, which results in approximately 55h.

In all cases, for the LA-RSM, consistency and continuity of the Pareto fronts is observed, given the optimization generated by second-order polynomial equations. However, it is possible to observe that the true nature of the optimization of an isogrid structure is composed of discontinuous Pareto fronts. Also, even with the same search spaces in both methodologies, usin the LA-FEM method was possible to find solutions with larger ranges of critical lambda (Case I) and natural frequencies (Case III). For this reason, the solution via TOPSIS for LA-FEM ends up being more displaced in relation to LA-RSM.

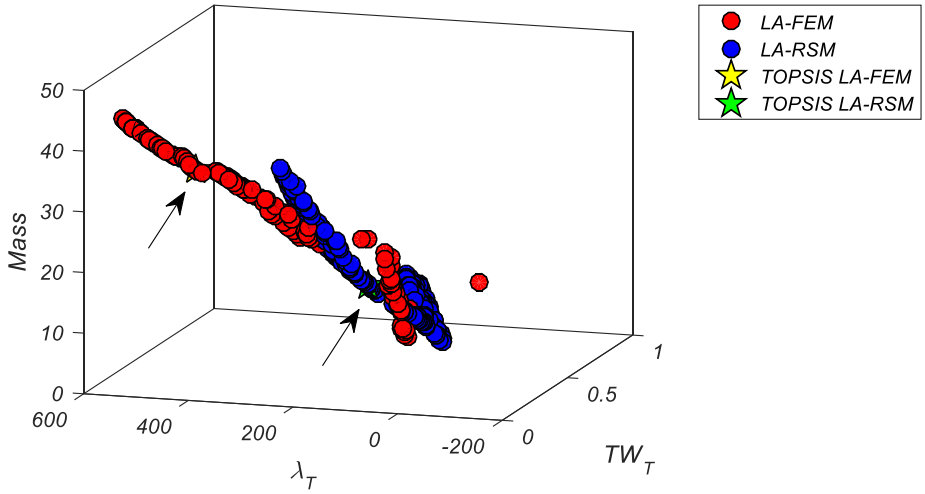

(a) Case I - Torsion

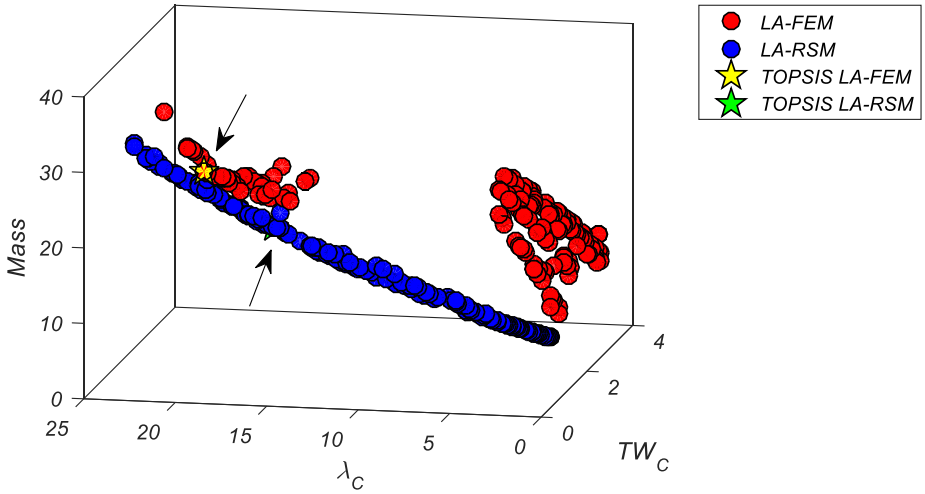

(b) Case II – Compression

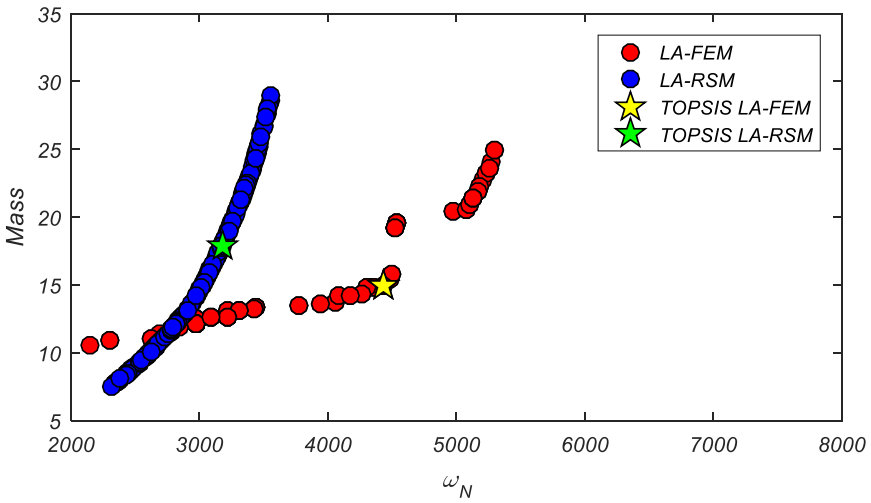

(c) Case III - Modal

Figure 4.4 – Pareto fronts generated for LA-FEM and LA-RSM

Three metrics are used in this work to compare these generated Pareto fronts: IGD, SP and MS. The lower the IGD, the closer the analyzed Pareto front approached the true Pareto front. The smaller the SP, the less spaced the solutions are from each other and the larger the MS, the greater the interval between the solutions found. In this way, the smaller the IGD and SP and the larger the MS, the better the Pareto front. As in this problem there is no true Pareto front to be used as a reference, a Pareto front was generated that is composed of the solutions of the two methodologies for each case. These results are shown in Table 4.7.

Table 4.7 – Statistical comparison of Pareto fronts

Case	Methodology	IGD	SP	MS
I	LA – FEM	5.55	1.70	0.87
	LA-RSM	56.65	1.18	0.77
II	LA – FEM	4.06	0.51	0.57
	LA-RSM	0.02	0.26	0.45
III	LA – FEM	13.38	53.73	1.92
	LA-RSM	683.59	3.10	0.89
IV	LA – FEM	35	30	0.99
	LA-RSM	830.51	15.32	0.84

As expected, given the ease of the optimization problem with second order polynomial functions, the SP of the LA-RSM methodology is smaller in all cases. This result can also indicate the presence of discontinuity between the solutions, confirming the non-continuous

nature of the Pareto front of the multi-objective optimization problem of an isogrid structure. MS indicates how diverse the solutions found are and for all cases, the LA-FEM Methodology was higher, as can also be seen in Figure 4.5.

One of the most important metrics is the IGD, as it is the metric that guarantees better solutions when using TOPSIS or a solution closer to the ideal solution. In all situations, the LA-FEM presented better values, with the exception of Case II. However, a high discontinuity of the real problem can be observed in part of this region, not identified by the RSM. The difference in IGD is even greater on the hyper-dimensional Pareto fronts generated in Case IV - A case with six objectives or dimensions. For this reason, the optimal solutions for this work are those found by LA-FEM.

All the solutions using TOPSIS highlighted in Figure 4.5 are in Table 4.8. The LA-RSM methodology finds the optimal decision variables from metamodels. When entering them into the FEM for a conference simulation, there may be an error due to polynomial approximations of the metamodeling. For this methodology, the Error is calculated, also represented in Table 4.8. The Difference (Diff) is also calculated for the objectives found between the LA-FEM and LA-RSM methodologies. It is important to emphasize that using only the Diff to assess which solution is better in multi-objective optimization is insufficient.

For Case I, LA-FEM found a solution with 3 times the mass with less than half the TW and 32.5 times the capacity to support a buckling load. However, for this case, a small error is observed using the LA-RSM, since the solution determined by TOPSIS in this methodology is close to the true Pareto front (LA-FEM) of the problem, as can be seen in Figure 4.4(a).

Approximately half of the TW and 18 times the load capacity for only a 16% increase in mass was found by the LA-FEM in the Compression case. In this, significant errors were identified for the TW and the critical Lambda. It can be seen in Figure 4.5(b) that the solution found by LA-RSM is close to the discontinuous region found by LA-FEM. Still, this was the only case in which the methodology using the metamodel had a higher IGD than the one using the direct link with the FEM. Therefore, the feasibility of this point may be questionable.

As for the case of modal performance (Case III), the LA-RSM methodology found an 18.7% smaller mass, but with a first natural frequency 32.9% smaller. It can be seen in Figure 4.5(c) that the point found by the LA-RSM is not far from the Pareto front found by the LA-FEM. Thus, it presents a minor error. However, even the two methodologies having the same

search space, can be seen a much larger number of solutions in LA-FEM for higher natural frequencies.

Table 4.8 – Optimized decision variables for all the fours multi-objective design optimization cases.

Case		Decision Variables			Objectives					
		φ (°)	δ_h (*mm*)	δ_c (*mm*)	TW_T	Error	λ_T	Error	M (g)	Error
I	LA-FEM	40.00	6.00	3.64	0.03	-	395.81	-	37.55	-
	LA-RSM	25.12	2.54	2.00	0.08	0.66%	12.18	0.05%	12.96	0.04%
				Diff(%)	+166.7		-96.9		-65.5	
		φ (°)	δ_h (*mm*)	δ_c (*mm*)	TW_C	Error	λ_C	Error	M (g)	Error
II	LA-FEM	25.07	6.00	4.13	0.26	-	18.71	-	20.84	0%
	LA-RSM	23.31	3.66	2.18	0.57	10.4%	1.10	8.17%	17.83	1.35%
				Diff(%)	+119.2		-94.1		-14.4	
		φ (°)	δ_h (*mm*)	δ_c (*mm*)	ω_n (Hz)		Error	M (g)		Error
III	LA-FEM	40.00	2.00	2.00	4433.7		-	14.95		-
	LA-RSM	30.17	2.00	2.00	2972.1		0.1%	12.15		0.03%
				Diff(%)	-32.9			-18.7		
		φ (°)	δ_h (*mm*)	δ_c (*mm*)	TW_C	TW_T	λ_C	λ_T	ω_n	M (g)
V	LA-FEM	40	5.81	6.00	0.31	0.07	18.76	522.02	6682	43.93
	LA-RSM	40	2.70	4.20	1.14	0.10	6.10	62.10	5884	24.70
				Error (%)	23.7	40	0.16	0.03	0	0.04
				Diff(%)	+276.7	+42.9	-67.5	-88.1	-11.9	-43.8

The more objectives, the more complex the multi-objective optimization problem becomes. As seen, the isogrid tube optimization problem in small dimensions generated discontinuities and despite being visually difficult, it can be projected that more discontinuities will have for Case IV. This difference is evidenced by the difference in IGD in Table 4.7. The LA-RSM found a solution with a mass 43.8% smaller, however it obtained a TW greater than 1, which indicates a failure of the structure. The LA-FEM methodology found safe TW values and critical lambda values 3 times higher for compression and 8 times higher for torsion.

The results found in this work can be compared to those from Junqueira *et al*. (2019) and Francisco *et al.* (2021), as seen in Table 4.9. Difference 1 is the percentage difference between the results of this study and those of Junqueira *et al*. (2019). Difference 2 is for Francisco *et al.* (2021). There is no comparison for Case IV because this study is the first to do so.

This work significantly improves all the optimization objectives for Case I compared to other works in the literature, finding a smaller mass, a larger critical lambda and a smaller TW for the torsion case. In the case of compression, it also finds a mass and a TW smaller than all

the other related studies; however, it has a lower critical λ, even though it has an expressive value of 18.71.

Table 4.9 – Comparison of studies on the optimization of the Isogrid Tube

Case	Objective	Junqueira *et al.* (2019)	Francisco *et al.* (2021)	Present Study	Difference 1 (%)	Difference 2 (%)
I	TW_T	0.13	0.33	0.03	-77	-90.90
	λ_T	777	387.45	395.81	-49.05	+2.16
	M (g)	82.2	72.34	37.55	-54.3	-48.09
II	TW_C	0.68	0.83	0.26	-61.76	-68.67
	λ_C	33	22.93	18.71	-43.3	-18.40
	M (g)	82.20	38.31	20.84	-74.64	-45.69
III	ω_n (Hz)	2683	2905.91	4433.70	+65.25	+52.57
	M (g)	82.20	13.25	14.95	-81.81	+12.8

For case 3, it finds higher natural frequency values given the direct connection between Ansys and the optimization algorithm, having increased by at least 52.57% the best found in the literature with only 12.8% more mass. Figure 4.5 shows the isogrid tubes optimized for each of the Cases in this study using the LA-FEM.

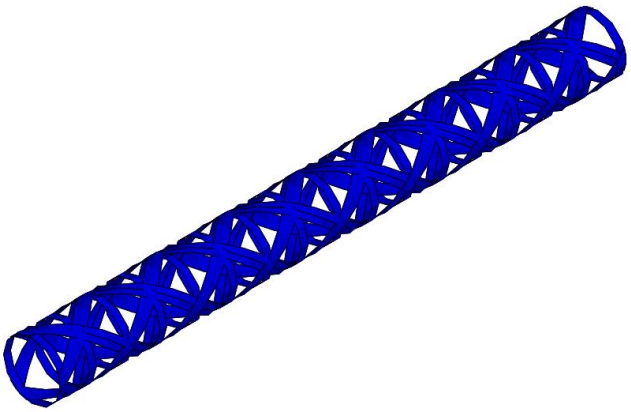

(a) Torsion design

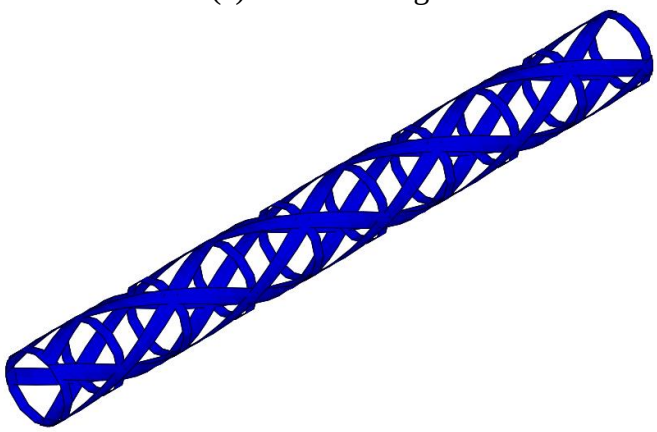

(b) Compression design

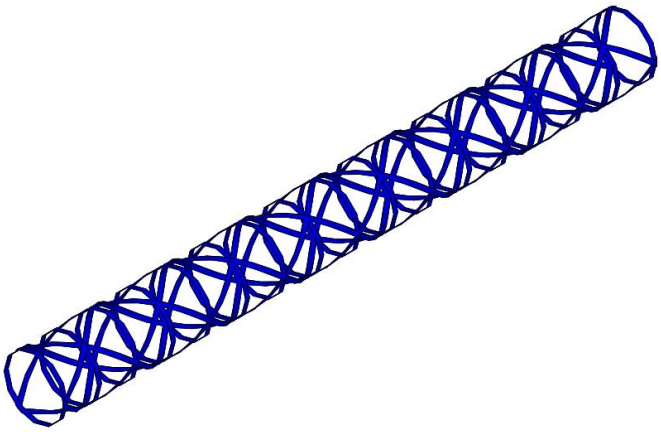

(c) Modal design

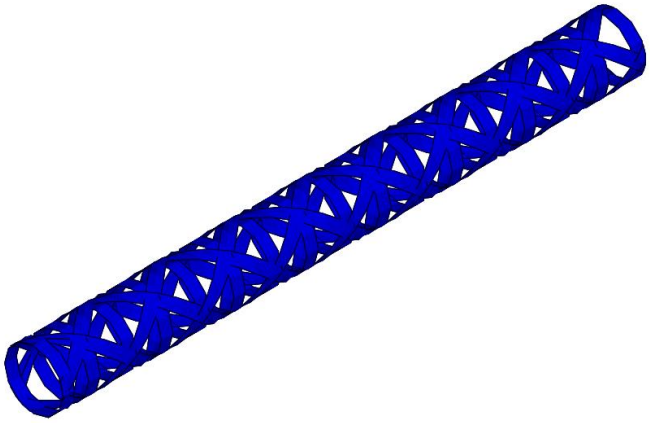

(d) Torsion, Compression and Modal design

Figure 4.5 – Isogrid tubes after deep optimization using TOPSIS

4.4 Chapter Conclusion

This Chapter presents a deep multi-objective optimization of the CFRP isogrid tube considering six objectives: structural mass, Tsai-Wu failure index and instability coefficient (for compression and torsion efforts), and natural frequency. The objectives are divided into three cases for comparison with the literature: torsion, compression, and modal. The optimizations are considered using the direct link between the MOLA and the finite element method software and using metamodeling through the response surface methodology.

The LA-FEM methodology revealed part of the real nature of the Pareto fronts for this type of problem for the first time in literature and allowed the evaluation of regions where the application of the response surface methodology is successful or not. Also, even with the same

search spaces, this methodology allowed to find a range of non-dominated solutions with higher critical lambdas and natural frequencies. Design variables were found with significant improvement compared to the most recent study in the literature. In the case of torsion, it allowed a mass reduction by 48.09%, an increase in the critical lambda of buckling by 2.16%, and a reduction in Tsai-Wu by 90.90%. For Compression, mass reduction by 45.69%, critical lambda reduction by 18.40%, and Tsai-Wu reduction by 68.67%. For the Modal Case, it allowed an increase of up to 52.57% in natural frequency for an increase of only 12.8% in mass. These design variables allowed the identification of a safe and lightweight isogrid tube.

It is important to note that this work does not seek to say which methodology is better, whether optimization by FEM updating or by metamodeling. Although for this application it was concluded that LA-FEM was the best, it is computationally expensive and relies on the availability of other software, while metamodeling is a method that has allowed great advances in optimization when there is no such resource and not even explicit equations.

(Intentionally left Blank)

Chapter 5

Multi-objective Sensor Placement Optimization of Helicopter Rotor Blade Based on Feature Selection

Helicopters have gained importance due to their capabilities of aircraft travel speed (200-300 km/h) and maneuverability, which ensures movement along the shortest route and vertical takeoff (KHABAROV & KOMSHIN, 2021). Its most important element is the main rotor blade (MRB), which is usually made of composite material. Due to the intense in-service conditions of aerodynamics, temperature variation, and accelerations, damage can be induced in these structures (AHMAD *et al*., 2020; VOICU *et al*., 2020).

Efficient systems, as Structural Health Monitoring (SHM), allow early identification of damage through non-destructive inspection and integrated sensors exploring vibration/modal measures in order to avoid catastrophic failures. The method is based on the principle that damage changes natural frequencies, mode shapes, modal strain, energy, wave propagation, and damping ratios (GOMES *et al*., 2018; GOMES & GIOVANI, 2020; PEREIRA *et al*., 2021a). Then, using inverse modeling and computational intelligence, it is possible to identify damage.

The main techniques used are meta-heuristics, neural networks, non-probabilistic methodologies, and time-series analyses. However, there is no methodology that is very effective for all problems. New technologies have been proposed and there is space for new ones (BURGOS *et al*., 2020). Still at the beginning of the century, the first works using SHM and inverse methods associated with finite element method (FEM) updating on MRB appeared.

Pawar & Ganguli (2003) proposed a genetic fuzzy system to find the location and extent of damage. In the study, a fuzzy system qualifies the changes in natural frequencies in four damage levels and the Genetic Algorithm (GA) (HOLLAND, 1975) optimizes its rule-base and membership functions. Despite being qualitative damage identification and the author used a simplified MRB (beam), the methodology was accurate.

The same authors repeat this in two other studies: *i*) using displacements measures instead natural frequencies and residual life classes instead damage levels to create a prediction model that provided the helicopter rotor blade life (PAWAR & GANGULI, 2003), and *ii*) changing the genetic fuzzy system by the Support Vector Machine (SVM) classifier. The authors were successful even in noisy situations (PAWAR & JUNG, 2007). Reddy & Ganguli (2003) also used machine learning algorithms. In this case, artificial neural networks (ANN) with modal data generated by the FEM to accurately identify damage to MRB. The authors also concluded that the first 5 mode shapes were sufficient for this.

After a few years without further studies, Gomes *et al.* (2020b) was the first to propose a methodology for identifying damage in MRB that was able to locate and quantify the damage severity. The proposed inverse method used the FEM updating associated with the Bat Optimization Algorithm (BA) (YANG & HOSSEIN, 2012) and the authors uniformly distributed 10 sensors on the blade structure and got good results.

As seen, few works were dedicated to propose SHM methodologies for identifying damage in MRB and none of them proposed a MRB sensor placement optimization (SPO) method. However, modern and efficient methodologies have been proposed to identify damage in other types of structures, including FEM updating, frequency response function, ground excitation, signal processing, new machine learning algorithms, among others. The most accurate is the FEM updating and has two fronts: *i*) the direct problem modeling, where a numerical model of the structure is made, and *ii*) the model is constantly evaluated by an optimization algorithm that minimizes an objective function composed by structural characteristics (MILAD *et al*., 2019; GOMES *et al*., 2018b; ASSIS & GOMES, 2021).

The methodology efficiency and the quality of the answers strongly depend on the optimization algorithm used (PEREIRA et al., 2021a; YANG, 2014). Consequently, many meta-heuristics have been proposed for damage identification and SPO, most are dealing with only one objective: *i*) GA (GOMES *et al*., 2018; PAWAR & GANGULI, 2003; WOEDECCKI *et al*., 2018), *ii*) Ant Colony Optimization (ACO) (BRAUN et al., 2015; MISHRA et al., 2019; YU & XU, 2011), *iii*) Particle Swarm Optimization (PSO) (CHEN & YU, 2018; KAVEH & MANIAT, 2015; QIAN *et al*., 2012), *iv*) Firefly Algorithm (FA) (PAN *et al*., 2016; ZHOU *et al*., 2014; ZHOU *et al*., 2019), *v*) Sunflower Optimization (SFO) (GOMES *et al*., 2019), *vi*) BA (GOMES *et al*., 2020b; KANG *et al*., 2015; ZENZEN *et al*., 2018), and *vii*) Wolf Algorithm (Yi *et al*., 2017), among others.

However, recent studies indicate that the use of multi-objective meta-heuristics, given their ability to evaluate several metrics at the same time, has found better results both in SPO and in damage identification (GOMES *et al*., 2018; ALKAYEM *et al*., 2017; ZHOU *et al*., 2021). Even so, the number of workers using multi-objective algorithms in SHM is uncommon. According to Pereira *et al*. (2021d), the vast majority uses the Non-sorting Genetic Algorithm II (NSGA-II) (ZHOU *et al*., 2021; ALEXANDRINO *et al*., 2020) or the Multi-objective PSO (MOPSO) (CHA & BUYUKOZTURK, 2015; ALKAYEM *et al*., 2018).

Still, being that the fundamental principle of SHM is to select the smallest possible number of measurement locations from a structure and represent the system with the highest possible accuracy (BARTHORPE & WORDEN, 2009), which are obviously conflicting objectives, there is no work in the literature considering any kind of structure that proposes a methodology to approach this. In this Chapter, MOLA will be used to propose a new SHM methodology.

Firstly, a real AS350 MRB will be experimentally tested to obtain its modal parameters. A numerical model will be elaborated in FEM and an inverse method using the constrained Lichtenberg Algorithm will find the mechanical properties that fit the numerical and experimental models. Then, will be proposed a methodology to address the SPO problem using the MOLA and Feature Selection (FS), which is an important and modern area in data mining that seeks to optimize input data series for machine learning algorithms (SHARMA & KAUR, 2021).

The multi-objective optimization problem will have as one of the objectives the number of sensors. The other objectives will be defined as one of the 7 well-known metrics of SPO in

literature: Kinetic Energy, Effective Independence, Average Driving-Point Residue, Eigenvalue Vector Product, Information Entropy, Fisher Information Matrix, and Modal Assurance Criterion. The new methodology, named Multi-objective Sensor Selection and Placement Optimization based on Lichtenberg Algorithm (MOSSPOLA) will present the sensor configurations (SC) (number and locations) and the results will be compared/analyzed for the MRB case study. Finally, a damage identification test problem will be presented considering triaxial mode shapes displacements and noise.

The major contributions of this Chapter are: *i*) to propose a multi-objective sensor placement optimization methodology considering the number of sensors as one of the objectives complementary to others 7 well-known metrics of SPO; *ii*) develop and apply feature selection techniques for SPO considering discrete MO optimization; *iii*) to apply the proposed methodology in a real aeronautical SPO case study; and *iv*) Validate all the found optimal sensor configurations in an inverse damage identification problem. The Chapter is organized as follows: Section 5.1 presents the theoretical background. Section 5.2 presents the methodology of this work. Section 5.3 brings the results and discussions, and Section 5.4 concludes the Chapter.

5.1 Theoretical Background

The concepts necessary for the understanding of this research are: *i*) damages in MRB; *ii*) modal data and damage identification; *iii*) the main metrics used to analyze modal data; *iv*) State of art about multi-objective optimization in SHM - well discussed in Chapter 2; *v*) Multi-objective Lichtenberg Algorithm - well discussed in Chapter 3; and *v*) what is feature selection and how does it relate to meta-heuristics.

5.1.1 Damage in Main Helicopter Rotor Blade

Composite materials have low weight, high strength, remarkable stiffness related to their specific mass, and a high capacity to withstand fatigue and corrosion. These reasons justify their use in MRB. However, they may have failure mechanisms due to manufacturing defects or severe conditions in flight, due to aerodynamics, temperature variation, and acceleration loads (AHMADA *et al*, 2020).

Small defects in blade fabrication, such as autoclave molding, resin transfer mold or resin film infusion, can progress severely when in operation. The main damages resulting from this are: non-uniformly positioned laminae, uneven distributed resin, missing or cut fibers, incomplete resin maturation, porosity or trapped air bubbles, signs of wear or scratches on the material, and fiber or weave undulation (HOU & ZHANG, 2012).

In operation, overloads, environmental factors or impact with foreign objects can aggravate previous manufacturing defects or give rise to new damages. Some examples are: fracture of matrix, fiber breakage, debonding, delamination, fiber waviness, and creep deformation (VOICU *et al*., 2020). The most critical and important damage is delamination, which can lead the entire structure to failure, as the material strength is proportional to the degree of delamination. This damage is the loss of stiffness in the material due to spaces formed between the adjacent layers of a laminate and is the main source of cracks in composite structures (PANTANO, 2019; LATIFI *et al*., 2015).

5.1.2 Damage Monitoring using Vibration Signals and Modal Data

Damages cause structural degradation and change natural frequencies, mode shapes, modal strain energy and damping ratios in very particular ways. Then, it is possible to identify the damage using inverse modeling and computational intelligence analyzing the output modal parameters of the system (PEREIRA *et al*., 2021a; BURGOS *et al*., 2020). The main and most used modal properties are natural frequencies and mode shapes (GOMES & GIOVANI, 2020).

Both have their advantages and drawbacks. According to Gopalakrishnan *et al*. (2011), natural frequencies have low sensitivity in determining damage location when compared to mode shapes. However, according to Worden & Friswell (2009), natural frequencies can be estimated very accurately (1% error) without a complete modal test. A single random excitation test can determine them through a basic spectral analysis.

Determining the modal properties of any structure solving the involved differential equations such as the helicopter MRB is not an easy task. Advances in computing and FEM make it possible, where the variation of the global stiffness matrix can be summarized as shown in Equation (5.1). So, the insertion of the damage in the structure, composed of N elements and nodes, is simplified. Many authors have successfully used this equation to represent delaminations in composite materials (GOMES *et al*., 2020b; GOMES *et al*., 2019):

$$\Delta K = \sum_{k=1}^{N} \alpha_K K_K \tag{5.1}$$

where α is a scalar multiplier (between 0 and 1) that modifies the original K stiffness in the k element.

The FEM works as a black box that delivers modal outputs and intelligent computational techniques can be used for data processing through formulated and appropriate objective functions.

5.1.3 Modal Metrics in Structural Health Monitoring

Most objective functions designed to be used in SPO or damage identification use modal metrics and can be maximized or minimized. Some well-known are: Kinetic Energy (KE) (HEO *et al*., 1997), Effective Independence (EfI) (YANG & LU, 2017), Average Driving-Point Residue (ADPR) (BARTHORPE & WORDEN, 2009), Eigenvalue Vector Product (EVP) (BARTHORPE & WORDEN, 2009), Information Entropy (IE) (YUEN & KUOK, 2015; YIN *et al*., 2017), Fisher Information Matrix (FIM) (YANG *et al*., 2018c; BENNER *et al*., 2017), and Modal Assurance Criterion (MAC) (JIN *et al*., 2015).

The KE metric gives a measure of the dynamic contribution of each element of FEM to each of the target mode shapes and can be calculated through Equation (5.2):

$$KE_{in} = \Phi_{in} \sum_{j} M_{ij} \Phi_{jn} \omega_n^2 \tag{5.2}$$

where Φ is the mode shape matrix, M is the mass matrix, i and j refers to the degrees of freedom and n, the n-th mode (HEO *et al*., 1997).

Efi (KAMMER, 1991) is one of the most used metric in large structures, which is an efficient unbiased estimator. Its objective is to select positions of measurements linearly independent providing high information. The covariance matrix of the estimated error can be expressed in Equation (5.3). Note that unlike KE, mass is not considered.

$$EfI = diag(\Phi \left[\Phi^T \Phi \right]^{-1} \Phi^T) = diag(QQ^T) \tag{5.3}$$

where Q is an orthonormal matrix and Φ is the mode shape matrix. This metric has a few drawbacks: *i*) it might choose sensor locations with less energy content, just like KE, what can leave sensing incomplete and bring vulnerability in noisy conditions (CAO *et al*., 2020; MEO &

ZUMPANO, 2005), and *ii*) it presented poor results under conditions of uncertainty (KAMMER, 1992).

The ADPR provides a measure of the contribution of any point to the global response. For all *N* mode shapes, the ADPR in the *i*-th DOF can be calculated using Equation (5.4).

$$ADPR_i = \sum_{i=1}^{N} \frac{\Phi_{ij}^2}{\omega_j} \tag{5.4}$$

where ω_j is the *j*-th natural frequency and Φ is the mode shape matrix.

The EVP calculates the product of the mode shapes for its locations for *N* modes to be measured: a maximum for this product is a point with optimum measurement candidate. In the *i*-th, it can be calculated by Equation (5.5):

$$EVP_i = \prod_{j=1}^{N} \left| \Phi_{ij} \right| \tag{5.5}$$

IE (JAYNES, 1979) is an efficient metric to finding the best combination of structural tests that can minimize the negative consequence of uncertainty. The metric is based on a Bayesian statistical method, where a probability density function $p(\Theta|D)$ (Equation 5.6) is used to quantify the uncertainties in the parameters Θ. The calculation is defined in Equation (5.7).

$$p(\theta \mid D) = c\left[J(\theta; D)\right]^{-(NN_0-1)/2} \pi_\theta(\theta) \tag{5.6}$$

$$H(D) = E_\theta\left[-\ln p(\theta \mid D)\right] = -\int p(\theta \mid D) \ln p(\theta \mid D) d\theta \tag{5.7}$$

where E_Θ is the mathematical expectation to Θ, D is the dynamic test data, $J(\Theta|D)$ is the fit measure between the measured and the response time histories, N_0 is the number of DOF of the structure and N is the number of sampled data. Note that, while EfI gives the relative importance of the chosen DOF, IE is related to the total maximum limit of entropy.

The FIM is the main metric used in SPO, where the optimal sensor configuration is taken as the one that maximizes the norm of the FIM and minimizes the expected Bayesian loss function involving the trace of the inverse of the FIM (GOMES *et al*., 2018). The array of sensors can be given in the form of an estimation problem with a corresponding FIM given in Equation (5.8) (KAMMER, 1991). The modal response is estimated based on the data measured by the sensors.

$$Q = \Phi_S^T W \Phi_S \tag{5.8}$$

where W is a weighting matrix and Q, when maximized, results in the minimization covariance matrix error. This results in the maximization of the signal intensity and the independence of the main directions (RAO *et al*., 2015).

MAC is a metric proposed by Allemang & Brown (1982) and used by Carne and Dohrmann (1994) in SPO. It aims to find sensor locations to ensure that all inner products between distinguishable shape vectors have relatively small cosines. It allows comparison of the different mode shapes and is defined by Equation (5.9).

$$MAC = \frac{(\Phi_i^T \Phi_J)^2}{(\Phi_i^T \Phi_i)(\Phi_j^T \Phi_J)} \tag{5.9}$$

where Φ_i and Φ_j are the *i*-th and *j*-th column vectors in matrix Φ. The matrix MAC values range between 0 and 1, where 1 indicates a high similarity between the modal vectors. So whether it is an OSP or damage identification problem, it is desired to maximize the sum of diagonal values. Note that EfI is MAC^{-1} (TAN & ZHANG, 2019).

Many studies show significant correlation and statistical equality between: *i*) EfI, KE, and FIM (LI *et al*., 2007), *ii*) MAC and IE (YI & LI, 2012), and *iii*) FIM, KE, EI, EVP and ADPR, where the authors also conclude that EfI presented the worst result (GOMES *et al*., 2018b). Table 5.1 summarizes and shows the objective functions derived from these metrics to be used in SPO or Damage Identification.

Table 5.1 – Sensor placement objective functions used in Structural Health Monitoring

Metric	Objective function
KE	$J = max(KE)$
EfI	$J = max(sum(diag(QQ^T)))$
ADPR	$J = max(ADPR)$
EVP	$J = max(EVP)$
IE	$J = min(H(D))$
FIM	$J = max\|det(Q)\|$
MAC	$J = max(diag(MAC))$

5.1.4 Feature Selection and Metaheuristics

Feature Selection (FS) is an area in data mining that aims to minimize the number of features and maximize the machine learning algorithm accuracy. Its most important approach is the wrapper-based method, which using some search strategy selects different subsets within a

dataset and seeks to select those that present the best accuracy values. Sharma & Kaur (2021) analyzed 166 articles and showed that FS methodologies using meta-heuristics have generated the best results.

In the feature selection problem, features form a vector of length equal to the number of original problem features, whose values of the selected features is 1 and those eliminated is 0. So, the optimization process is considered binary and, therefore, it is a discrete optimization. The meta-heuristics need adaptations for greater efficiency, i. e., adapt them for binary optimization.

Several algorithms and adaptations have been proposed, most of which are single objective: Dynamic Salp Swarm Algorithm (DSSA) (TUBISHAT *et al*., 2020), Improved Equlibrium Optimizer (IEO) (AHMED et al., 2021), binary Emperor Penguin Optimizer (BEPO) (DHIMAN *et al*., 2021), among others. Most of these works use a classifier to evaluate selected subsets, as k-Nearest Neighbors (KNN) or Support Vector Machine (SVM).

5.2 Numerical-Experimental Methodology

The methodology of this study is divided into three steps: *i*) numerically model an AS 350 MRB that is similar to a real one experimentally tested; *ii*) develop and apply MOSSPOLA in it; and *iii*) to apply the SC found in damage identification.

5.2.1 Numerical and Adjusted Rotor Blade

The first step of this work was the elaboration of a numerical MRB that is feasible with a real one. Two approaches could be adopted: *i*) Direct modeling: use FEM software, create a model with identical geometry to the blade, with insertion of each of the materials with exact geometry (sections of aluminum, fiberglass reinforced polyester, carbon fiber reinforced plastics, wood, and/or epoxy laminates) (AHMAD *et al*., 2020); or *ii*) inverse modeling: to create a unique blade geometry with only one material and use a search algorithm to identify the mechanical properties that make it behave like the real one.

Having a real MRB of the AS-350 helicopter, and considering that the direct method, even if perfect, cannot predict the state of the blade to be used, which is already retired and can count on aging, fatigue, and wear damage that can alter its original properties, the inverse

method becomes advantageous. Then it is necessary to find the real MRB natural frequencies to compare with those calculated by a meta-heuristic.

A test bench was made using the 1704-A Bruel & Kjaer equipment, which has its own software, see Figure 5.1. The blade is fixed by its root and is freely supported. The test was the Multiple-inputs-single-output, where well-spaced blade nodes received sinusoidal impulses of the same peak through a hammer, but only one accelerometer collected the signals. According to Avitabile (AVITABILE, 2001), this is a simple method that allows good modal understanding.

The accelerometer can measure the blade's amplitude of motion as a function of time. When the excitation impulse has its frequency close to any of the natural frequencies, the amplitude naturally increases. This analog and time domain data are acquired using photon+ device and it is filtered using anti-aliasing. Then, it is digitized using the analog-to-digital converter. Applying the Fast Fourier Transform (FFT), the Frequency Response Function (FRF) can be obtained to better interpret the natural frequencies.

So, the numerical model of the blade was created in the ANSYS® APDL software, see Figure 5.2. The blade has a total length of 4665 mm, whose aerodynamic section is 3880 mm and has a NACA0012 profile, which generated two symmetrical shells in this region. Each one has shell elements (SHELL281), being 8 nodes per element and 6 degree of freedom per node. The material used, whose mechanical properties will be investigated, is composed of 12 layers with 1.08 mm each.

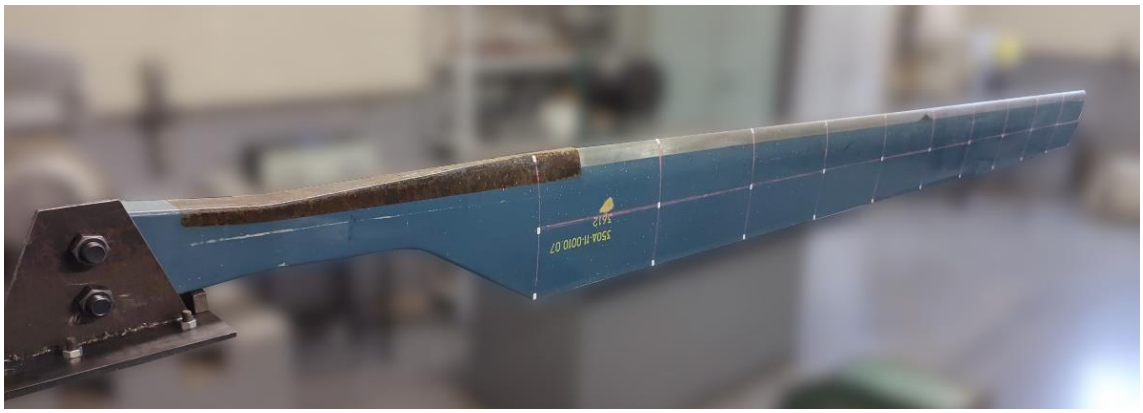

Figure 5.1 – Clamped AS 350 main rotor blade on the test bench.

Having as references the real natural frequencies, the inverse method will be performed by the LA with the parameters in Table 5.4. The optimization problem is described by Equation 5.10. When the difference is zero, the natural frequencies of the numerical and real MRB are equal. It is a minimization problem with five variables, $\vec{X} = \{ E_1 , E_2 , \nu_{12} , G_{12} , \rho \}$, being the

equivalent mechanical properties of the blade, i.e., longitudinal and transversal modulus of elasticity, Poisson's coefficient, and density.

$$\begin{aligned} &\min F(\boldsymbol{X})=\sum_i \left(\omega(\vec{\boldsymbol{X}})_i^{exp} - \omega(\vec{\boldsymbol{X}})_i^{LA}\right)^2 \\ &\textit{subject to:} \\ &70 \leq \boldsymbol{E_1} \leq 140\ GPa \\ &5 \leq \boldsymbol{E_2} \leq 10\ GPa \\ &0.2 \leq \boldsymbol{\nu_{12}} \leq 0.33 \\ &5 \leq \boldsymbol{G_{12}} \leq 10\ \ GPa \\ &1300 \leq \boldsymbol{\rho} \leq 1700\ kg/m^3 \\ &g_1(\vec{\boldsymbol{X}}) = G_{12}/E_1 > 0 \\ &g_2(\vec{\boldsymbol{X}}) = \sqrt{E_2/E_1} - |\boldsymbol{\nu_{12}}| > 0 \end{aligned} \tag{5.10}$$

where ω^{exp} and ω^{LA} are the experimental and calculated natural frequencies, respectively. The constraints g_i guarantee a solution that has a positive definite elasticity matrix (BLEDZKI, 1999).

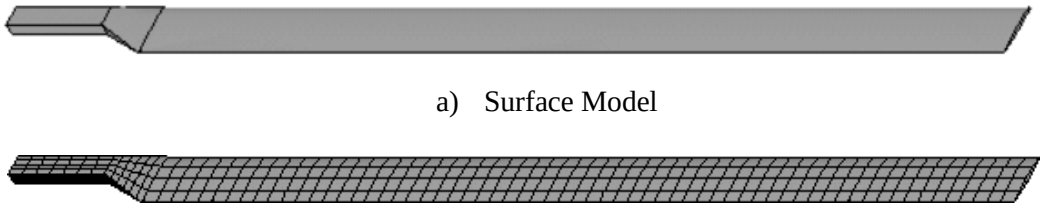

a) Surface Model

b) 2266 Nodes and 746 Elements

Figure 5.2 – Numerical model of the AS 350 main rotor blade skin.

5.2.2 Multi-objective Sensor Placement

The FEM allows evaluating the nodal displacements due to the mode shapes. Therefore, each node of any structure is a candidate point for sensor allocation. All works in Table 2.5 that use meta-heuristics in SPO elaborate an optimization problem in which the number of sensors is fixed. For each of them, a search space is defined that varies from the smallest to the last node number of the structure (upper and lower bounds). Non-overlapping and distancing constraints can be added and each Sensor Configurations (SC) found uses some SPO metric for evaluation, which could be any of those present in Table 5.1.

In this way, the SPO work even for a small structure can be exhausting and direct evaluation between the metrics and analysis of their behavior may be unfeasible, since several

SC can be found for the same metric. Still, the amount of SC found is even greater for larger structures and the amount of local minimum for a given metric can be expressive. The use of multi-objective optimization algorithms having the number of sensors as an objective not only shows how each metric can behave with the increase of the number of sensors, but it can eliminate any SC that is dominated through the Pareto dominance relationship. Thus, many SC that would be local minimum in a single-objective optimization are eliminated and a detailed discussion of the behavior of these metrics in the Pareto region can be made.

Despite ensuring an advance in SPO, this has not been done before in literature. Programming a meta-heuristic to optimize with a number of variables and evaluations in objective functions for a variable number of sensors is not an easy task. It becomes possible with the advancement of FS and multi-objective meta-heuristics. Combining both, a new methodology is proposed in this work.

5.2.2.1 Multi-objective Sensor Selection and Placement Optimization based on Lichtenberg Algorithm

The Multi-objective Sensor Selection and Placement Optimization based on Lichtenberg Algorithm (MOSSPOLA) uses MOLA to perform a SPO based on FS. Like any multi-objective meta-heuristic, MOLA is a continuous optimization algorithm that needs conflicting objectives to properly converge in the objective space, what obviously happens when using the number of sensors and any of the metrics in Table 5.1 as objectives.

MOLA will select a sensor using the value 1 and not select using 0. For this, the algorithm needs to be conditioned to work in a binary optimization. It is important to emphasize to the reader that a single round is precarious and generates poor results. Thus, there are two main groups in the literature to convert a continuous optimization algorithm to binary: *i*) general approaches, in which the operators of the algorithm are not modified, such as transfer function, great value priority, and angle modulation, and *ii*) specific approaches, in which the algorithm structure is modified, such as Boolean, set-based, or quantum binary techniques (CRAWFORD *et al*., 2017).

The most effective and easiest method is to implement a transfer function and there are two main groups: *s-shaped* and *v-shaped.* The last is considered the best because it does not force the population to take values 0 or 1 and has a higher probability of not selecting factors when associated with meta-heuristics (GHOSH *et al*., 2020).

Using a *v-shaped* transfer function, two steps are needed to put the population in a binary search space. They are represented respectively by Equations 5.11 and 5.12 (MIRJALILI & LEWIS, 2013). Each continuous element of the vector of decision variables in MOLA is an input.

$$T(\Delta x) = \left| \frac{\Delta x}{\sqrt{\Delta x^2 + 1}} \right| \tag{5.11}$$

The value generated in Equation 5.11 is used in Equation 5.12 to calculate the probability of changing each element to 0 or 1. The *rand* is a randomly generated number between 0 and 1. When $T(\Delta x)$ has a small value, the chance of inverting the element's value is also small.

$$X_{t+1} = \begin{cases} \neg X_t, rand < T(\Delta x_{t+1}) \\ X_t, rand \geq T(\Delta x_{t+1}) \end{cases} \tag{5.12}$$

The FEM identifies the node position through the number assigned to it, which generates a vector of candidate sensors equal to the number of nodes *n*, i.e., $\overrightarrow{S_c} = \{1, \ldots, n\}$. In the same way, the MOLA generates another binary vector of the same length ($\overrightarrow{B}$), which through Equation 5.13 generates the selected sensors vector ($\overrightarrow{S_s}$):

$$\overrightarrow{S_S} = \overrightarrow{S_C} * \overrightarrow{B^T} \tag{5.13}$$

For each *Pop* of each N_{iter}, a vector $\overrightarrow{S_s}$ is generated and evaluated in the two objective functions: sum of the number of sensors and in the objective function related to the metric *M*, *J(M)*, which can be any one of Table 5.1. Then a solution is generated in the objective space and through the Pareto dominance relationship, dominated solutions are excluded. That is, for a fixed number of sensors, any solution generated with worse metric values is excluded, remaining the smallest. Likewise, considering a fixed metric value, any generated solution that has a greater number of sensors is eliminated. Throughout all iterations, the best solutions are stored and make up the Pareto front. The optimization problem is expressed in Equation 5.14. Note that in this methodology it is impossible to have sensors overlapping.

$$\begin{aligned} & F(\overrightarrow{S_s}) = \left\{ \min(length(\overrightarrow{S_s}) ; \max(J\left(M(\overrightarrow{S_s})\right) \right\} \\ & \textit{where:} \\ & \overrightarrow{S_S} = \overrightarrow{S_C} * \overrightarrow{B^T} \end{aligned} \tag{5.14}$$

$$\overrightarrow{S_C} = \{1, ..., n\}$$
$$\vec{B} = \{a_1, ..., a_n\}$$

where each a_i is obtained using Equations 5.11 and 5.12 through the continuous x values between 0 and 1 calculated by MOLA. More objectives could be considered at the same time; however, it is desired to discuss and compare each of the metrics in the results.

5.2.2.2 Main Rotor Blade case study

For application in the MRB, some simplifications can be adopted in order to reduce the dimensionality of the problem. The larger the search space for any meta-heuristic, the greater the optimization challenge. Simplifications and, consequently, better answers can be obtained by decreasing the number of variables or narrowing upper and lower bounds (YANG, 2014).

In MRB, there are 2266 nodes as shown in Figure 5.2(b). As it is a relatively complex structure, there are regions of the structure in the FEM where there is no logical sequence for enumerating the nodes. Furthermore, the developed MRB model generated two symmetrical shells in relation to the NACA0012 profile. Thus, for each node in the upper shell, there is a corresponding node in the lower shell. For the SPO and damage identification problem, this difference does not matter, but for the meta-heuristic, it doubles its dimensionality.

Furthermore, even considering only the upper shell, not all nodes need to be evaluated. 34 well-spaced and distributed FEM MRB nodes were chosen to compose $\overrightarrow{S_C}$. They are represented in Figure 5.3. In this way, this vectors no longer starts at 1 and goes up to the number of nodes, but has the numbers of the selected nodes.

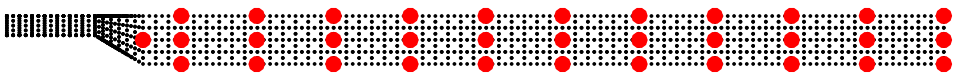

Figure 5.3 - Candidate positions (design space) for the sensor placement optimization.

With $\overrightarrow{S_C}$ defined, MOLA can run the optimization problem of Equation 5.14 for each of the 7 metrics in Table 5.1. This results in 7 optimization problems. Another consideration in this work is in relation to the displacements of these nodes. The FEM provides it in the directions *x*, *y*, and *z*, however, as will be shown in the results, the mode shapes of the MRB promote triaxial movements. So, in this work, the triaxial displacement (ΔS) for each node will be considered and is calculated by Equation 5.15.

$$\Delta S = \sqrt{\Delta x^2 + \Delta y^2 + \Delta z^2} \tag{5.15}$$

5.2.3 Damage Identification

After determining the optimal SC, some will be applied to delamination identification for testing. As stated in Section 1 of this chapter, it is one of the most serious damage in composites and can be modeled through Equation 5.1 in FEM. Using this, a selected element in MRB suffers a defined stiffness reduction. Thus, there are two design variables involved, $\vec{x} = (N_e, \alpha)$, where N_e is the element number and α is the damage rate. Note that the stiffness reduction is $\beta = 1 - \alpha$.

The LA will be chosen to perform the inverse optimization problem associated with FEM updating. The Equation 5.16 brings the objective function used and the optimization problem (PEREIRA *et al.*, 2021a). Note that the mode shapes are used in the position of the sensors found.

$$\begin{aligned} &\min\ J_\Phi = \sum_{i=1}^{n} \sqrt{\left(1 - \frac{\Phi_{i,s}^{LA}}{\Phi_{i,s}^{real}}\right)^2} \\ &\textit{subject to:} \\ &1 \leq \boldsymbol{N_e} \leq 358 \\ &0 \leq \boldsymbol{\alpha} \leq 1 \end{aligned} \tag{5.16}$$

where $\Phi_{i,s}^{LA}$ are the nodal displacements obtained by FEM and LA to the mode shape *i* and $\Phi_{i,s}^{real}$ are the known mode shapes with known damage, which could be collected directly in the MRB or in this case, it will be provided by a direct method. The null difference indicates that the mode shapes are the same and so, the damage is identified. Examples of MRB damage in root, central and tip sections can be seen in Figure 5.4. The methodology of this Chapter is summarized in Figure 5.5.

. After initial simulations for some SC, additional simulations considering noise will be done. Obviously, a helicopter blade is not a static structure and is susceptible to this. The noise will be ramdom and modeled through Equation 5.17 (GANGULI, 2001):

$$\Delta\phi_{noise} = \Delta\phi(1 + ua) \tag{5.17}$$

where *a* is a noise percentage and *u* is a normal random number known as white Gaussian noise *N(0,1)*.

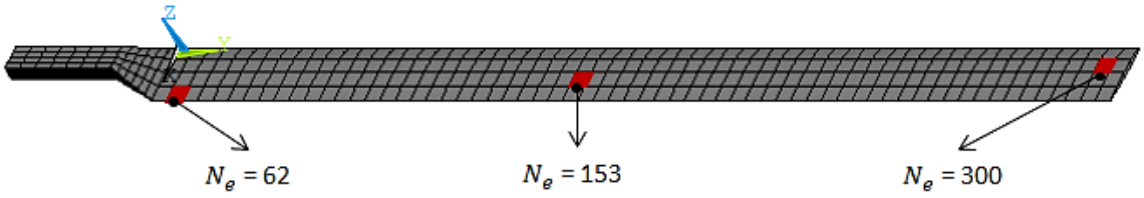

Figure 5.4 – Damage sites in three different scenarios: root, central and tip sections**.**

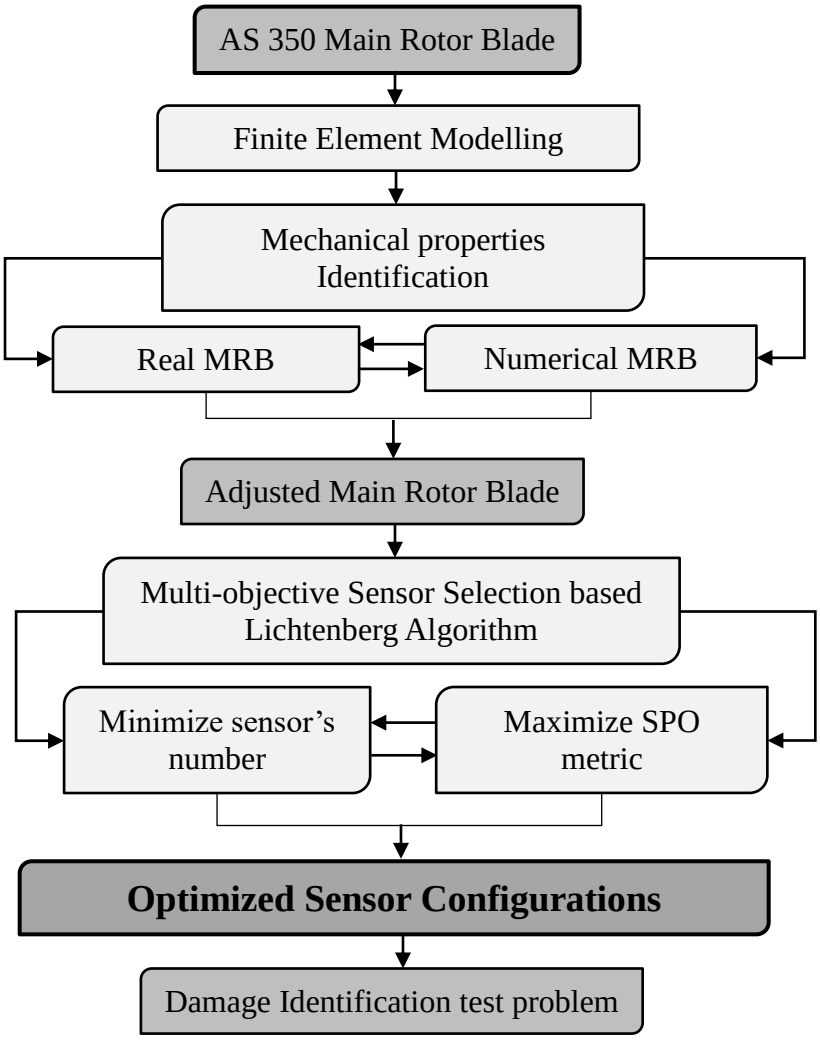

Figure 5.5 – General Methodology Flowchart

5.3 Results and Discussions

5.3.1 Adjusted Numerical Model of Main Rotor Blade

The first step to properly adjust the numerical model was to define the range and which natural frequencies to use. Tamer *et al*. (2021) studied vibrations in real helicopters and concluded that the excitation frequencies found in the MRB under normal conditions range from 20 to 25 Hz. In adverse and dangerous situations, it can reach 50 Hz. Therefore, in the bench test of Figure 5.1, it was aimed to find the natural frequencies in the range from 0 to 50 Hz.

The FRF for different excitation points was found and clearly presents the MRB resonant frequencies. Six experimental natural frequencies were found and were confirmed by the phase component of the FRF which presented a delta of 180°. See Figure 5.6. Reddy & Ganguli (2003) recommended using at least 5 modes for reliable damage identification and considering the operating range of the helicopter, these six natural frequencies will be used.

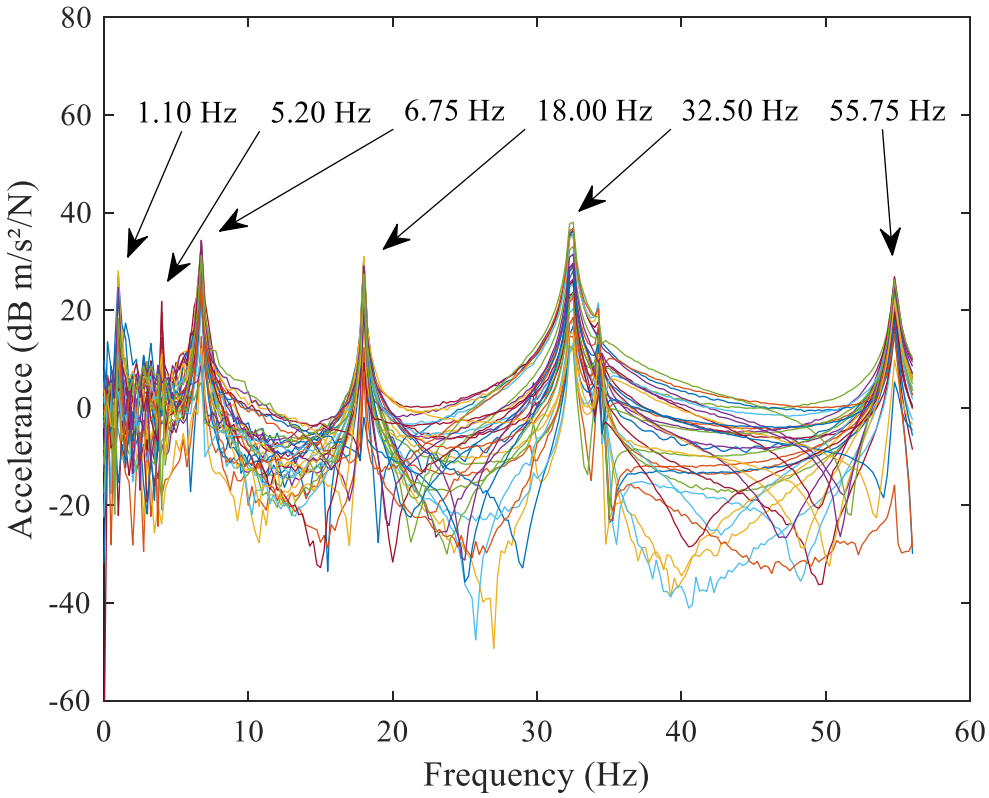

Figure 5.6 – Experimental AS 350 helicopter rotor blade FRF (accelerance).

So, the optimization problem of Equation 5.10 is performed by LA using the parameters of Table 5.2.

Table 5.2 – Recommended MOLA control parameters

R_c	N_p	S	ref	Pop	N_{iter}
200	10^6	1	0.4	80	100

After 5 simulations, the equivalent mechanical properties that make the natural frequencies of the numerical model get closer to the real are in Table 5.3.

Table 5.3 – Numerical MRB Mechanical Properties

E_1 (GPa)	E_2 (GPa)	v_{12}	G_{12} (GPa)	ρ (kg/m^3)
134.7518	9.0011	0.2642	7.3202	1491.10

By inserting them into the numerical MRB, the numerical natural frequencies ($\omega_{numerical}$) can be calculated. It is important to emphasize that in the range from 0 to 56 Hz, there are at least 10 MRB natural frequencies in experimental studies, as well as those calculated by the FEM in this study. Some of them are close and could be superimposed in Figure 5.6. For this reason, the authors chose the first 6 natural frequencies to be used in this study and they are represented in Figure 5.7. These mode shapes are named as: a) 1st Flapping; b) 1st Lagging; c) 2nd Flapping; d) 3rd Flapping; e) 1st Torsional; and f) 5th Flapping. The results are consistent with the literature (REDDY & GANGULI, 2003; SANTOS *et al.*, 2016; MUGNAINI *et al.*, 2022).

Table 5.4 shows the experimental natural frequencies obtained and the MRB numerical natural frequencies adjusted by the LA after optimization. Then it calculates the difference (Diff) between them. With the exception of 1st Lagging mode shape, that has a major displacement in the *x* direction, the error was less than 1% for all others. A small difference happens because the algorithm had to meet six natural frequencies at the same time. It is important to note that in none of these natural frequencies is damage present.

Table 5.4 – Natural Frequencies Comparison after adjustment

Mode	ω_{exp} (Hz)	$\omega_{numerical}$ (Hz)	**Diff (%)**
# 1	1.10	1.10	0.00
# 2	5.20	5.48	5.38
# 3	6.75	6.69	-0.89
# 4	18.00	17.84	-0.89
# 5	32.50	32.50	0.00
# 6	55.75	55.73	-0.05

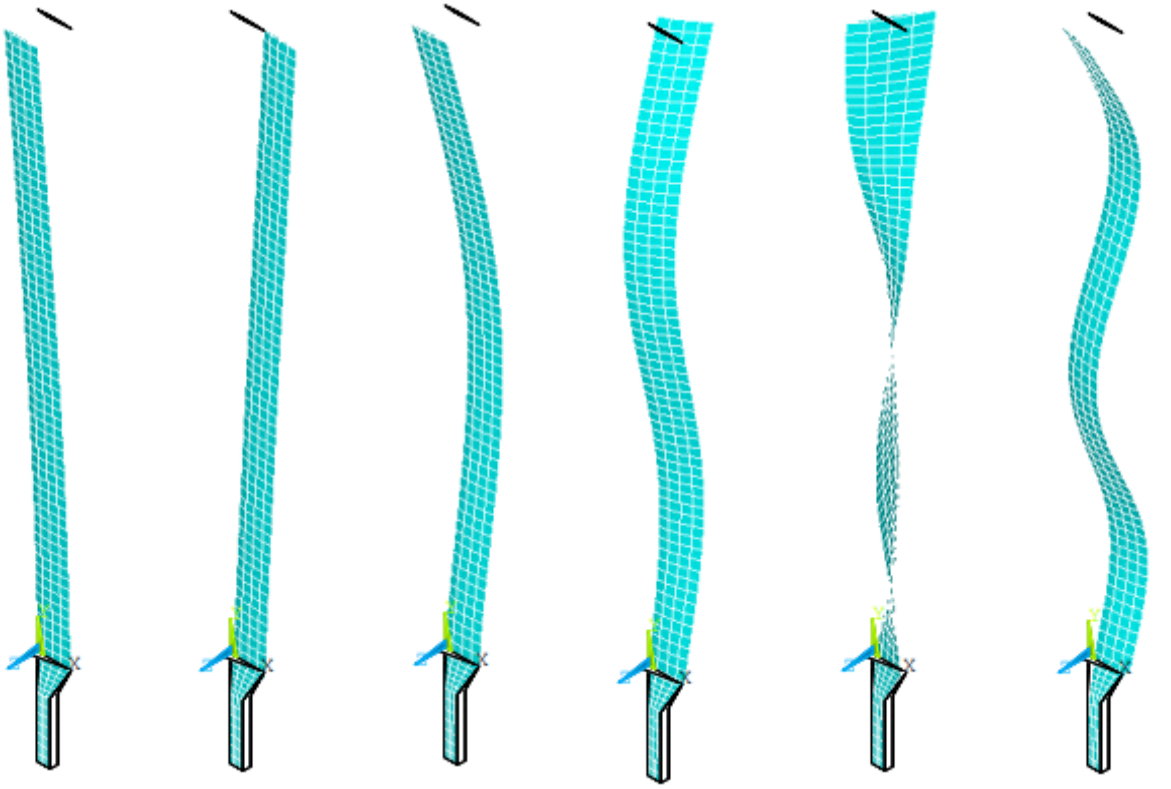

a) 1.10 Hz b) 5.48 Hz c) 6.69 Hz d) 17.84 Hz e) 32.50 Hz f) 55.73 Hz

Figure 5.7 – Numerical MRB natural frequencies and Mode Shapes

5.3.2 Sensor Placement Optimization Results

With a feasible numerical MRB, MOSSPOLA can be applied to identify sensor configurations using Equation 5.14, the MOLA Parameters in Table 5.2, and considering the first six mode shapes from Figure 5.7. There are seven bi-objective optimization problems named as the metric that is being evaluated: KE, EfI, ADPR, EVP, IE, FIM, and MAC.

All Pareto fronts are in Figure 5.8. It is possible to see that are solutions for sensor placement from one to all the 34 candidate sensors for all the seven considered metrics. Also, whatever the metric, with the increase in the number of sensors, the level of information acquired from the MRB always increases.

The results show two PF families: linear and convex. Although the ranges of metric values are different, it is possible to observe that the KE, EfI, IE, FIM, and MAC metrics have linear PF. Hence, in the Pareto optimal region, the amount of information collected in the structure grows linearly with the addition of sensors and it would even be possible to propose first-degree equation models. This fact suggests a strong correlation between these metrics,

which has already been observed in the literature: *i*) between EfI, KE, and FIM (GOMES *et al*., 2018b; LI *et al*., 2007), and *ii*) between MAC and IE (YI & LI, 2012).

The other series is those metrics that form a convex PF when related to the number of sensors: ADPR and EVP. Although there is this correlation between them, it is possible to observe that for less than 5 sensors, the EVP metric is quite sensitive with the addition of them. Both no longer have a significant improvement in metric value above 20 sensors for ADPR and above 10 for EVP. Sensor numbers that also determine the boundaries values that these metrics grow rapidly with a linear increase in the number of sensors.

These PF families can be compared with each other using a Pareto front comparison metric called Hypervolume (HV). This metric uses a reference vector *r* to calculate the space between it and the non-dominated solutions in PF. In a normalized objective space, *r* is a unit vector with number of objectives length. The higher the HV, the more convergent and coverage is the PF at the same time (KUMAR *et al*., 2021). The results of mean after 10 independent runs for all metrics are in Table 5.5. Obviously convex Pareto fronts have higher HV, so two series were created.

Although all metrics have found solutions, the best metrics are KE and EVP, as they presented the highest HV within their series. That is, they managed to have the greatest convergence and coverage. The EfI had the worst HV value in linear PF, which already had the performance of its sensor configurations criticized (GOMES *et al*., 2018b). The fact that solutions exist for any number of sensors confirms MOLA's ability to solve the sensor selection problem.

Table 5.5 – Average obtained Hypervolume values in MO.

Metric	HV
Linear Pareto Fronts	
KE	**0.655**
EfI	0.567
IE	0.613
FIM	0.624
MAC	0.574
Convex Pareto Front	
ADPR	0.723
EVP	**0.853**

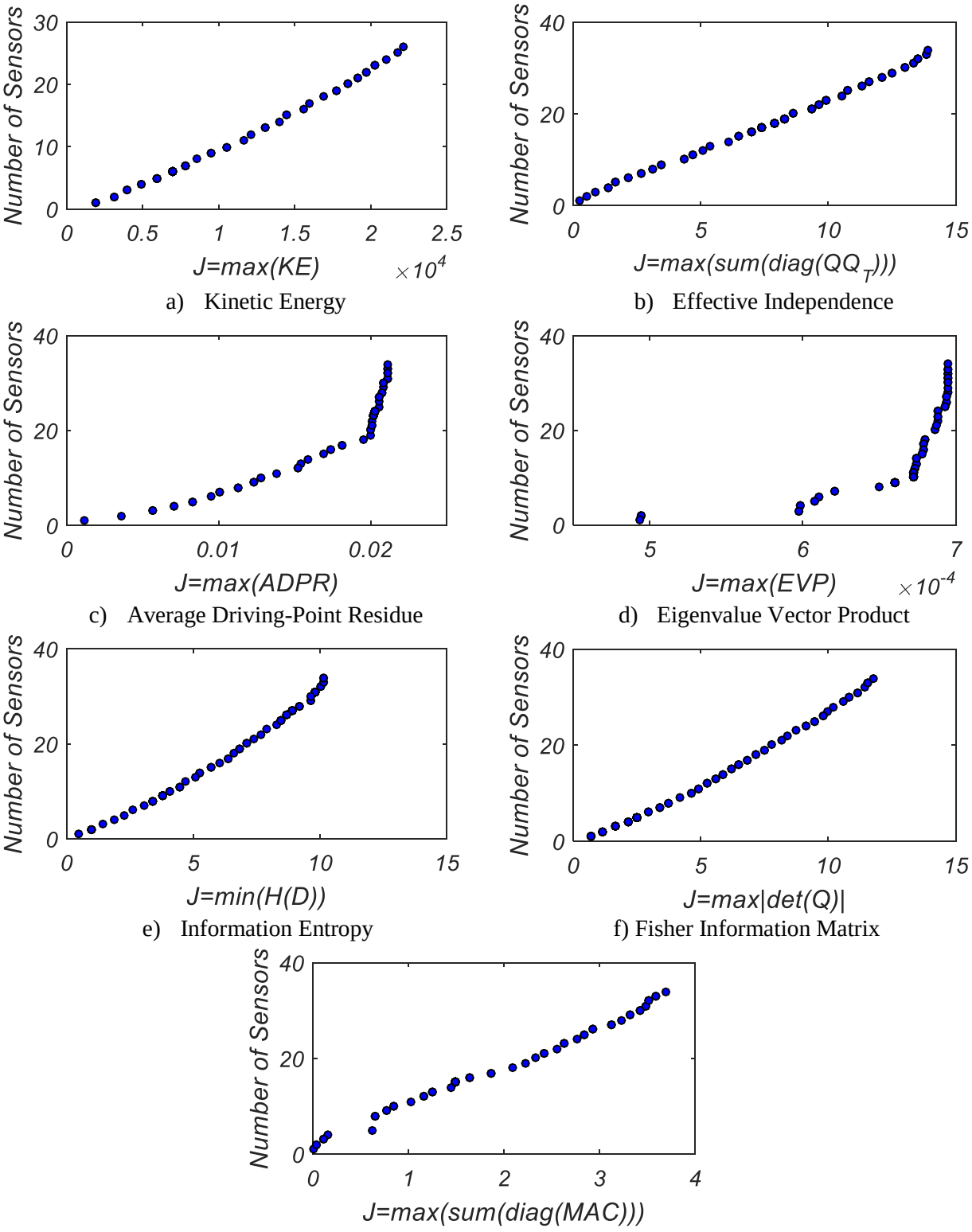

a) Kinetic Energy

b) Effective Independence

c) Average Driving-Point Residue

d) Eigenvalue Vector Product

e) Information Entropy

f) Fisher Information Matrix

g) Modal Assurance Criterion

Figure 5.8 - Behavior of SPO metrics in relation to the number of sensors in the Pareto front for a helicopter blade

However, these discussions are concerned in analyzing the metrics behavior in relation to sensors number, i. e., considering just PF. The solutions found by all metrics for 6, 8 and 10 sensors are in Figures 5.9, 5.10, and 5.11, respectively. Six sensors were chosen as the minimum number because it is equal to the mode shapes number used in this work (Figure 5.7). The same will be applied in the damage identification. A common but not necessary recommendation found in the literature. Ten sensors are considered the maximum sensors number because in a study without SPO, it already showed good results for MRB damage identification (REDDY & GANGULI, 2003; GOMES *et al*., 2020b).

In general terms, can be seen in the 3 Figures that there was no configuration repetition for any metric, given the size and complexity of the MRB. Still, the only place that always has at least one sensor is at the MRB tip, given that according to Figure 5.7, it is the region with the greatest nodal displacement for all mode shapes. Right behind comes the central region that has significant displacements after the second mode shape.

Considering 6 sensors (Figure 5.9), the IE and EfI metrics had the worst distribution of sensors along the blade, allocating more than half of the sensors in the tip section. Few metrics allocated sensors in the roots section, which is expected to have less nodal displacement. Therefore, IE and MAC did not allocate any sensors in this region. Equally important, the EfI metric was the only one that did not allocate points in the dynamic central region, which proves the disadvantage of this metric in prefer to select low signal strength points. The metrics that had the best distribution were KE, EVP and FIM. Perhaps it is no coincidence that they have the best HV values in Table 5.5.

Increasing to 8 sensors (Figure 5.10), the sensors offer gets bigger and it is possible to notice smaller differences. However, IE and FIM allocate most of the sensors between the center and the tip of the MRB. KE, EfI, and MAC have a similar and more uniform sensor distribution along the blade. ADPR and EVP also allocate the sensors evenly and similarly to each other, however the EVP is more attracted to the blade tip. Here, can be seen a metrics grouping similar to the PF series in Figure 5.8.

As for 10 sensors, once again the IE makes a bad distribution of the sensors, having almost all of them at the blade tip, being accompanied by the ADPR and the MAC that allocate more sensors in the central and tip section blade. KE, EfI, EVP and FIM make a more uniform allocation of sensors, in which once again the sensor configurations of KE and EfI are similar. Considering only the sensor configurations for all metrics and sensor numbers, only KE and EVP

did not make a bad sensor distribution. Still, they were the only ones to have at least one sensor in each of the blade sections: root, central ant tip. Even knowing that the largest nodal displacements are in the central and tip part, may be welcome to have at least one sensor in the root section to better diagnose possible damage in this section.

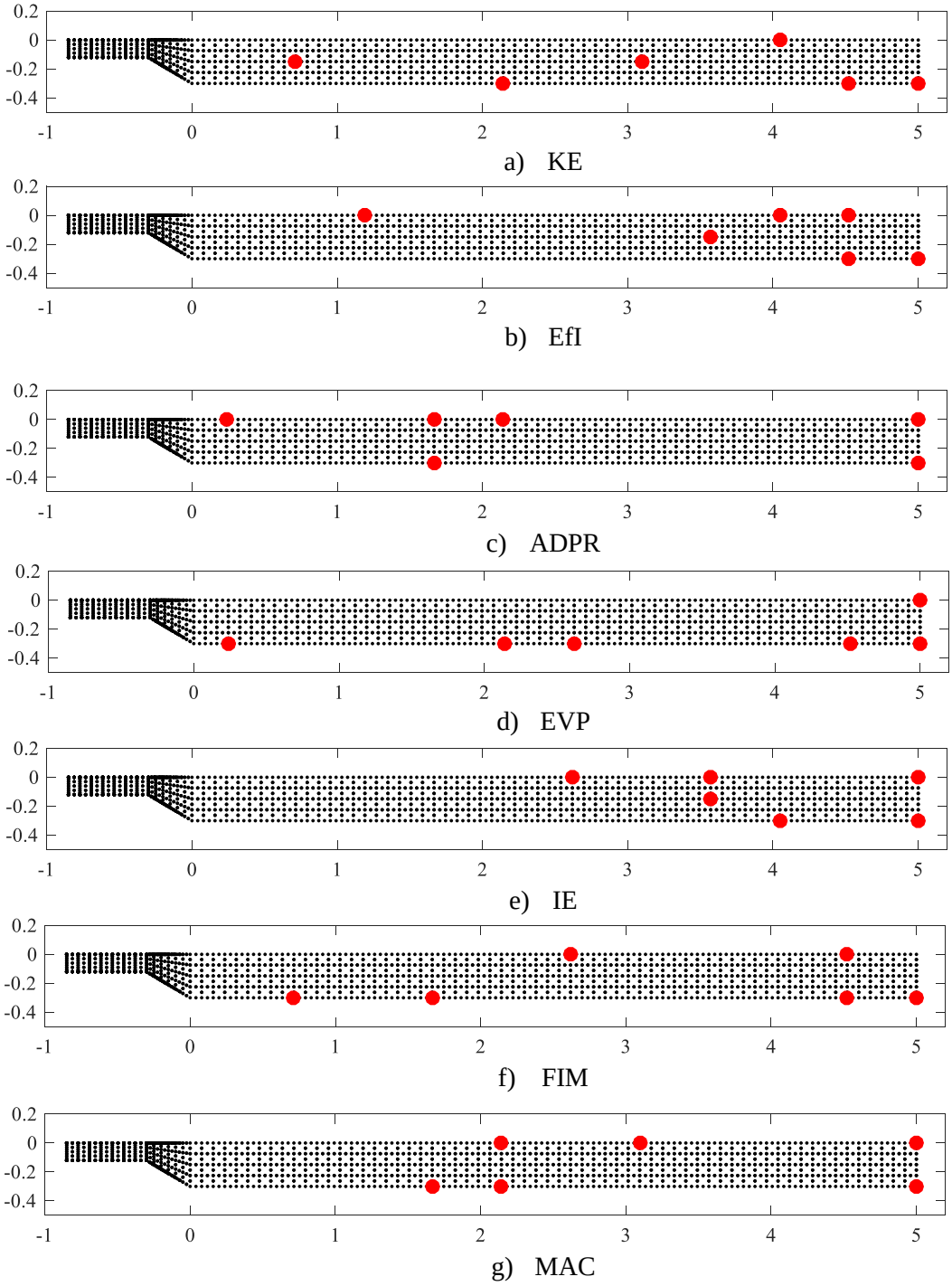

Figure 5.9 – Best Configurations for six sensors considering different SPO metrics.

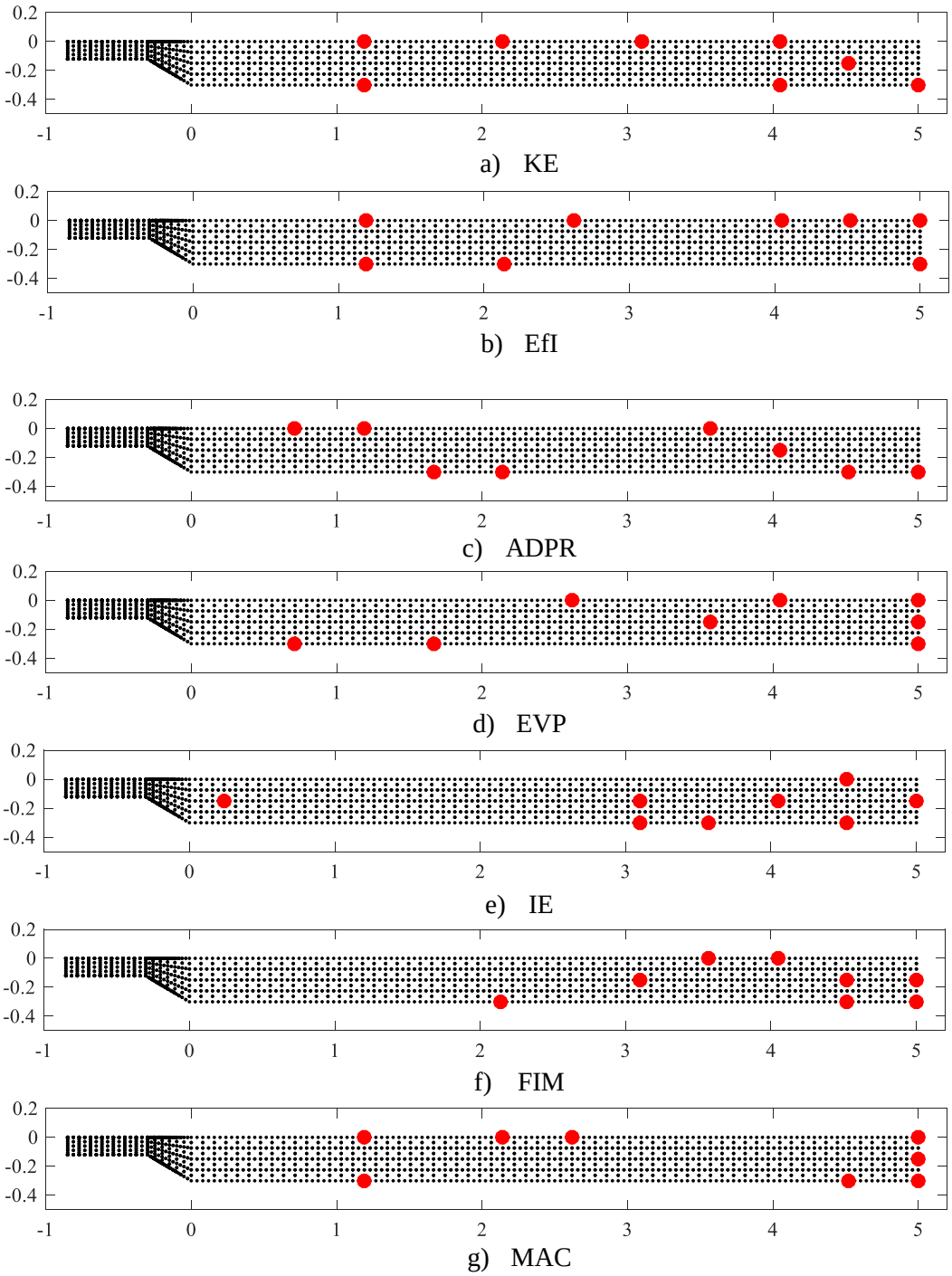

Figure 5.10 – Best Configurations for eight sensors considering different SPO metrics.

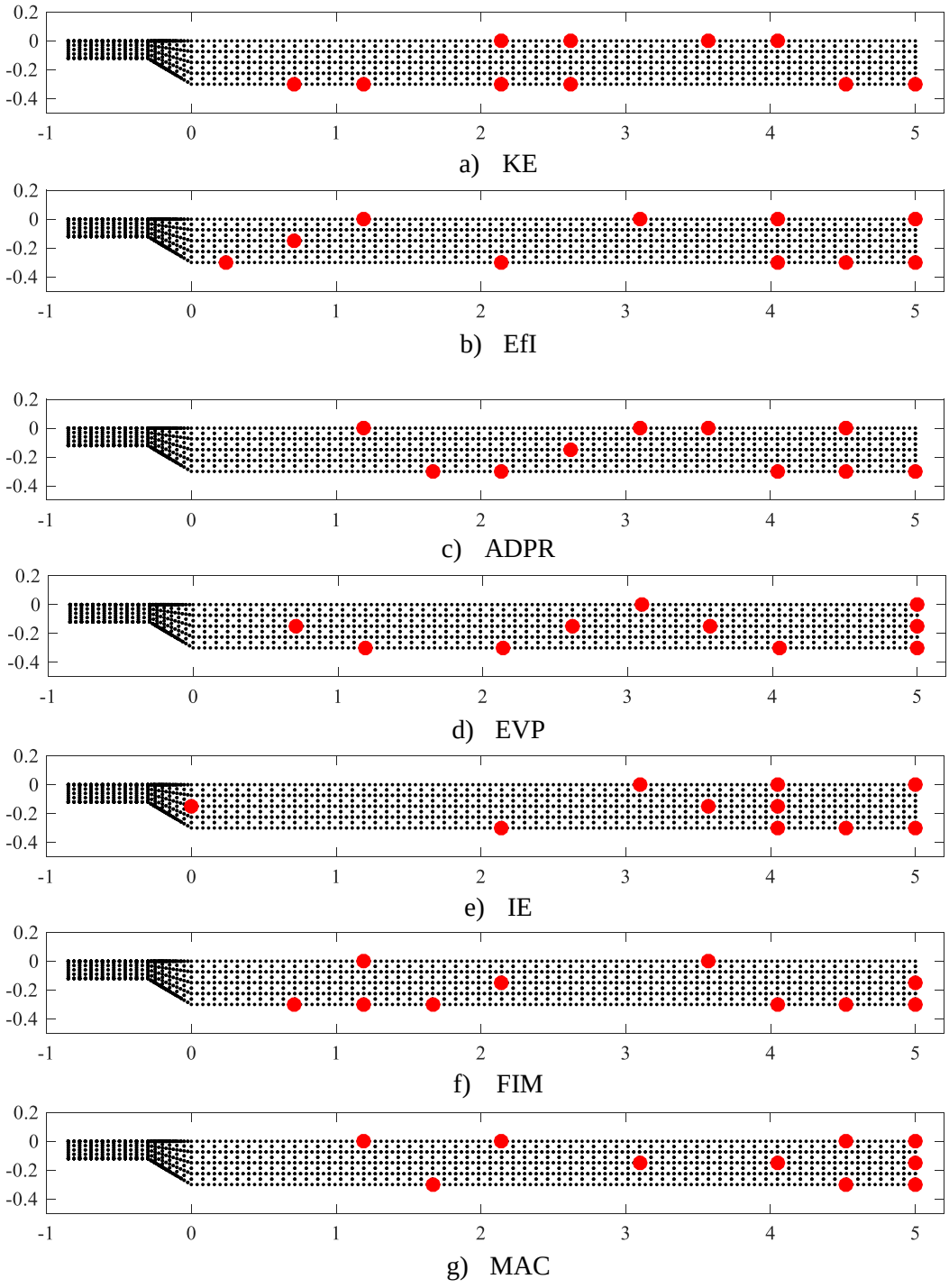

Figure 5.11 – Best Configurations for ten sensors considering different SPO metrics.

Figure 5.12 shows how the distribution of sensors for these metrics varies, starting from 1 to 34 sensors. The first observation is that for a single sensor, both metrics select the greatest nodal displacement point for the six considered mode shapes. As the sensors number increases, both metrics seek a better sensors distribution, being the EVP metric that always has the largest

amplitude. However, this metric also tends to place the maximum sensors number at the blade tip, which decreases the sensors density other regions.

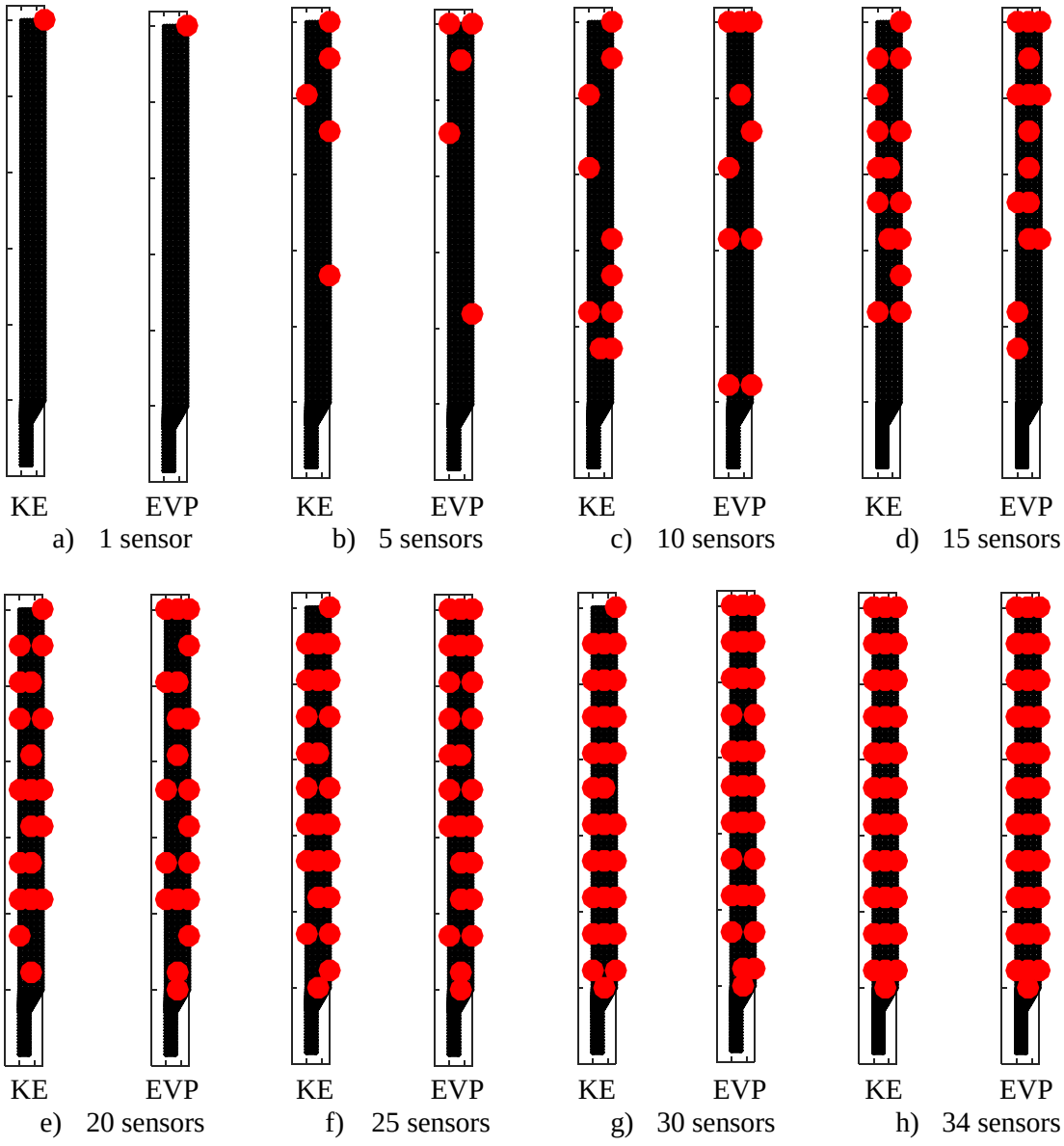

Figure 5.12 – Sensor distribution variation as sensor availability increases for the higher HV metrics

A confluence between better sensor distribution and higher HV is evidenced, which was not expected, as it is the first time in the literature that these metrics are compared using multi-objective optimization. The EVP has a higher HV value due to its PF nature, and it is not correct to say that it is better than KE, which has another PF form. Still, Figure 5.12 is unable to answer which of these metrics might be better for sensing. Thus, both will be applied in damage identification for final comparison.

5.3.3 Damage Identification using Optimal Sensor Configuration

Being the smallest number of sensors needed in the structure equal to the number of mode shapes being used, which in this work are 6 (Figure 5.7), for comparison of KE and EVP, damage in the central region of the blade will be considered with 10 and 6 sensors (Figures 5.10a, 5.10d, 5.8a, and 5.8d), without noise. Then, 3% will be added through Equation 5.17.

The damage identification will be performed by LA with the parameters in Table 5.2 and the optimization problem defined in Equation 5.16. Five simulations will be considered for each case. The results are in Table 5.6 and the convergence graphs for the element number (N_e) and the damage rate (α) are in Figure 5.13.

Table 5.6 – Delamination Identification considering the damage scenario N_e = 153 and α = 0.1

	KE 0% Noise 10 Sensors		**EVP** 0% Noise 10 sensors		**KE** 0% Noise 6 Sensors		**EVP** 0% Noise 6 sensors		**KE** 3% Noise 6 Sensors		**EVP** 3% Noise 6 sensors	
Run	N_e	α	N_e	α	N_e	α	N_e	α	N_e	α	N_e	α
# 1	153	0.1000	153	0.1000	153	0.1001	153	0.0992	153	0.1032	153	0.1328
# 2	153	0.1001	153	0.1000	153	0.0999	154	0.1335	153	0.1103	157	0.0804
# 3	153	0.1000	153	0.1000	153	0.1000	153	0.0999	153	0.0896	153	0.1403
# 4	153	0.1000	153	0.1000	153	0.0999	153	0.1000	153	0.1226	154	0.1391
# 5	153	0.1000	153	0.1001	153	0.1000	153	0.0999	153	0.0911	149	0.1234
Avg.	**153**	**0.1000**	**153**	**0.1000**	**153**	**0.1000**	**153.2**	**0.1056**	**153**	**0.1034**	**153.2**	**0.1232**
SD	**0**	**0**	**0**	**0**	**0**	**0**	**0.5**	**0.0151**	**0**	**0.0138**	**2.86**	**0.0248**
Error(%)	**0**	**0**	**0**	**0**	**0**	**0**	**0.13**	**5.6**	**0**	**3.4%**	**0.13**	**23.2%**

With 10 sensors, both metrics found sensor configurations 100% accurate in identifying the location and damage severity. This also happened for the KE metric for 6 sensors. For the EVP, the use of the minimum number of sensors brought an error of 0.13% to determine the location and 5.6% to determine the severity. With the addition of noise, the KE metric continues to be 100% accurate in locating damage, but has an error of only 3.4% in identifying the severity. The EVP metric presents an error of 0.13% in the location identification and 23.2% in the severity quantization. Therefore, the KE metric demonstrates more accuracy and consistency than the EVP, having in all cases lower standardize deviation.

Despite being plotted with only one run, the graphs in Figure 5.13 confirm Table 5.6. Regarding the damage rate, regardless of the metric, the exact value is not reached when noise is present. For damage location, only the EVP metric with noise misses the exact location. It is still

possible to observe that the LA using the KE metric for 6 and 10 sensors, with or without noise, finds the damage location with up to 10 iterations.

To better validate the KE six sensors metric distribution, damages will be simulated in the root and tip sections, in addition to the central section in Table 5.6. See these damages in Figure 5.4. The results also consider 3% noise and are in Table 5.7.

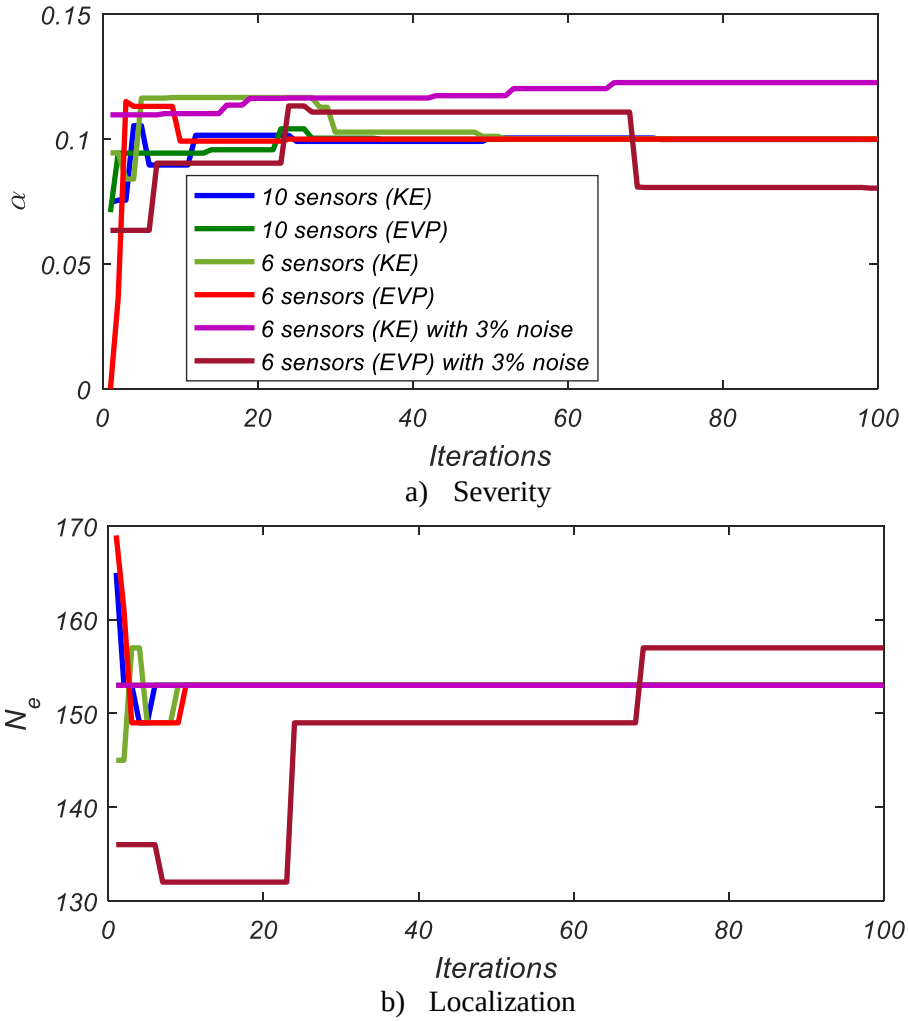

a) Severity

b) Localization

Figure 5.13 – Convergence curves for the inverse damage identification problem

Damage location identification continues to be accurately found for all simulations and blade sections. However, there is a greater error in the severity identification when the damage is in tip section (50.6%) and smaller when it is in root section (1.3%), when compared to the damage in the central region. This shows that the change in the modal properties of the blade is greater the closer the damage is to the root section.

Table 5.7 – Delamination Identification results for the root and tip sections using KE

	Root section		**Tip section**	
	N_e	α	N_e	α
Target	62	0.1	300	0.1
# 1	62	0.0922	300	0.1532
# 2	62	0.1021	300	0.1226
# 3	62	0.0985	300	0.1801
# 4	62	0.1131	300	0.1206
# 5	62	0.1005	300	0.1767
Avg.	**62**	**0.1013**	**300**	**0.1506**
SD	**0**	**0.0076**	**0**	**0.0285**
Error (%)	**0**	**1.3**	**0**	**50.6**

5.4 Chapter Conclusion

This Chapter proposed an innovative Structural Health Monitoring methodology for optimal positioning of sensors in an AS350 helicopter main rotor blade considering the experimental modal responses, feature selection techniques and the Multi-objective Lichtenberg optimization Algorithm. With the number of sensors as one objective to be minimized, the 7 well-known metrics in the literature composed a bi-objective problem, where non-dominated solutions in different Pareto were obtained, evaluated and discussed.

First, an inverse problem was able to identify the mechanical properties that adjusted the real and numerical model with a 5.38% error for the second natural frequency and less than 1% for the other five. Then, the Multi-objective Sensor Selection and Placement Optimization based Lichtenberg Algorithm found two families of Pareto fronts: linear and convex. It was not only possible to find a correlation between the metrics, but also to associate those that provided a better sensor distribution with a higher Hypervolume value. The metrics Kinetic Energy and Eigenvalue Product were the best from your families and 10 and 6 sensor configurations from both were selected for delamination identification in the central section blade. With 10 sensors and no noise, both were 100% accurate in identifying damage. Just like KE for 6 sensors. However, the EVP metric has a 0.13% error when identifying the position and 5.6% when quantifying the severity. With the addition of 3% noise, the KE metric continued to hit the exact position of the damage, but had a 3.4% error when quantifying the severity. In the same situation, EVP presented an error of 0.13% for locating and 23.2% for quantifying the damage severity. Six sensors KE metric distribution proved to be more accurate and consistent. So, it was

tested in identifying damage in the root and tip sections, where it continued to hit the exact damage location, but had more difficulty in finding the severity as the damage moved away from the root section (1.3, 3.4, and 50.6% for the root, central and tip sections, respectively).

MOSSPOLA not only found the sensor configuration for the helicopter blade that allowed accurate damage identification in noise situations, but also found sensor configurations for each metric and for each number of sensors, proving to be an algorithm capable of solving the basic problem of Structural Health Monitoring. Finally, the methodology proposed and applied in this study can be reproduced in any other type of mechanical, civil, naval or aerospace structure.

(Intentionally left Blank)

Chapter 6

General Conclusions

The current state of the art in multi-objective optimization shows a trend towards using meta-heuristics, the development of new algorithms, and the use of *a posteriori* decision-making techniques to solve complex engineering problems, where the decision maker tries to come up with all possible optimal solutions to the problem before choosing the best one. This tendency was confirmed in this study via the literature review that considered recent studies on the multi-objective optimization of complex problems, and discussed the drawbacks of deterministic, enumerative, stochastic algorithms, and *a priori* and *interactive* decision-making techniques.

Although evolutionary and swarm-based algorithms are currently the most used algorithms in the literature (mainly NSGA-II and MOPSO), these algorithms are being challenged by new and more powerful meta-heuristics with more appropriate routines for specific problems, such as the Multi-objective Grey Wolf Optimizer. The best metaheuristic for a specific problem is the one that delivers the best convergence, coverage, at the lowest possible computational cost.

Supported by this trend and in the best knowledge of the authors, the first hybrid multi-objective metaheuristic in literature, the first inspired by the physical phenomenon of radial intra-cloud lightning and Lichtenberg figures and the first multi-objective metaheuristic registered in Brazil was created.

The Multi-objective Lichtenberg Algorithm was compared with six other metaheuristics in the ZDT and CEC 2009 test suites. The IGD, SP, and MS were used to measure the convergence and coverage of the results. The MOLA proved to be a promising algorithm, resulting in the best mean MS value for all 13 test functions used, with the best mean IGD value at 6, and came in second in other tests, still showing competitive SP values. Among all the compared algorithms, MOLA was the one that had more times the best average values of IGD and MS, outperformed the most used algorithms in the literature: NSGA-II, MOPSO, MOEA/D, and the modern and powerful MOGWO and MOGOA. Visually, the MOLA found many non-dominated-solutions, with great distance between extreme solutions (high MS). Still, analyzing the boxplot of the results, this algorithm proved to be very consistent. In the three real-world constrained engineering problems, the algorithm found non-dominated solutions that practically overlapped the real ones. Well tested, the algorithm was then applied to two complex engineering problems where the use of methods that are based on gradients or that require explicit equations could not be applied.

The first was the deep multi-objective optimization of the CFRP isogrid tube considering three cases for comparison with the literature: torsion, compression, and modal performance. The optimizations are considered using the LA-FEM and LA-RSM methodologies. The first methodology revealed part of the real nature of the Pareto fronts for this type of problem for the first time in literature and allowed the evaluation of regions where the application of the response surface methodology is successful or not.

Even with the same search spaces, this methodology was able to find a range of non-dominated solutions with higher critical lambdas and natural frequencies. Design variables were found with significant improvement compared to the most recent study in the literature. In the case of torsion, it allowed a mass reduction by 48.09%, an increase in the critical lambda of buckling by 2.16%, and a reduction in Tsai-Wu by 90.90%. For Compression, mass reduction by 45.69%, critical lambda reduction by 18.40%, and Tsai-Wu reduction by 68.67%. For the Modal Case, it allowed an increase of up to 52.57% in natural frequency for an increase of only 12.8% in mass. These design variables allowed the identification of a safe and lightweight isogrid tube.

The second complex application consisted of the proposition of an innovative Structural Health Monitoring methodology for optimal positioning of sensors in an AS350 helicopter main rotor blade considering the experimental modal responses, feature selection techniques and the Multi-objective Lichtenberg optimization Algorithm. With the number of sensors as one

objective to be minimized, the 7 well-known metrics in the literature composed a bi-objective problem, where non-dominated solutions in different Pareto fronts were obtained, evaluated and discussed.

The Multi-objective Sensor Selection and Placement Optimization based on the Lichtenberg Algorithm found two families of Pareto fronts: linear and convex. It was not only possible to find a correlation between the metrics, but also to associate those that provided a better sensor distribution with a higher Hypervolume value. The metrics Kinetic Energy and Eigenvalue Product were the best from your families and 10 and 6 sensor configurations from both were selected for delamination identification in the central section blade. With 10 sensors and no noise, both were 100% accurate in identifying damage. Just like KE for 6 sensors. However, the EVP metric has a 0.13% error when identifying the position and 5.6% when quantifying the severity. With the addition of 3% noise, the KE metric continued to hit the exact position of the damage, but had a 3.4% error when quantifying the severity. In the same situation, EVP presented an error of 0.13% for locating and 23.2% for quantifying the damage severity. Six sensors KE metric distribution proved to be more accurate and consistent. So, it was tested in identifying damage in the root and tip sections, where it continued to hit the exact damage location, but had more difficulty in finding the severity as the damage moved away from the root section (1.3, 3.4, and 50.6% for the root, central and tip sections, respectively).

MOSSPOLA not only found the sensor configuration for the helicopter blade that allowed accurate damage identification in noise situations, but also found sensor configurations for each metric and for each number of sensors, proving to be an algorithm capable of solving the basic problem of Structural Health Monitoring.

Therefore, this Dissertation not only allowed the understanding of the State of Art in the subject, but also enabled the creation of a new metaheuristic that demonstrates good results where was applied. Consequently, it allows to find innovative results in different areas. It is important to emphasize that as stated in Chapter 2, there is no metaheuristic alone that can be excellent in any type of problem.

6.1 Future Works

Some suggestions for future work can be suggested as a continuation of this doctoral dissertation:

- Generalized study of the tuning of MOLA´s parameters.
- Application of chaos theory and levy flights distribution to improve algorithm results.
- MOLA Algorithm Improvement: code reductions or updates.
- Export MOLA from Matlab® to Python, a free and powerful programming language that has been more used.
- Application of MOLA in several other mechanical structures designs using FEM updating which, as seen, can deliver very good results. This can be repeated with the first two items and using other metaheuristics.
- Deepen the study of SPO in the MRB improving the numerical model by adding dynamic boundary conditions: blade rotation, centrifugal forces, run-out, aerodynamic conditions, etc.
- Test other binarization models for the SPO problem when adapting MOLA to MOSSPOLA.
- Application of MOSSPOLA in other structures for SPO study. This can be repeated with the first two items and using other metaheuristics.
- Develop new algorithms that can present better results and reap all the fruits of this dissertation again.

Chapter 7

Publications and Patents

The fifteen papers (Section 7.1) and the seven patents (Section 7.2) presented below were published **during** the Doctorate (March/2020 – August/2022). It is important to note that the doctorate subject (multi-objective optimization) is a continuation of the masters (mono-objective optimization) and therefore, they are related.

7.1 Publications

- Pereira JLJ, Chuman M, Cunha SS Jr, Gomes GF (2021) **Lichtenberg optimization algorithm applied to crack tip identification in thin plate-like structures**. Engineering & Computations. https://doi.org/10.1108/EC-12-2019-0564
- Pereira JLJ, Francisco MB, Cunha SS Jr, Gomes GF (2021). **A powerful Lichtenberg Optimization Algorithm: A damage identification case study**. Engineering Applications of Artificial Intelligence. https://doi.org/10.1016/j.engappai.2020.104055
- Pereira JLJ, Francisco MB, Diniz CA, Oliver GA, Cunha SS Jr, Gomes GF (2021). **Lichtenberg Algorithm: A Novel Hybrid PHYSICS-Based Meta-Heuristic For**

Global Optimization. Expert Systems with Applications. https://doi.org/10.1016/j.eswa.2020.114522

- Pereira, J.L.J., Oliver, G.A., Francisco, M.B. *et al.* (2021). **A Review of Multi-objective Optimization: Methods and Algorithms in Mechanical Engineering Problems**. Archives of Computational Methods in Engineering. https://doi.org/10.1007/s11831-021-09663-x
- Pereira JLJ, Guilherme Antônio Oliver, Matheus Brendon Francisco, Sebastião Simões Cunha Jr, Guilherme Ferreira Gomes. **Multi-objective lichtenberg algorithm: A hybrid physics-based meta-heuristic for solving engineering problems**, Expert Systems with Applications. Volume 187. 2022. 115939. https://doi.org/10.1016/j.eswa.2021.115939
- Pereira, J.L.J., Francisco, M.B., Ribeiro, R.F. *et al.* **Deep multiobjective design optimization of CFRP isogrid tubes using lichtenberg algorithm**. *Soft Comput* 26, 7195–7209 (2022). https://doi.org/10.1007/s00500-022-07105-9
- Pereira, J. L. J., Matheus Brendon Francisco, Lucas Antônio de Oliveira, João Artur Souza Chaves, Sebastião Simões Cunha Jr, Guilherme Ferreira Gomes. **Multi-objective sensor placement optimization of helicopter rotor blade based on Feature Selection**. Mechanical Systems and Signal Processing. Volume 180. 2022c. 109466. ISSN 0888-3270. https://doi.org/10.1016/j.ymssp.2022.109466.
- Francisco MB, Junqueira DM, Oliver GA, Pereira JLJ, Cunha SS Jr, Gomes GF (2021). **Design optimizations of carbon fibre reinforced polymer isogrid lower limb prosthesis using particle swarm optimization and Lichtenberg algorithm**. Engineering Optimization. https://doi.org/10.1080/0305215X.2020.1839442
- Francisco, M. B. ; Pereira, J. L. J. ; Roque, L. ; Machado, S. ; Cunha jr, S. S. ; Gomes, G. F. (2021). **A Statistical Analysis of High-Performance Prosthetic Isogrid Composite Tubes Using Response Surface Method**. Engineering Computations. https://doi.org/10.1108/EC-04-2020-0222
- Francisco, M. B., Pereira, J. L. J., Oliver, G. A., Da Silva, F. H. S., Cunha, S. S., Gomes, G. F. (2021). **Multi-objective Design Optimization of CFRP Isogrid Tubes Using SunFlower Multi-Objective Optimization Based on Metamodel**. Computers and Structures. https://doi.org/10.1016/j.compstruc.2021.106508

- Francisco, M. B., Pereira, J. L. J., Oliver, G. A., Roque, L. R., Cunha, S. S., Gomes, G. F. (2021). **A review on the energy absorption response and structural applications of auxetic structures**. Mechanics of Advanced Materials and Structures. https://doi.org/10.1080/15376494.2021.1966143
- Oliver, G. A., Pereira, J. L. J., Francisco, M. B. ; Ancelotti, A. C. ; Gomes, G. F. (2021). **Parameter tuning for wavelet transform-based damage index using mixture design**. Engineering with Computers. https://doi.org/10.1007/s00366-021-01481-w
- Oliver, G. A., João Luiz Junho Pereira, Matheus Brendon Francisco & Guilherme Ferreira Gomes (2022) **The influence of delamination parameters on the wavelet based damage index in CFRP structures**, Mechanics of Advanced Materials and Structures. https://doi.org/10.1080/15376494.2022.2028204
- T. A. Z. de Souza, J. L. J. Pereira, M. B. Francisco, C. A. R. Sotomonte, B. Jun Ma, G. F. Gomes & C. J. R. Coronado (2022) **Multi-objective optimization for methane, glycerol, and ethanol steam reforming using lichtenberg algorithm**, International Journal of Green Energy. https://doi.org/10.1080/15435075.2022.2050375

  Diniz, C.A., Pereira, J.L.J., da Cunha, S.S. et al. **Drop-off Location Optimization in Hybrid CFRP/GFRP Composite Tubes Using Design of Experiments and SunFlower Optimization Algorithm**. Appl Compos Mater (2022). https://doi.org/10.1007/s10443-022-10046-z

7.2 Patents

- Pereira, J. L. J.; Cunha JR, S. S. ; Gomes, G. F. **Lichtenberg Algorithm Optimization (LA)**. 2019. Patent: Computer Program. Registration number: BR512019002567-9. Registration Date: 11/11/2019. Instituição de registro: INPI - *Instituto Nacional da Propriedade Industrial*.
- Pereira, J. L. J.; Diniz, C. A.,Cunha JR, S. S. ; Gomes, G. F. **Algoritmo Neuro-Fuzzy para predição de Tensão Residual em Fibra de Carbono Reforçado com Polímeros e com grau de porosidade**. 2019. Patent: Computer Program.

Registration number: BR512019002568-7. Registration Date: 11/11/2019. Instituição de registro: INPI - *Instituto Nacional da Propriedade Industrial*.

- Pereira, J. L. J.; Cunha JR, S. S. ; Gomes, G. F. **Multi-objective Lichtenberg Algorithm (MOLA)**. 2021. Patent: Computer Program. Registration number: BR512021000195-8. Registration Date: 01/01/2021. Instituição de registro: INPI - *Instituto Nacional da Propriedade Industrial*.
- PEREIRA, J. L. J.; GOMES, G. F. **Multi-objective Sunflower Optimization (MOSFO)**. 2021. Patent: Computer Program. Registration number: BR512021002620-9. Registration Date: 27/10/2021. Instituição de registro: INPI - *Instituto Nacional da Propriedade Industrial*.
- Francisco, M. B. ; Cunha jr, S. S. ; Pereira, J. L. J. ; Gomes, G. F. **Software de Análise Numérica e Mecânica de uma Estrutura Isogrid**. 2021. Patent: Computer Program. Registration number: BR512021002621-7. Registration Date: 15/10/2021. Registration institution: INPI - *Instituto Nacional da Propriedade Industrial*.
- Francisco, M. B. ; Cunha jr, S. S. ; Pereira, J. L. J.; Gomes, G. F. **Software de Análise Numérica e Mecânica de uma Estrutura Tubular Auxética**. 2021. Patent: Computer Program. Registration number: BR512022000231-0. Registration Date: 23/12/2021. Registration institution: INPI - *Instituto Nacional da Propriedade Industrial*.
- Pereira, J. L. J.; Francisco, M. B., Cunha JR, S. S. ; Gomes, G. F. **Multi-objective Sensor Selection and Placement Optimization based on Lichtenberg Algorithm (MOSSPOLA)**. 2022. Patent: Computer Program. Registration number: BR512022000511-5. Registration Date: 07/02/2022. Instituição de registro: INPI - *Instituto Nacional da Propriedade Industrial*.

REFERENCES

Abidi, M. H., Al-Ahmari, A. M., Umer, U., & Rasheed, M. S. (2018). **Multi-objective optimization of micro-electrical discharge machining of nickel-titanium-based shape memory alloy using MOGA-II**. Measurement, 125, 336–349.

Afshari, H., Hare, W., & Tesfamariam, S. (2019). **Constrained multi-objective optimization algorithms: Review and comparison with application in reinforced concrete structures**. Applied Soft Computing, 83, 105631.

Ahmad, K., Baig, Y., Rahman, H., & Hasham, H. J. (2020). **Progressive failure analysis of helicopter rotor blade under aeroelastic** loading. Aviation, 24(1), 33-41.

Ahmed, Shameem, Kushal Kanti Ghosh, Seyedali Mirjalili, and Ram Sarkar. (2021). **AIEOU: Automata-based improved equilibrium optimizer with U-shaped transfer function for feature selection**, Knowledge-Based Systems, 228: 107283.

Ahire, P. G., Patil, U. S. and Kadam, M. S. "**Genetic algorithm based optimization of the process parameters for manual metal arc welding of dissimilar metal joint**", *Procedia Manuf.*, vol. 20, pp. 106-112, 2018.

Ahmadi, P., Hajabdollahi, H., and Dincer, I., **Cost and entropy generation minimization of a cross flow plate fin heat exchanger using multi-objective genetic algorithm**, Journal of Heat Transfer, vol. 133, no. 2,pp. 021801–021810, 2011.

Akl, W.; El-sabbagh, A.; Baz, A. **Optimization of the static and dynamic characteristics of plates with isogrid stiffeners**. Finite Elements in Analysis and Design, v. 44, n. 8, p. 513-523, 2008.

Al Dawood, Z. I. A., and A. M. Saadoon, "**Multi response optimization of submerged arc welding using Taguchi fuzzy logic based on utility theory**", *Int. J. Sci. Res.*, vol. 6, no. 12, pp. 475-481, 2017.

Alexandrino, P. D. S. L., Gomes, G. F., & Cunha Jr, S. S. (2020). **A robust optimization for damage detection using multi-objective genetic algorithm, neural network and fuzzy decision making**. Inverse Problems in Science and Engineering, 28 (1), 21-46.

Alkayem, N. F., Cao, M., Zhang, Y., Bayat, M., & Su, Z. (2017). **Structural damage detection using finite element model updating with evolutionary algorithms: a survey**. Neural Computing and Applications, 30(2), 389–411.

Alkayem, N. F., Cao, M., & Ragulskis, M. (2018). **Damage Diagnosis in 3D Structures Using a Novel Hybrid Multiobjective Optimization and FE Model Updating Framework**. Complexity, 2018, 1–13.

Allemang, R.J., & Brown, D.L. (1982). A Correlation Coefficient for Modal Vector Analysis.

Almeida, F. A., Gomes, G. F., Paula, V. R., Correa, J. E., Paiva, A. P., Gomes, J. H. F. & Turrioni, J. B. (2018). **A Weighted Mean Square Error Approach to the Robust Optimization of the Surface Roughness in an AISI 12L14 Free-Machining Steel-Turning Process**. Journal of Mechanical Engineering.

Almeida, F. A., Santos, A. C. O., Paiva, A. P., Gomes, G. F., & Gomes, J. H. F. (2020). **Multivariate Taguchi loss function optimization based on principal components analysis and normal boundary intersection**. Engineering with Computers.

Arian Nik M, Fayazbakhsh K, Pasini D, Lessard L (2012) **Surrogatebased multi-objective optimization of a composite laminate with curvilinear fibers**. Compos Struct 94(8):2306–2313

Asanjarani, A., Dibajian, S. H., & Mahdian, A. (2017). **Multi-objective crashworthiness optimization of tapered thin-walled square tubes with indentations**. Thin-Walled Structures, 116, 26–36.

Ashjari M, Khoshravan MR. **Multi-objective optimization of a functionally graded sandwich panel under mechanical loading in the presence of stress constraint**. J Mech Behav Mater 2017;26(3–4):79–93.

Assis, F. M., & Gomes, G. F. (2021). **Crack identification in laminated composites based on modal responses using metaheuristics, artificial neural networks and response surface method: a comparative study**. Archive of Applied Mechanics.

Avitabile, P. **Experimental Modal Analysis: A Simple Non-Mathematical Presentation**. Sound And Vibration, Lowell, jan. 2001.

Back T (1996) **Evolutionary algorithms in theory and practice: evolution strategies, evolutionary programming, genetic algorithms**. Oxford University Press, Oxford

Bahadormanesh, N., Rahat, S., & Yarali, M. (2017). **Constrained multi-objective optimization of radial expanders in organic Rankine cycles by firefly algorithm**. Energy Conversion and Management, 148, 1179–1193.

Baril, C.; Yacout, S.; Clément, B. **Design for Six Sigma through collaborative multi-objective optimization**. Computers and Industrial Engineering, v. 60, p. 43–55, 2011.

Barthorpe RJ, Worden K (2009) **Sensor placement optimization**. Encyclopedia of Structural Health Monitoring.

Belinato, G., Almeida, F. A., Paiva, A. P., Freitas Gomes, J. H., Balestrassi, P. P., & Rosa, P. A. R. C. (2018). **A multivariate normal boundary intersection PCA-based approach to reduce dimensionality in optimization problems for LBM process**. Engineering with Computers.

Benayoun, B. Roy, and B. Sussman. **Electre: Une methode pour guider le choix en presence de points de vue multiple**. Direction Scientifique, 1966. Note de Travail, No. 49.

Benner P, Herzog R, Lang N, Riedel I, Saak J (2017) **Comparison of model order reduction methods for optimal sensor placement for thermo-elastic models.**

Bilel, N., Mohamed, N., Zouhaier, A., & Lotfi, R. (2016). **An improved imperialist competitive algorithm for multi-objective optimization**. Engineering Optimization, 48(11), 1823–1844. doi:10.1080/0305215x.2016.1141204

Bledzki *et al.* (1999). **Determination of elastic constants of glass/epoxy unidirectional laminates by the vibration testing of plates**. Composites Science and Technology, 59(13):2015–2024

Brans J. P., P. Vincke, and B. Mareschal. **How to select and how to rank projects: the PROMETHEE method**. European Journal of Operational Research, 24(2):228–238, February 1986.

Branke J, Kaußler T, Schmeck H (2001) **Guidance in evolutionary multi-objective optimization**. Adv Eng Softw 32:499– 507

Brassard G and Bratley P. **Algorithmics: Theory and Practice**. Prentice-Hall, Englewood Cliffs, New Jersey, 1988.

Brito, T. G.; Paiva, A. P.; Ferreira, J. R.; Gomes, J. H. F.; Balestrassi, P. P. **A normal boundary intersection approach to multiresponse robust optimization of the surface roughness in end milling process with combined arrays**. Precision Engineering, Elsevier Inc., v. 38, n. 3, p. 628–638, 2014. ISSN 01416359.

Byun, H. S. and Lee, K. H., "**A Decision Support System for the Selection of a Rapid Prototyping Process using the Modified TOPSIS Method**," The International Journal of Advanced Manufacturing Technology, Vol. 26, No. 11-12, pp. 1338-1347, 2005.

Braun, C. E., L.D. Chiwiacowsky, A.T. Gomez, **Variations of Ant Colony Optimization for the solution of the structural damage identification problem**, Procedia Comput. Sci. 51 (2015) 875–884

Brito, T. G.; Paiva, A. P.; Paula, T. I.; Dalosto, D. N.; Ferreira, J. R.; Balestrassi, P. P. **Optimization of AISI 1045 end milling using robust parameter design**. International Journal of Advanced Manufacturing Technology, v. 84, n. 5-8, p. 1185–1199, 2016. ISSN 14333015.

Burgos, D. A. T., Vargas, R. C. G., Pedraza, C., Agis, D., &Pozo, F. (2020). **Damage Identification in Structural Health Monitoring: A Brief Review from its Implementation to the Use of Data-Driven Applications**. Sensors, 20(3), 733.

Cao, X., Chen, J., Xu, Q., & Li, J. (2020). **A distance coefficient-multi objective information fusion algorithm for optimal sensor placement in structural health monitoring**. Advances in Structural Engineering, 136943322096437.

Carne TG and Dohrmann CR. **A modal test design strategy for model correlation**. Albuquerque, NM: Sandia National Labs, 1994.

Cha Y, Buyukozturk O (2015) **Structural damage detection using modal strain energy and hybrid multi-objective optimization**. Comput Aided Civ Infrastruct Eng 30:347–358

Chen, F., Wang, Y., Sun, S., Ma, Z., & Huang, X. (2018). **Multi-objective optimization of mechanical quality and stability during micro resistance spot welding**. The International Journal of Advanced Manufacturing Technology.

Chen, L. Yu, **A new structural damage detection strategy of hybrid PSO with Monte Carlo simulations and experimental verifications**, Measurement 122 (2018b) 658–669.

Chiandussi, G.; Codegone, M.; Ferrero, S.; Varesio, F.E. **Comparison of multi-objective optimization methodologies for engineering applications**. [S.l.]:Eslsevier Ltd, 2012. 912-942p.

Choudhary, A., M. Kumar and D. R. Unune, "**Experimental investigation and optimization of weld bead characteristics during submerged arc welding of AISI 1023 steel**", *Defence Technol.*, vol. 15, no. 1, pp. 72-82, Feb. 2019

Coello Coello CA, Corte´s NC (2005) **Solving multi-objective optimization problems using an artificial immune system**. Genet Program Evol Mach 6(2):163–190

Coello C., Lamont B., Van Veldhuizen, D. **Evolutionary Algorithms for Solving Multi-Objective Problems**. Springer US, 2007. DOI 10.1007/978-0-387-36797-2.

Cohon, J. L. and Marks, D. H.. **A Review and Evaluation of Multi-objective Programming Techniques**. Water Resources Research, 11(2):208–220, apr 1975.

Cohon, J. L. **Multi-objective Programming and Planning**. Academic Press, 1978.

Colombo, M.D. Todd, C. Sbarufatti, M. Giglio. (2022). **On statistical Multi-Objective optimization of sensor networks and optimal detector derivation for structural health monitoring.** Mechanical Systems and Signal Processing. Volume 167, Part A , 108528. ISSN 0888-3270.

Crawford, R. Soto, G. Astorga, J. García, C. Castro, F. Paredes, **Putting continuous metaheuristics to work in binary search spaces**, Complexity 2 (2017) 1–19.

Cui, Y., Geng, Z., Zhu, Q., & Han, Y. (2017). **Review: Multi-objective optimization methods and application in energy saving**. Energy, 125, 681–704.

Custódio AL, Madeira JFA, Vaz AIF, Vicente LN. **Direct multisearch for multi-objective optimization**. SIAM J Optim 2011;21(3):1109–40.

DAS, I.; DENNIS, J. E. **Normal-Boundary Intersection: A New Method for Generating the Pareto Surface in Nonlinear Multicriteria Optimization Problems**. SIAM Journal on Optimization, v. 8, n. 3, p. 631–657, 1998. ISSN 1052-6234.

Deb, K. (2008) **Introduction to evolutionary multi-objective optimization**. In: Multi-objective Optimization, Springer, pp 59–96

Deb, K., S. Agrawal, A. Pratab, and T. Meyarivan. **A Fast Elitist Non Dominated Sorting Genetic Algorithm for Multi-Objective Optimization: NSGA-II**. In M. Schoenauer, K. Deb, G. Rudolph, X. Yao, E. Lutton, J. J. Merelo, and H.-P. Schwefel, editors, Proceedings of the Parallel Problem Solving from Nature VI Conference, pages 849–858, Paris, France, 2000. Springer. Lecture Notes in Computer Science No. 1917.

Dhiman, G., Singh, K. K., Soni, M., Nagar, A., Dehghani, M., Slowik, A., Cengiz, K. (2020). **MOSOA: A New Multi-objective Seagull Optimization Algorithm**. Expert Systems with Applications, 114150.

Dhiman, G., Krishna Kant Singh, Adam Slowik, Victor Chang, Ali Riza Yildiz, Amandeep Kaur, Meenakshi Garg. (2020b). **EMOSOA: A New Evolutionary Multi-objective Seagull Optimization Algorithm for Global Optimization**. International Journal of Machine Learning and Cybernetics.

Dhiman, Gaurav, Diego Oliva, Amandeep Kaur, Krishna Kant Singh, S Vimal, Ashutosh Sharma, and Korhan Cengiz. 2021. **BEPO: A novel binary emperor penguin optimizer for automatic feature selection**, Knowledge-Based Systems, 211: 106560.

Dinh-Cong, D., Nguyen-Thoi, T. **An effective damage identification procedure using model updating technique and multi-objective optimization algorithm for structures made of functionally graded materials.** Engineering with Computers (2021).

Diniz, C. A., Mendez, Y. A. D., Almeida, F. A., Cunha Jr, S. S. **Optimum Design of Composite Structures with Ply Dropp-Offs using Responde Surface Methodology**. Engineering Computations, 2021.

Duckstein, L. **Multi-objective Optimization in Structural Design: The Model Choice Problem**. In E. Atrek, R. H. Gallagher, K. M. Ragsdell, and O. C. Zienkiewicz, editors, New Directions in Optimum Structural Design, pages 459–481. John Wiley and Sons, 1984.

Dumbhare, A. P., Dubey, S., V. Deshpande, Y., Andhare, A. B., & Barve, P. S. (2018). **Modelling and multi-objective optimization of surface roughness and kerf taper angle in abrasive water jet machining of steel**. Journal of the Brazilian Society of Mechanical Sciences and Engineering, 40(5).

Ebrahimi-Nejad, S., Kheybari, M., & Borujerd, S. V. N. (2020). **Multi-objective optimization of a sports car suspension system using simplified quarter-car models**. Mechanics & Industry, 21(4), 412.

Emmerich, M. T. M., & Deutz, A. H. (2018). **A tutorial on multi-objective optimization: fundamentals and evolutionary methods**. Natural Computing, 17(3), 585–609. doi:10.1007/s11047-018-9685-y

Fadaee, M., & Radzi, M. A. M. (2012). **Multi-objective optimization of a stand-alone hybrid renewable energy system by using evolutionary algorithms: A review**. Renewable and Sustainable Energy Reviews, 16(5), 3364–3369.

Fan et al.(2009) Hualin Fan, Daining Fang, Liming Chen, Zheng Dai, e Wei Yang. **Manufacturing and testing of a cfrc sandwich cylinder with kagome cores**. Composites Science and Technology, 69(15-16):2695–2700.

Fan, H., Zhang, J., Zhang, W. & Liu, B. (2020). **Multiparameter and Multiobjective Optimization Design Based on Orthogonal Method for Mixed Flow Fan**. Energies, 13(11), 2819.

Ferentinos, K. P. & Tsiligiridis, T. A. (2007). **Adaptive design optimization of wireless sensor networks using genetic algorithms**. Computer Networks, 51(4), 1031–1051.

Fonseca, C. M. & Fleming, P. J. **An overview of evolutionary algorithms in multi-objective optimization**. Technical report, Department of Automatic Control and Systems Engineering, University of Sheffield, Sheffield, U. K., 1994.

Fonseca C. M. , Fleming PJ (1993) **Genetic algorithms for multi-objective optimization: Formulation discussion and generalization**. In: Proceedings of the International Conference on Genetic Algorithms, vol 93. Citeseer, pp 416–423

Forcellese, **Archimede et al. Manufacturing of Isogrid Composite Structures by 3D Printing**. Procedia Manufacturing, v. 47, p. 1096-1100, 2020.

Fossati, G. G., L.F.F. Miguel, W.J.P. Casas, **Multi-objective optimization of the suspension system parameters of a full vehicle model**, Optim. Eng. 20, 151–177 (2019)

Fourman M. P.. Compaction of Symbolic Layout using Genetic Algorithms. In J. J. Grefenstette, editor, **Genetic Algorithms and their Applications: Proceedings of the First International Conference on Genetic Algorithms**, pages 141–153. Lawrence Erlbaum, Hillsdale, New Jersey, 1985

Francisco MB, Junqueira DM, Oliver GA, Pereira JLJ, Cunha SS Jr, Gomes GF (2021). **Design optimizations of carbon fibre reinforced polymer isogrid lower limb prosthesis using particle swarm optimization and Lichtenberg algorithm**. Engineering Optimization. https://doi.org/10.1080/0305215X.2020.1839442

Francisco, M. B., Pereira, J. L. J., Oliver, G. A., Silva, F. H. S., Cunha, S. S., Gomes, G. F. (2021b). **Multi-objective Design Optimization of CRP Isogrid Tubes Using SunFlower Multi-Objective Optimization Based on Metamodel**. Computers and Structures.

Francisco M, Roque L, Pereira J, Machado S, da Cunha SS, Gomes GF. (2021c) **A statistical**

analysis of high-performance prosthetic isogrid composite tubes using response surface method. Eng Comput (Swansea, Wales). https://doi.org/10.1108/EC-04-2020-0222.

Franco Correia VM, Aguilar Madeira JF, Araújo AL, Mota Soares CM. **Multi-objective optimization of ceramic-metal functionally graded plates using a higher order model.** Compos Struct 2018;183:146–60.

Franco Correia VM, Aguilar Madeira JF, Araújo AL, Mota Soares CM. **Multi-objective optimization of functionally graded material plates with thermo-mechanical loading**. Compos Struct 2019;207:845–57

Gandibleux, N. Mezdaoui, and A. Fr´eville. **A Tabu Search Procedure to Solve Combinatorial Optimisation Problems**. In R. Caballero, F. Ruiz, and References 667 R. E. Steuer, editors, Advances in Multiple Objective and Goal Programming, volume 455 of Lecture Notes in Economics and Mathematical Systems, pages 291–300. Springer-Verlag, 1997.

Ganguli (2001) Ranjan Ganguli. **A fuzzy logic system for ground based structural health monitoring of a helicopter rotor using modal data**. Journal of Intelligent Material Systems and Structures, 12(6):397–407.

Gao, Z., Shao, X., Jiang, P., Wang, C., Zhou, Q., Cao, L., & Wang, Y. (2016). **Multi-objective optimization of weld geometry in hybrid fiber laser-arc butt welding using Kriging model and NSGA-II**. Applied Physics A, 122(6).

Gaudêncio, D. J. H., Almeida, F. A., Turrioni, J. B., Costa Quinino, R., Balestrassi, P. P., & Paiva, A. P. (2019). **A multiobjective optimization model for machining quality in the AISI 12L14 steel turning process using fuzzy multivariate mean square error**. Precision Engineering.

Ghasemi, A. R., & Hajmohammad, M. H. (2016). **Multi-objective optimization of laminated composite shells for minimum mass/cost and maximum buckling pressure with failure criteria** under external hydrostatic pressure. Structural and Multidisciplinary Optimization, 55(3), 1051–1062.

Ghosh, K. K., Ritam Guha, R., Bera S. K. **S-Shaped versus V-Shaped Transfer Functions for Binary Manta Ray Foraging Optimization in Feature Selection Problem**. Research Square, 2020.

Gupta, S. K., Pandey, K., & Kumar, R. (2016a). **Multi-objective optimization of friction stir welding process parameters for joining of dissimilar AA5083/AA6063 aluminum alloys using hybrid approach**. Proceedings of the Institution of Mechanical Engineers, Part L: Journal of Materials: Design and Applications, 232(4), 343–353.

Gupta, S. K., Pandey, K., & Kumar, R. (2016b). **Artificial intelligence-based modelling and multi-objective optimization of friction stir welding of dissimilar AA5083-O and AA6063-T6 aluminium alloys**. Proceedings of the Institution of Mechanical Engineers, Part L: Journal of Materials: Design and Applications, 232(4), 333–342

Ghachi, R. F., Alnahhal, W. I., Abdeljaber, O., Renno, J., Haque, A. B. M. T., Shim, J., & Aref, A. (2020). **Optimization of Viscoelastic Metamaterials for Vibration Attenuation Properties**. International Journal of Applied Mechanics.

Goicoechea, L. Duckstein, and M. Fogel. **Multi-objective programming in watershed management: A study of the Charleston watershed**. Water Resources Research, 12(6):1085–1092, December 1976.

Goldberg D. E. **Genetic Algorithms in Search, Optimization and Machine Learning**. Addison-Wesley Publishing Company, Reading, Massachusetts, 1989.

Gomes, G. F., & Giovani, R. S. (2020). **An efficient two-step damage identification method using sunflower optimization algorithm and mode shape curvature (MSDBI–SFO).** Engineering with Computers. https://doi.org/10.1007/s00366-020-01128-2.

Gomes, G. F., Souza Chaves, J. A., & de Almeida, F. A. (2020b). **An inverse damage location problem applied to AS-350 rotor blades using bat optimization algorithm and multiaxial vibration data**. Mechanical Systems and Signal Processing, 145, 106932.

Gomes G. F., Sebastiao Simões da Cunha Jr., Antonio Carlos Ancelotti Jr., **A sunflower optimization (SFO) algorithm applied to damage identification on laminated composite plates**, Eng. Comput. 35 (2) (2019) 619–626

Gomes, G. F., Almeida, F. A., Silva Lopes Alexandrino, P., Cunha, S. S., Sousa, B. S., & Ancelotti, A. C. (2018). **A multi-objective sensor placement optimization for SHM systems considering Fisher information matrix and mode shape interpolation**. Engineering with Computers.

Gomes, G. F., S.S. da Cunha, P.D.S.L. (2018b). Alexandrino, B.S. de Sousa, A.C. Ancelotti, **Sensor placement optimization applied to laminated composite plates under vibration**, Struct. Multidiscipl. Optimiz. 58 (5) 2099–2118.

Gomes, J **Método dos polinômios canônicos de misturas para otimização multi-objetivo**. Itajubá, Minas Gerais, Brasil: Doctoral Thesis - Postgraduate Program in Production Engineering – Universidade Federal de Itajubá, 2013.

Gopalakrishnan *et al*. (2011)**. Computational techniques for damage detection, classification and quantification**. Em Computational Techniques for Structural Health Monitoring, pages 407–461. Springer.

Gunantara, N. (2018). **A review of multi-objective optimization: Methods and its applications**. Cogent Engineering, 5(1), 1–16.

Guo, X., Wu, Y., Xie, L., Cheng, S., & Xin, J. (2015). **An Adaptive Brain Storm Optimization Algorithm for Multi-objective Optimization Problems**. Lecture Notes in Computer Science, 365–372.

Haimes Y. Y., Lasdon L. S. and Wismer D. A. **On a Bicriterion Formulation of the Problems of Integrated System Identification and System Optimization**. IEEE Transactions on Systems, Man, and Cybernetics, 1(3):296–297, July 1971.

Hajela, P. and Lin, C. Y. **Genetic search strategies in multicriterion optimal design**. Structural Optimization, 4:99–107, 1992.

Heidari AA, Mirjalili S, Faris H, Aljarah I, Mafarja M, Chen H. **Harris hawks optimization: Algorithm and applications**. 2019. Future Generation Computer Systems 97:849-872

Heo G, Wang M and Satpathi D. **Optimal transducer placement for health monitoring of long span bridge**. Soil Dyn Earthq Eng 1997; 16(7–8): 495–502

Holland J. **Adaptation in natural and artificial systems**. Ann Arbor, MI, USA: University of Michigan Press; 1975.

Horn, J., N. Nafpliotis. **Multi-objective Optimization using the Niched Pareto Genetic Algorithm**. Technical Report IlliGAl Report 93005, University of Illinois at Urbana-Champaign, Urbana, Illinois, USA, 1993.

Horn, J., N. Nafpliotis, and D. E. Goldberg. **A Niched Pareto Genetic Algorithm for Multi-objective Optimization**. In Proceedings of the First IEEE Conference on Evolutionary Computation, IEEE World Congress on Computational Intelligence, volume 1, pages 82–87, Piscataway, New Jersey, June 1994. IEEE Service Center.

Hou, W. Zhang, **Advanced Composite Materials defects/damages and health monitoring**, in Proceedings of the IEEE 2012 Prognostics and System Health Management Conference (PHM-2012 Beijing), Beijing, pp. 1-5, (2012).

Huybrechts, S. M.; Hahn, S. E.; Meink, T. E. **Grid stiffened structures: a Survay of fabrication, analysis and design methods**. 12 ICCM Proceedings, (1999).

Hwang, C. L. & Yoon, K. P. (1981). **Multiple Attribute Decision Making: Methods and Applications**. Berlin/Heidelberg/New York: Springer-Verlag.

Ikeya K, Shimoda M, Shi J-X (2016) **Multi-objective free-form optimization for shape and thickness of shell structures with composite materials**. Compos Struct 135:262–275

Jadhav, Prakash; MANTENA, P. Raju. **Parametric optimization of grid-stiffened composite panels for maximizing their performance under transverse loading**. Composite structures, v. 77, n. 3, p. 353-363, 2007.

Jaimes *et al.*(2009) Antonio López Jaimes, Saúl Zapotecas Martınez, e Carlos A Coello Coello. **An introduction to multi-objective optimization techniques**. Optimization in Polymer Processing, páginas 29–57.

Jason R. Schott. **Fault tolerant design using single and multicriteria genetic algorithm optimization** 1995:199–200.

Jaynes ET. **Where do we stand on maximum entropy?** In: The maximum entropy formalism,

Cambridge, MA, 2–4 May 1979.

Jin H, Xia J and Wang YQ. **Optimal sensor placement for space modal identification of crane structures based on an improved harmony search algorithm**. J Zhejiang Univ: Sc A 2015; 16(6): 464–477.

Jiang, R., D. Wang, **Optimization of Suspension System of Self-Dumping Truck Using TOPSIS-based Taguchi Method Coupled with Entropy Measurement**, SAE Technical Paper, 2016-2001-1385 (2016)

Jiang, R., D. Wang, **Optimization of Vehicle Ride Comfort and Handling Stability Based on TOPSIS Method**, SAE Technical Paper, 2015-200-1348 (2015)

Jiang, P., Wang, C., Zhou, Q., Shao, X., Shu, L., & Li, X. (2016). **Optimization of laser welding process parameters of stainless steel 316L using FEM, Kriging and NSGA-II**. Advances in Engineering Software, 99, 147–160.

Jin Y, Sendhoff B (2002) **Fuzzy preference incorporation into evolutionary multi-objective optimization**. In: Proceedings of the 4th Asia-Pacific Conference on Simulated Evolution and Learning, vol 1, pp 26–30.

Joyce T., Herrmann J.M. (2018) **A Review of No Free Lunch Theorems, and Their Implications for Metaheuristic Optimisation**. In: Yang XS. (eds) Nature-Inspired Algorithms and Applied Optimization. Studies in Computational Intelligence, vol 744. Springer, Cham.

Junqueira, Diego Morais et al. **Design optimization and development of tubular isogrid composites tubes for lower limb prosthesis**. Applied Composite Materials, v. 26, n. 1, p. 273-297, 2019.

Kalantari M, Dong C, Davies IJ (2016) **Multi-objective robust optimisation of unidirectional carbon/glass fibre reinforced hybrid composites under flexural loading**. Compos Struct 138:264–275

Kammer DC. **Sensor placement for on-orbit modal identification and correlation of large space structures.** J Guid Control Dynam 1991; 14(2): 251–259.

Kammer DC. **Effects of noise on sensor placement for on-orbit modal identification of large space structures**. J Dyn Syst 1992; 114(3): 436–443.

Kang, J. Kim, J.M. Kim, **Reliable fault diagnosis for incipient low-speed bearings using fault feature analysis based on a binary bat algorithm**, Inform. Sci. 294 (2015) 423–438

Kanou, S. Nabavi, and J. Jam. **Numerical modeling of stresses and buckling loads of isogrid lattice composite structure cylinders**. International Journal of Engineering, Science and Technology, 5(1):42–54, 2013.

Kaveh, M. Maniat, **Damage detection based on MCSS and PSO using modal data**, Smart Struct. Syst. 15 (5) (2015) 1253–1270

Karimi, M., Hall, M., Buckham, B., & Crawford, C. (2016). **A multi-objective design optimization approach for floating offshore wind turbine support structures**. Journal of Ocean Engineering and Marine Energy, 3(1), 69–87.

Khabarov, S. S., & Komshin, A. S. (2021). **Fiber-Optic Measurement Technology and the Phase-Chronometric Method for Controlling and Monitoring the Technical Condition of Aircraft Structures**. Measurement Techniques, 64(2), 131–138.

Kim G, Park Y (2004) **An improved updating parameters method and finite element model updating using multi-objective optimisation technique**. Mech Syst Signal Process 18(1):59–78.

Kim, S., & Frangopol, D. M. (2016). **Efficient multi-objective optimisation of probabilistic service life management**. Structure and Infrastructure Engineering, 13(1), 147–159. doi:10.1080/15732479.2016.1198405

Kitayama, S., Miyakawa, H., Takano, M., & Aiba, S. (2016). **Multi-objective optimization of injection molding process parameters for short cycle time and warpage reduction using conformal cooling channel**. The International Journal of Advanced Manufacturing Technology, 88(5-8), 1735–1744.

Kitayama, S., Yokoyama, M., Takano, M., & Aiba, S. (2017). **Multi-objective optimization of variable packing pressure profile and process parameters in plastic injection molding**

for minimizing warpage and cycle time. The International Journal of Advanced Manufacturing Technology, 92(9-12), 3991–3999.

Knowles JD, Corne DW (2000) **Approximating the nondominated front using the Pareto archived evolution strategy**. Evol Comput 8:149–172

Kumar R., Sehijpal Singh, Paramjit Singh Bilga, Jatin, Jasveer Singh, Sunpreet Singh, Maria-Luminiţa Scutaru, Cătălin Iulian Pruncu. **Revealing the benefits of entropy weights method for multi-objective optimization in machining operations: A critical review**. Journal of Materials Research and Technology. Volume 10. 2021. Pages 1471-1492. ISSN 2238-7854.

Kursawe, F. **A Variant of Evolution Strategies for Vector Optimization**. In H.-P. Schwefel and R. Manner, editors, Parallel Problem Solving from Nature. 1st Workshop, PPSN I, pages 193–197, Dortmund, Germany, October 1991. Springer-Verlag. Lecture Notes in Computer Science No. 496.

Lakshmi, K.; Rao, A. Rama Mohan. **Optimal design of laminate composite isogrid with dynamically reconfigurable quantum PSO**. Structural and Multidisciplinary Optimization, v. 48, n. 5, p. 1001-1021, 2013.

Latifi, F.P. van der Meer, L.J. Sluys, **A level set model for simulating fatigue-driven delamination in composites**, International Journal of Fatigue, Vol. 80, pp. 434–442, (2015)

Lee D, Morillo C, Bugeda G, Oller S, Onate E (2012) **Multilayered composite structure design optimisation using distributed/parallel multi-objective evolutionary algorithms**. Compos Struct 94(3): 1087–1096.

Leguizamón, G., & Coello Coello, C. A. (2011). **Multi-Objective Ant Colony Optimization: A Taxonomy and Review of Approaches**. Series in Machine Perception and Artificial Intelligence, 67–94.

Li D, Li H and Fritzen C. **The connection between effective independence and modal kinetic energy methods for sensor placement**. J Sound Vib 2007; 305(4–5): 945–955.

Li, H., Wang, X., Wei, Y., Liu, T., Gu, J., Li, Z., … Liu, Y. (2017). **Multi-Objective Optimizations of Biodegradable Polymer Stent Structure and Stent Microinjection Molding Process**. Polymers, 9(12), 20.

Li, P., Huang, L., & Peng, J. (2018). **Sensor Distribution Optimization for Structural Impact Monitoring Based on NSGA-II and Wavelet Decomposition**. Sensors, 18(12), 4264.

Li, K., Yan, S., Zhong, Y., Pan, W., & Zhao, G. (2018b). **Multi-Objective Optimization of the Fiber-reinforced Composite Injection Molding Process using Taguchi method, RSM, and NSGA-II**. Simulation Modelling Practice and Theory.

Li, C. Lai, Q. Zheng, et al. (2019) **Design and mechanical properties of hierarchical isogrid structures validated by 3D printing technique**. Materials & Design, https://doi.org/10.1016/j.matdes.2019.107664

Li, Y., Wei, K., Yang, W., & Wang, Q. (2020). **Improving wind turbine blade based on multi-objective particle swarm optimization**. Renewable Energy. doi:10.1016/j.renene.2020.07.067

Lichtenberg, G. C., **Novi. Comment. Gött.** Vol. 8, 168, 1777.

Lin, W., Yu, D., Zhang, C., Zhang, S., Tian, Y., Liu, S., & Luo, M. (2016). **Multi-objective optimization of machining parameters in multi-pass turning operations for low-carbon manufacturing**. Proceedings of the Institution of Mechanical Engineers, Part B: Journal of Engineering Manufacture, 231(13), 2372–2383.

Lin, J.-F., Xu, Y.-L., & Law, S.-S. (2018). **Structural damage detection-oriented multi-type sensor placement with multi-objective optimization**. Journal of Sound and Vibration, 422, 568–589.

Liu, H., Li, Y., Duan, Z., & Chen, C. (2020). **A review on multi-objective optimization framework in wind energy forecasting techniques and applications**. Energy Conversion and Management, 224, 113324.

Liu, Q., Li, X., Liu, H., & Guo, Z. (2020b). **Multi-objective metaheuristics for discrete optimization problems: A review of the state-of-the-art**. Applied Soft Computing, 93, 106382.

Long Q.,Xue Wu,Changzhi Wu. **Non-dominated sorting methods for multi-objective optimization: Review and numerical comparison**. Journal of Industrial & Management optimization. 2021

Lostado Lorza, R., Escribano García, R., Fernandez Martinez, R., & Martínez Calvo, M. (2018). **Using Genetic Algorithms with Multi-Objective Optimization to Adjust Finite Element Models of Welded Joints**. Metals, 8(4), 230.

Lu, C., Gao, L., Li, X., Zheng, J., & Gong, W. (2018). **A multi-objective approach to welding shop scheduling for makespan, noise pollution and energy consumption**. Journal of Cleaner Production, 196, 773–787.

Lu, C., Gao, L., Li, X., & Xiao, S. (2017). **A hybrid multi-objective grey wolf optimizer for dynamic scheduling in a real-world welding industry**. Engineering Applications of Artificial Intelligence, 57, 61–79.

Madhavi. **Design and analysis of filament wound composite pressure vessel with integrated-end domes**. Defence science journal, 59(1):73–81, 2009.

Mahfouf, M.-Y. Chen, and D. A. Linkens. **Adaptive Weighted Particle Swarm Optimisation for Multi-objective Optimal Design of Alloy Steels**. In Parallel Problem Solving from Nature - PPSN VIII, pages 762–771, Birmingham, UK, September 2004. Springer-Verlag. Lecture Notes in Computer Science Vol. 3242.

Mane, S. U. & Rao, M. R. N. **Many-Objective Optimization: Problems and Evolutionary Algorithms – A Short Review**. International Journal of Applied Engineering Research ISSN 0973-4562 Volume 12, Number 20 (2017) pp. 9774-9793

Marler, R. T., & Arora, J. S. (2004). **Survey of multi-objective optimization methods for engineering**. Structural and Multidisciplinary Optimization, 26(6), 369–395.

Mariano, C. E. and E. Morales. **MOAQ an Ant-Q Algorithm for Multiple Objective Optimization Problems**. In W. Banzhaf, J. Daida, A. E. Eiben, M. H. Garzon, V. Honavar, M. Jakiela, and R. E. Smith, editors, Genetic and Evolutionary Computing COnference (GECCO 99), volume 1, pages 894–901, San Francisco, California, July 1999. Morgan Kaufmann.

Mei-Ping Song, & Guo-Chang Gu. (n.d.). **Research on particle swarm optimization: a review**. Proceedings of 2004 International Conference on Machine Learning and Cybernetics (IEEE Cat. No.04EX826).

Meo M and Zumpano G. **On the optimal sensor placement techniques for a bridge structure**. Eng Struct 2005; 27(10): 1488–1497.

Merrill, F. H., and Von Hippel, A. (1939). **The atomphysical Interpretation os Lichtenberg Figures and Their Application to the study of Gas Discharge**. *Journal of Applied Physics*, 10(12), 873-887.

Messac A, Mattson CA (2002) **Generating well-distributed sets of Pareto points for engineering design using physical programming**. Optim Eng 3:431–450.

Mia, M., Gupta, M. K., Lozano, J. A., Carou, D., Pimenov, D. Y., Królczyk, G., … Dhar, N. R. (2018). **Multi-objective Optimization and Life Cycle Assessment of Eco-friendly Cryogenic N2 assisted Turning of Ti-6Al-4V**. Journal of Cleaner Production.

Miettinen, K. (1998). **No-Preference Methods**. International Series in Operations Research & Management Science, 67–76.

Milad Jahangiri, M.A. Najafgholipour, S.M. Dehghan, M.A. Hadianfard. (2019) **The efficiency of a novel identification method for structural damage assessment using the first vibration mode data**, J. Sound Vibr. 458. 1–16.

Mirjalili S, Lewis A (2013) **S-shaped versus V-shaped transfer functions for binary particle swarm optimization**. Swarm Evolut Comput 9:1–14

Mirjalili, S., Saremi, S., Mirjalili, S. M., & Coelho, L. dos S. (2016). **Multi-objective grey wolf optimizer: A novel algorithm for multi-criterion optimization**. Expert Systems with Applications, 47, 106–119.

Mirjalili, S., Jangir, P., & Saremi, S. (2016b). **Multi-objective ant lion optimizer: a multi-objective optimization algorithm for solving engineering problems**. Applied Intelligence, 46(1), 79–95. doi:10.1007/s10489-016-0825-8

Mirjalili, Seyedeh Zahra; Mirjalili, Seyedali; Saremi, Shahrzad; Faris, Hossam; Aljarah, Ibrahim (2017). **Grasshopper optimization algorithm for multi-objective optimization problems**. Applied Intelligence.

Mishra, S.K. Barman, D. Maity, D.K. Maiti, **Ant lion optimisation algorithm for structural damage detection using vibration data**, J. Civil Struct. Health Monitor. 9 (1) (2019) 117–136.

Moleiro, F., Madeira, J. F. A., Carrera, E., & Reddy, J. N. (2020). **Design optimization of functionally graded plates under thermo-mechanical loadings to minimize stress, deformation and mass**. Composite Structures, 112360.

Monarchi. D. E., C. C. Kisiel, and L. Duckstein. **Interactive multi-objective programming in water resources: a case study.** Water Resources Research, 9(4):837–850, August 1973.

Montalvo-Urquizo, J., Niebuhr, C., Schmidt, A., & Villarreal-Marroquín, M. G. (2018). **Reducing deformation, stress, and tool wear during milling processes using simulation-based multiobjective optimization**. The International Journal of Advanced Manufacturing Technology, 96(5-8), 1859–1873.

Montgomery, D. C. (2017). **Design and analysis of experiments**. John wiley & sons.

Mostaghim, S., and J. Teich. **Strategies for Finding Good Local Guides in Multi-objective Particle Swarm Optimization (MOPSO)**. In 2003 IEEE Swarm Intelligence Symposium Proceedings, pages 26–33, Indianapolis, Indiana, USA, April 2003. IEEE Service Center.

Mugnaini, V.,Luca Zanotti Fragonara, Marco Civera. **A machine learning approach for automatic operational modal analysis**. Mechanical Systems and Signal Processing. Volume 170. 2022.

NBR ISO 10328-1: **Próteses - Ensaio Estrutural para Próteses de Membro Inferior: configurações de ensaio**. Associação Brasileira de Normas Técnicas, Rio de Janeiro (2002).

Neumann and Morgenstern. **Theory of Games and Economic Behavior**. Princeton University Press, Princeton, New Jersey, 1944.

Niu, Y., Jiao, F., Zhao, B., & Wang, D. (2017). **Multiobjective optimization of processing parameters in longitudinal-torsion ultrasonic assisted milling of Ti-6Al-4V**. The International Journal of Advanced Manufacturing Technology, 93(9-12), 4345–4356.

Ojstersek, R., Brezocnik, M & Buchmeister, B. (2020**). Multi-objective optimization of production scheduling with evolutionary computation: A review**. International Journal of Industrial Engineering Computations , 11(3), 359-376.

Okabe, T., Oya, Y., Yamamoto, G., Sato, J., Matsumiya, T., Matsuzaki, R., … Obayashi, S. (2017). **Multi-objective optimization for resin transfer molding process**. Composites Part A: Applied Science and Manufacturing, 92, 1–9.

Olorunda O, Engelbrecht AP. **Measuring exploration/exploitation in particle swarms using swarm diversity**. (2008) IEEE Congress on Evolutionary Computation (IEEE World Congress on Computational Intelligence), 2008. IEEE, pp 1128- 1134.

Omkar S, Mudigere D, Naik GN, Gopalakrishnan S (2008). **Vector evaluated particle swarm optimization (VEPSO) for multi-objective design optimization of composite structures**. Comput Struct 86(1):1–14.

Osyczka, A. **An Approach to Multicriterion Optimization Problems for Engineering Design**. Computer Methods in Applied Mechanics and Engineering, 15:309–333, 1978.

Paiva, A. P.; Gomes, J. H. F.; Peruchi, R. S.; Leme, R. C.; Balestrassi, P. P. **A multivariate robust parameter optimization approach based on Principal Component Analysis with**

combined arrays. Computers & Industrial Engineering, Elsevier Ltd, v. 74, n. August, p. 186–198, 2014. ISSN 03608352.

Pan, L. Yu, Z.P. Chen, W.F. Luo, H.L. Liu, **A hybrid self-adaptive Firefly-Nelder-Mead algorithm for structural damage detection**, Smart Struct. Syst. 17 (6) (2016) 957–980.

Panagant, N., Pholdee, N., Wansasueb, K., Bureerat, S., Yildiz, A. R., & Sait, S. M. (2019**). Comparison of recent algorithms for many-objective optimisation of an automotive floor-frame**. International Journal of Vehicle Design, 80(2/3/4), 176.

Panagant, N., Pholdee, N., Bureerat, S. *et al.* **A Comparative Study of Recent Multi-objective Metaheuristics for Solving Constrained Truss Optimisation Problems**. Arch Computat Methods Eng (2021). https://doi.org/10.1007/s11831-021-09531-8.

Pantano, **Cohesive Model for the Simulation of Crack Initiation and Propagation in Mixed-Mode I/II in Composite Materials**, Applied Composite Materials, Vol. 26, No. 4, pp. 1207-1225, (2019).

Paula, T. I., Gomes, G. F., Freitas Gomes, J. H., & Paiva, A. P. (2019). **A Mixture Design of Experiments Approach for Genetic Algorithm Tuning Applied to Multi-objective Optimization**. Optimization of Complex Systems: Theory, Models, Algorithms and Applications, 600–610.

Parsopoulos, K., and M. Vrahatis. **Particle Swarm Optimization Method in Multi-objective Problems**. In Proceedings of the 2002 ACM Symposium on Applied Computing (SAC'2002), pages 603–607, Madrid, Spain, 2002. ACM Press.

Park, H.-S., Nguyen, T.-T., & Dang, X.-P. (2016). **Multi-objective optimization of turning process of hardened material for energy efficiency**. International Journal of Precision Engineering and Manufacturing, 17(12), 1623–1631.

Parkinson A. R, Balling R. J., Hedengren J. D. **Optimization Methods for Engineering Design: Applications and Theory**. Brigham Young University, 2013.

Pawar, P. M., & Ganguli, R. (2003). **Genetic fuzzy system for damage detection in beams and helicopter rotor blades**. Computer Methods in Applied Mechanics and Engineering, 192(16-18), 2031–2057.

Pawar, P., & Ganguli, R. (2007). **Fuzzy-Logic-Based Health Monitoring and Residual-Life Prediction for Composite Helicopter Rotor**. Journal of Aircraft, 44(3), 981–995.

Pawar, P. M., & Sung Nam Jung. (2007b). **Support Vector Machine based Online Composite Helicopter Rotor Blade Damage Detection System**. Journal of Intelligent Material Systems and Structures, 19(10), 1217–1228.

Peng, Y., Wang, X., Xiong, X., & Xu, P. (2016). **Crashing analysis and multi-objective optimisation of duplex energy-absorbing structure for subway vehicle**. International Journal of Crashworthiness, 21(4), 338–352.

Pereira JLJ, Francisco MB, Diniz CA, Oliver GA, Cunha SS Jr, Gomes GF (2021). **Lichtenberg Algorithm: A Novel Hybrid PHYSICS-Based Meta-Heuristic For Global Optimization**. Expert Systems with Applications. https://doi.org/10.1016/j.eswa.2020.114522

Pereira JLJ, Chuman M, Cunha SS Jr, Gomes GF (2021b) **Lichtenberg optimization algorithm applied to crack tip identification in thin plate-like structures**. Engineering & Computations. https://doi.org/10.1108/ EC-12-2019-0564

Pereira JLJ, Francisco MB, Cunha SS Jr, Gomes GF (2021c). **A powerful Lichtenberg Optimization Algorithm: A damage identification case study**. Engineering Applications of Artificial Intelligence. https://doi.org/10.1016/j.engappai.2020.104055.

Pereira, J.L.J., Oliver, G.A., Francisco, M.B. *et al.* (2021d). **A Review of Multi-objective Optimization: Methods and Algorithms in Mechanical Engineering Problems**. Arch Computat Methods Eng.

Pereira JLJ, Guilherme Antônio Oliver, Matheus Brendon Francisco, Sebastião Simões Cunha Jr, Guilherme Ferreira Gomes. (2022). **Multi-objective lichtenberg algorithm: A hybrid physics-based meta-heuristic for solving engineering problems**. Expert Systems with Applications. Volume 187, 115939, ISSN 0957-4174 .

Pereira, J.L.J., Francisco, M.B., Ribeiro, R.F. *et al*. **Deep multiobjective design optimization of CFRP isogrid tubes using lichtenberg algorithm**. *Soft Comput* 26, 7195–7209 (2022b). https://doi.org/10.1007/s00500-022-07105-9

Pereira, J. L. J., Matheus Brendon Francisco, Lucas Antônio de Oliveira, João Artur Souza Chaves, Sebastião Simões Cunha Jr, Guilherme Ferreira Gomes. **Multi-objective sensor placement optimization of helicopter rotor blade based on Feature Selection**. Mechanical Systems and Signal Processing. Volume 180. 2022c. 109466. ISSN 0888-3270. https://doi.org/10.1016/j.ymssp.2022.109466.

Perera, R., & Ruiz, A. (2008). **A multistage FE updating procedure for damage identification in large-scale structures based on multi-objective evolutionary optimization**. Mechanical Systems and Signal Processing, 22(4), 970–991. doi:10.1016/j.ymssp.2007.10.004

Prakash, C., Singh, S., Singh, M., Antil, P., Aliyu, A. A. A., Abdul-Rani, A. M., & Sidhu, S. S. (2018). **Multi-objective Optimization of MWCNT Mixed Electric Discharge Machining of Al–30SiCp MMC Using Particle Swarm Optimization**. Materials Horizons: From Nature to Nanomaterials, 145–164.

Prakash, C., Kansal, H. K., Pabla, B. S., & Puri, S. (2016). **Multi-objective optimization of powder mixed electric discharge machining parameters for fabrication of biocompatible layer on β-Ti alloy using NSGA-II coupled with Taguchi based response surface methodology**. Journal of Mechanical Science and Technology, 30(9), 4195–4204.

Qian, Maosen Cao, Zhongqing Su, Jiangang Chen, **A hybrid particle swarm optimization (PSO)-simplex algorithm for damage identification of delaminated beams**, Mathemat. Probl. Eng. 2012 (2012) 1–11.

Qu, S., Zhao, J., & Wang, T. (2016). **Experimental study and machining parameter optimization in milling thin-walled plates based on NSGA-II**. The International Journal of Advanced Manufacturing Technology, 89(5-8), 2399–2409.

Rangaiah, G. P., Zemin F., Hoadley A, F. **Multi-Objective Optimization Applications in Chemical Process Engineering: Tutorial and Review**. J. Process. 2020. doi:10.3390/pr8050508

Rao ARM, Lakshmi K, Kumar SK (2015) **Detection of delamination in laminated composites with limited measurements combining pca and dynamic qpso**. Adv Eng Softw 86:85–106

Rao, R. V., Rai, D. P., & Balic, J. (2016). **Multi-objective optimization of machining and micro-machining processes using non-dominated sorting teaching–learning-based optimization algorithm**. Journal of Intelligent Manufacturing.

Rao, R. V., Saroj, A., Ocloń, P., Taler, J., & Taler, D. (2017). **Single- and Multi-Objective Design Optimization of Plate-Fin Heat Exchangers Using Jaya Algorithm**. Heat Transfer Engineering, 39(13-14), 1201–1216.

Rao, R. V., and D. P. Rai, "**Optimization of submerged arc welding process parameters using quasi-oppositional based jaya algorithm**", *J. Mech. Sci. Technol.*, vol. 31, no. 5, pp. 2513-2522, May 2017.

Rao, R. V., Rai, D. P., & Balic, J. (2017). **Multi-objective optimization of abrasive waterjet machining process using Jaya algorithm and PROMETHEE Method**. Journal of Intelligent Manufacturing.

Rao, S. **Multi-objective Optimization in Structural Design with Uncertain Parameters and Stochastic Processes**. AIAA Journal, 22(11):1670–1678, November 1984.

Rao, S. **Game Theory Approach for Multi-objective Structural Optimization**. Computers and Structures, 25(1):119–127, 1986.

Rao & Rao (2009). Singiresu S Rao e Singiresu S Rao. **Engineering optimization: theory and practice**. John Wiley & Sons.

Ray T, Liew KM (2002) **A swarm metaphor for multiobjective design optimization**. Eng Optim 34:141–153.

Reddy, R. R. K., & Ganguli, R. (2003). **Structural damage detection in a helicopter rotor blade using radial basis function neural networks**. Smart Materials and Structures, 12(2), 232–241.

Ricci, J. T., Coimbra, R. F. F., & Gomes, G. F. (2021). **Multiobjective optimization of the LASER aircraft wing's composite structural design.** Aircraft Engineering and Aerospace Technology.

Ridha, H. M., Gomes, C., Hizam, H., Ahmadipour, M., Heidari, A. A., & Chen, H. (2021). **Multi-objective optimization and multi-criteria decision-making methods for optimal design of standalone photovoltaic system: A comprehensive review**. Renewable and Sustainable Energy Reviews, 135, 110202.

Rivas, D., R. Quiza, M. Rivas and R. E. Haber, "**Towards Sustainability of Manufacturing Processes by Multi-objective Optimization: A Case Study on a Submerged Arc Welding Process**" in *IEEE Access*, vol. 8, pp. 212904-212916, 2020

Sadollah, A., Eskandar, H., & Kim, J. H. (2015). **Water cycle algorithm for solving constrained multi-objective optimization problems**. Applied Soft Computing, 27, 279–298.

Saha, A., & Mondal, S. C. (2017). **Multi-objective optimization of manual metal arc welding process parameters for nano-structured hardfacing material using hybrid approach**. Measurement, 102, 80–89.

Sahu, N. K., & Andhare, A. B. (2018). **Multiobjective optimization for improving machinability of Ti-6Al-4V using RSM and advanced algorithms**. Journal of Computational Design and Engineering.

Sailender M., G. C. Reddy and S. Venkatesh, "**Influences of process parameters on weld strength of low carbon alloy steel in purged SAW**", *Mater. Today Proc.*, vol. 5, no. 1, pp. 2928-2937, 2018.

Santos, F. L. M., Peeters, B., Van der Auweraer, H., Góes, L. C. S., & Desmet, W. (2016). **Vibration-based damage detection for a composite helicopter main rotor blade**. Case Studies in Mechanical Systems and Signal Processing, 3, 22–27.

Silva, M. M., V. R. Batista, T. M. Maciel, M. A. dos Santos and T. L. Brasileiro, "**Optimization of submerged arc welding process parameters for overlay welding**", *Weld. Int.*, vol. 32, no. 2, pp. 122-129, Feb. 2018.

Schaffer, J. D. **Multiple Objective Optimization with Vector Evaluated Genetic Algorithms**. PhD thesis, Vanderbilt University, Nashville, Tennessee, 1985.

Schott, J. R. (1995). **Fault tolerance design using single and multicriteria genetic algorithm optimization**. DTIC document. Massachusetts Institute of Technology, Department of Aeronautics and Astronautics.

Schlieter T & Dlugosz A. **Structural Optimization of Aerofoils for Many Criteria. 26°International Conference**. Engineering Mechanics 2020. Brno, Czech Republic.

Senthil, S. M., Parameshwaran, R., Ragu Nathan, S., Bhuvanesh Kumar, M., & Deepandurai, K. (2020). **A multi-objective optimization of the friction stir welding process using RSM-based-desirability function approach for joining aluminum alloy 6063-T6 pipes**. Structural and Multidisciplinary Optimization

Serafini, P. **Simulated Annealing for Multiple Objective Optimization Problems**. In G. Tzeng, H. Wang, U. Wen, and P. Yu, editors, Proceedings of the Tenth International Conference on Multiple Criteria Decision Making: Expand and Enrich the Domains of Thinking and Application, volume 1, pages 283–292, Berlin, 1994. Springer-Verlag.

Sierra MR, Coello CAC (2005) **Improving PSO-based multi-objective optimization using crowding, mutation and ∈-dominance**. In: Evolutionary multi-criterion optimization, pp 505–519

Sivaiah, P., & Chakradhar, D. (2018). **Performance improvement of cryogenic turning process during machining of 17-4 PH stainless steel using multi objective optimization techniques**. Measurement. doi:10.1016/j.measurement.2018.12.094

Shanjeevi, C., Satish Kumar, S., & Sathiya, P. (2014). **Multi-objective optimization of friction welding parameters in AISI 304L austenitic stainless steel and copper joints**. Proceedings of the Institution of Mechanical Engineers, Part B: Journal of Engineering Manufacture, 230(3), 449–457.

Shao, Q., Xu, T., Yoshino, T., & Song, N. (2017). **Multi-objective optimization of gas metal arc welding parameters and sequences for low-carbon steel (Q345D) T-joints**. Journal of Iron and Steel Research, International, 24(5), 544–555.

Sharma, Manik; KAUR, Prableen. **A Comprehensive Analysis of Nature-Inspired Meta-Heuristic Techniques for Feature Selection Problem**. Archives of Computational Methods in Engineering, v. 28, n. 3, 2021.

Sorrentino, L. et al. **Manufacture of high performance isogrid structure by Robotic Filament Winding**. Composite Structures, v. 164, p. 43-50, 2017.

Sowrirajan, M., Koshy Mathews, P., & Vijayan, S. (2018). **Simultaneous multi-objective optimization of stainless steel clad layer on pressure vessels using genetic algorithm**. Journal of Mechanical Science and Technology, 32(6), 2559–2568.

Srinivas, N. & K. Deb. **Multi-objective Optimization Using Nondominated Sorting in Genetic Algorithm**s. Evolutionary Computation, 2(3):221–248, fall 1994.

Tan, Y., & Zhang, L. (2019). **Computational methodologies for optimal sensor placement in structural health monitoring: A review**. Structural Health Monitoring, 147592171987757.

Tamaki, H., Kita, H., & Kobayashi, S. (n.d.). **Multi-objective optimization by genetic algorithms: a review**. Proceedings of IEEE International Conference on Evolutionary Computation.

Tamer, A., Zanoni, A., Cocco, A. et al. **A numerical study of vibration-induced instrument reading capability degradation in helicopter pilots**. CEAS Aeronaut J 12, 427–440 (2021).

Tawhid, M. A., & Savsani, V. (2017). **Multi-objective sine-cosine algorithm (MO-SCA) for multi-objective engineering design problems**. Neural Computing and Applications

Teughels, A., J. Maeck, G. Roeck, **Damage assessment by FE model updating using damage functions**, Computers and Structures 80 (2002) 1869–1879

Thiele L, Miettinen K, Korhonen PJ, Molina J (2009) **A preference-based evolutionary algorithm for multi-objective optimization**. Evol Comput 17(3):411–436

Torres, A. F., F. B. Rocha, F. A. Almeida, J. H. F. Gomes, A. P. Paiva & P. P. Balestrassi, "**Multivariate stochastic optimization approach applied in a flux-cored arc welding process**", *IEEE Access*, vol. 8, pp. 61267-61276, 2020.

Totaro, G. et al. **Optimized design of isogrid and anisogrid lattice structures**. Proc. Of the 55-th int. Austronautical Congr, 2004.

Tubishat, Mohammad et al. **Improved Salp Swarm Algorithm based on opposition based learning and novel local search algorithm for feature selection**. Expert Systems with Applications, v. 145, p. 113122, 2020.

Turner, A. **From Lichtenberg to Lightning: Understanding Random Growth**. Newsletter of the London Mathematical Society, 2019.

Tripathy, S., & Tripathy, D. K. (2017). **Multi-response optimization of machining process parameters for powder mixed electro-discharge machining of H-11 die steel using grey relational analysis and topsis**. Machining Science and Technology, 21(3), 362–384.

Vasiliev, V. and A. Razin. **Anisogrid composite lattice structures for spacecraft and aircraft applications**. *Composite Structures* 76 (2006): 182-189.

Vo-Duy, T., Duong-Gia, D., Ho-Huu, V., Vu-Do, H. C., & Nguyen-Thoi, T. (2017). **Multi-objective optimization of laminated composite beam structures using NSGA-II algorithm**. Composite Structures, 168, 498–509. doi:10.1016/j.compstruct.2017.02.038

Voicu, Andrei-Daniel, Hadăr, Anton, Vlăsceanu, Daniel and Pastramă, Ştefan-Dan. (2020). **SHM Monitoring Methods and Sensors with Applications to Composite Helicopter Blades: A Review**. Acta Universitatis Cibiniensis. Technical Series, vol.72, no.1, pp.1-11.

Xin-Gang, Z., Ji, L., Jin, M., & Ying, Z. (2020). **An improved quantum particle swarm optimization algorithm for environmental economic dispatch**. Expert Systems with Applications, 113370.

Wakchaure, K. N., Thakur, A. G., Gadakh, V., & Kumar, A. (2018). **Multi-Objective Optimization of Friction Stir Welding of Aluminium Alloy 6082-T6 Using hybrid Taguchi-Grey Relation Analysis- ANN Method**. Materials Today: Proceedings, 5(2), 7150–7159.

Wang, H., Olhofer, M., & Jin, Y. (2017b). **A mini-review on preference modeling and articulation in multi-objective optimization: current status and challenges**. Complex & Intelligent Systems, 3(4), 233–245.

Wang, J., Yan, Z., Wang, M., Li, M., & Dai, Y. (2013). **Multi-objective optimization of an organic Rankine cycle (ORC) for low grade waste heat recovery using evolutionary algorithm**. Energy Conversion and Management, 71, 146–158.

Wang, L., Wang, T., Wu, J., & Chen, G. (2017). **Multi-objective differential evolution optimization based on uniform decomposition for wind turbine blade design**. Energy, 120, 346–361.

Wang Y, Ma Q, Li W (2012) **Structural damage detection by multi-objective intelligent algorithm**. In: The 15th world conference on earthquake engineering, Lisbon

Wang, Y., & Huo, X. (2018). **Multiobjective Optimization Design and Performance Prediction of Centrifugal Pump Based on Orthogonal Test**. Advances in Materials Science and Engineering, 2018, 1–10.

Warsi, S. S., Agha, M. H., Ahmad, R., Jaffery, S. H. I., & Khan, M. (2018). **Sustainable turning using multi-objective optimization: a study of Al 6061 T6 at high cutting speeds**. The International Journal of Advanced Manufacturing Technology.

Witten, T. A., Sander, L. M**. Diffusion-limited aggregation,** Phys. Rev. Lett. 27, 1983. p. 5687-5697.

Witten, T. A., Sander, L. M**. Diffusion-limited aggregation: a kinetic critical phenomenon**, Phys. Rev. Lett. 47, 1981. p. 1400-1403.

Wodecki, J., Anna Michalak, Radoslaw Zimroz. **Optimal filter design with progressive genetic algorithm for local damage detection in rolling bearings**. Mechanical Systems and Signal Processing. Volume 102. 2018.

Worden & Friswell (2009). **Modal–vibration-based damage identification**. Encyclopedia of Structural Health Monitoring.

Yang, X., & Hossein Gandomi, A. (2012). **Bat algorithm: a novel approach for global engineering optimization**. Engineering Computations, 29(5), 464–483.

Yang, Xin-She. **Nature-inspired optimization algorithms**. Elsevier, 2014.

Yang C, Lu Z (2017) **An interval effective independence method for optimal sensor placement based on non-probabilistic approach**. Sci China Technol Sci 60(2):186–198.

Yang, Y., Cao, L., Zhou, Q., Wang, C., Wu, Q., & Jiang, P. (2018a). **Multi-objective process parameters optimization of Laser-magnetic hybrid welding combining Kriging and NSGA-II**. Robotics and Computer-Integrated Manufacturing, 49, 253–262.

Yang, Y., Cao, L., Wang, C., Zhou, Q., & Jiang, P. (2018b). **Multi-objective process parameters optimization of hot-wire laser welding using ensemble of metamodels and NSGA-II**. Robotics and Computer-Integrated Manufacturing, 53, 141–152.

Yang C, Lu Z, Yang Z (2018c) **Robust optimal sensor placement for uncertain structures with interval parameters**. IEEE Sens J.

Yi TH and Li HN. **Methodology developments in sensor placement for health monitoring of civil infrastructures**. Int J Distrib Sens N 2012; 8(8): 612726.

Yi, T-H, Zhou, G-D, Li, H-N, Wang, C-W. **Optimal placement of triaxial sensors for modal identification using hierarchic wolf algorithm**. Struct Control Health Monit. 2017; 24:e1958.

Yifei, T., Z. Meng, L. Jingwei, L. Dongbo and W. Yulin, "**Research on intelligent welding robot path optimization based on GA and PSO algorithms**", *IEEE Access*, vol. 6, pp. 65397-65404, 2018.

Yin T, Yuen K-V, Lam H-F, Zhu H-P (2017) **Entropy-based optimal sensor placement for model identification of periodic structures endowed with bolted joints**. Comput Aid Civ Infrastruct Eng 32(12):1007–1024

Yoon, K. P., & Kim, W. K. (2017). **The behavioral TOPSIS**. Expert Systems with Applications, 89, 266–272.

Yu, P. Xu, **Structural health monitoring based on continuous ACO method**, Microelectron. Reliab. 51 (2) (2011) 270–278

Yuen K-V, Kuok S-C (2015) **Efficient bayesian sensor placement algorithm for structural identification: a general approach for multi-type sensory systems**. Earthq Eng Struct Dyn 44(5):757–774

Zadeh, L. A. **Optimality and Nonscalar-Valued Performance Criteria**. IEEE Transactions on Automatic Control, AC-8(1):59–60, 1963.

Zenzen, I. Belaidi, S. Khatir, M.A. Wahab, **A damage identification technique for beam-like and truss structures based on FRF and Bat Algorithm**, Comptes Rendus Mécanique 346 (12) (2018) 1253–1266.

Zhou, G. D., Yi, T.-H., Xie, M.-X., Li, H.-N., & Xu, J.-H. (2021). **Optimal Wireless Sensor Placement in Structural Health Monitoring Emphasizing Information Effectiveness and Network Performance**. Journal of Aerospace Engineering, 34(2), 04020112.

Zhang, H., Peng, Y., Hou, L., Tian, G., & Li, Z. (2019a). **A hybrid multi-objective optimization approach for energy-absorbing structures in train collisions**. Information Sciences.

Zhang, J., H. Zhu, C. Yang, Y. Li, & H. Wei. **Multi-objective shape optimization of helico-axial multiphase pump impeller based on NSGA-II and ANN**. Energy Conversion and Management, vol. 52, no. 1, pp. 538–546, 2011.

Zhang, L., S. Zhang, W. Zhang, **Multi-objective optimization design of in-wheel motors drive electric vehicle suspensions for improving handling stability**. Proceedings of the Institution of Mechanical Engineers, Part D: Journal of Automobile Engineering 233, 2232–2245 (2019b)

Zhang Q, Li H (2007) **MOEA/D: a multi-objective evolutionary algorithm based on decomposition**. IEEE Trans Evol Comput 11:712–731

Zhang, R., X. Wang, **Parameter study and optimization of a half-vehicle suspension system model integrated with an arm-teeth regenerative shock absorber using Taguchi method**, Mech. Sys. Signal Process. 126, 65–81 (2019c)

Zhang, Y., Xu, Y., Zheng, Y., Fernandez-Rodriguez, E., Sun, A., Yang, C., & Wang, J. (2019d). **Multiobjective Optimization Design and Experimental Investigation on the Axial Flow Pump with Orthogonal Test Approach**. Complexity, 2019, 1–14.

Zhang, J., Wang, J., Lin, J., Guo, Q., Chen, K., & Ma, L. (2015). **Multiobjective optimization of injection molding process parameters based on Opt LHD, EBFNN, and MOPSO**. The International Journal of Advanced Manufacturing Technology, 85(9-12), 2857–2872.

Zhang Q, Zhou A, Zhao S, Suganthan PN, Liu W, Tiwari S (2008) **Multiobjective optimization test instances for the CEC 2009 special session and competition. Special session on performance assessment of multi-objective optimization algorithms**, technical report, 264. University of Essex, Colchester, UK and Nanyang technological University, Singapore.

Zheng, Q., Jiang, D., Huang, C., Shang, X., Ju, S.: **Analysis of failure loads and optimal design of composite lattice cylinder under axial compression**. Compos. Struct.131, 885–894 (2015)

Zhou, G.-D., Yi, T.-H., Zhang, H., and Li, H.-N. (2014) **Energy-aware wireless sensor placement in structural health monitoring using hybrid discrete firefly algorithm**, Struct. Control Health Monit., 22, 648– 666.

Zhou G-D, Xie M-X, Yi T-H, Li H-N. **Optimal wireless sensor network configuration for structural monitoring using automatic-learning firefly algorithm**. Advances in Structural Engineering. 2019; 22(4):907-918.

Zitzler, E., Deb, K., & Thiele, L. **Comparison of Multi-objective Evolutionary Algorithms: Empirical Results.** Evolutionary Computation, 8(2):173–195, Summer 2000.

Zitzler, E., Laumanns, M., & Thiele, L. SPEA2: **Improving the Strength Pareto Evolutionary Algorithm**. In K. Giannakoglou, D. Tsahalis, J. Periaux, P. Papailou, & T. Fogarty, editors, EUROGEN 2001. Evolutionary Methods for Design, Optimization and Control with Applications to Industrial Problems, pages 95–100, Athens, Greece, 2001.

Zitzler, E. (1999). **Evolutionary algorithms for multiobjective optimization: Methods and applications**, vol 63.

Zitzler, E. & Thiele, L. **Multi-objective Evolutionary Algorithms: A Comparative Case Study and the Strength Pareto Approach**. IEEE Transactions on Evolutionary Computation, 3(4):257–271, November 1999.

Appendix

Appendix A – Test Functions

Table A.1 – ZDT Test Functions for validating the MOLA

ZDT1	ZDT2
Minimize $f_1(x) = x_1$	Minimize $f_1(x) = x_1$
Minimize $f_2(x) = g(x) \times h(f_1(x), g(x))$	Minimize $f_2(x) = g(x) \times h(f_1(x), g(x))$
Where $g(x) = 1 + \frac{9}{N-1} \sum_{I=2}^{N} x_i$	Where $g(x) = 1 + \frac{9}{N-1} \sum_{I=2}^{N} x_i$
$h(f_1(x), g(x)) = 1 - \sqrt{f_1(x) / g(x)}$	$h(f_1(x), g(x)) = 1 - (f_1(x) / g(x))^2$
$0 \le x_i \le 1, 1 \le i \le 30$	$0 \le x_i \le 1, 1 \le i \le 30$

ZDT3
Minimize $f_1(x) = x_1$
Minimize $f_2(x) = g(x) \times h(f_1(x), g(x))$
Where $g(x) = 1 + \frac{9}{29} \sum_{I=2}^{N} x_i$
$h(f_1(x), g(x)) = 1 - \sqrt{\frac{f_1(x)}{g(x)}} - (\frac{f_1(x)}{g(x)}) \times \sin(10\pi f_1(x))$
$0 \le x_i \le 1, 1 \le i \le 30$

Table A.2 – CEC 2009 test functions

Name	Mathematical formulation
UF1	$f_1(x) = x_1 + \frac{2}{\lvert j_1 \rvert}\sum_{j\in J_1}\left[x_j - \sin(6\pi x_1 + \frac{j\pi}{n})\right]^2,\ f_2(x) = 1-\sqrt{x} + \frac{2}{\lvert j_2 \rvert}\sum_{j\in J_2}\left[x_j - \sin(6\pi x_1 + \frac{j\pi}{n})\right]^2$ $J_1 = \{j \mid j \text{ is odd and } 2 \le j \le n\}, \quad J_2 = \{j \mid j \text{ is even and } 2 \le j \le n\}$
UF2	$f_1(x) = x_1 + \frac{2}{\lvert j_1 \rvert}\sum_{j\in J_1} y_j^2,\ f_2(x) = 1-\sqrt{x} + \frac{2}{\lvert j_2 \rvert}\sum_{j\in J_2} y_j^{\ 2}$ $J_1 \text{and } J_2 \text{are the same of } UF1$
UF3	$f_1(x) = x_1 + \frac{2}{\lvert j_1 \rvert}(4\sum_{j\in J_1} y_j^2 - 2\prod_{j\in j_1}\cos(\frac{20y_j\pi}{\sqrt{j}}) + 2),\ f_2(x) = \sqrt{x_1} + \frac{2}{\lvert j_2 \rvert}(4\sum_{j\in J_1} y_j^2 - 2\prod_{j\in j_2}\cos(\frac{20y_j\pi}{\sqrt{j}}) + 2)$ $J_1 \text{and } J_2 \text{are the same of } UF1; y_j = x_j - x_1^{0.5\left(1+^{3(j-2)}/_{n-2}\right)}, j = 2,3,\dots,n$
UF4	$f_1(x) = x_1 + \frac{2}{\lvert j_1 \rvert}\sum_{j\in J_1} h(y_j),\ f_2(x) = 1-x_2 + \frac{2}{\lvert j_2 \rvert}\sum_{j\in J_2} h(y_j)$ $J_1 \text{and } J_2 \text{are the same of } UF1, y_j = x_j - \sin\left(6\pi x_1 + \frac{j\pi}{n}\right), j = 2,3,\dots,n, h(t) = \frac{\lvert t \rvert}{1+e^{2\lvert t \rvert}}$
UF5	$f_1(x) = x_1 + (\frac{1}{2N} + \varepsilon)\lvert \sin(2N\pi x_1) \rvert + \frac{2}{\lvert J_1 \rvert}\sum_{j\in J_1} h(y_i)$ $f_2(x) = 1-x_1 + (\frac{1}{2N} + \varepsilon)\lvert \sin(2N\pi x_1) \rvert + \frac{2}{\lvert J_2 \rvert}\sum_{j\in J_2} h(y_i)$ $J_1 \text{and } J_2 \text{are the same of } UF1, \varepsilon > 0, y_j = x_j - \sin\left(6\pi x_1 + \frac{j\pi}{n}\right), j = 2,3,\dots,n, h(t) = 2t^2 - \cos(4\pi t) + 1$
UF6	$f_1(x) = x_1 + \max\left\{0, 2(\frac{1}{2N} + \varepsilon)\sin(2N\pi x_1)\right\} + \frac{2}{\lvert J_1 \rvert}\left(4\sum_{j\in j_1} y_j^2 - 2\prod_{j\in j_1}\cos(\frac{20y_j\pi}{\sqrt{j}}) + 2\right)$ $f_2(x) = 1-x_1 + \max\left\{0, 2(\frac{1}{2N} + \varepsilon)\sin(2N\pi x_1)\right\} + \frac{2}{\lvert J_2 \rvert}\left(4\sum_{j\in j_1} y_j^2 - 2\prod_{j\in j_2}\cos(\frac{20y_j\pi}{\sqrt{j}}) + 2\right)$ $J_1 \text{and } J_2 \text{are the same of } UF1, \varepsilon > 0, , y_j = x_j - \sin\left(6\pi x_1 + \frac{j\pi}{n}\right), j = 2,3,\dots,n$
UF7	$f_1(x) = \sqrt[5]{x_1} + \frac{2}{\lvert J_1 \rvert}\sum_{j\in J_1} y_j^2,\ f_2(x) = 1-\sqrt[5]{x_1} + \frac{2}{\lvert J_2 \rvert}\sum_{j\in J_2} y_j^2$ $J_1 \text{and } J_2 \text{are the same of } UF1, \varepsilon > 0, , y_j = x_j - \sin\left(6\pi x_1 + \frac{j\pi}{n}\right), j = 2,3,\dots,n$
UF8	$f_1(x) = \cos(0,5x_1\pi)\cos(0,5x_2\pi) + \frac{2}{\lvert j_1 \rvert}\sum_{j\in J_1}\left[x_j - 2x_2\sin(2\pi x_1 + \frac{j\pi}{n})^2\right]$

$$f_2(x) = \cos(0,5x_1\pi)\sin(0,5x_2\pi) + \frac{2}{|j_1|}\sum_{j\in J_1}\left[x_j - 2x_2\sin(2\pi x_1 + \frac{j\pi}{n})^2\right]$$

$$f_3(x) = \sin(0,5x_1\pi) + \frac{2}{|j_3|}\sum_{j\in J_3}\left[x_j - 2x_2\sin(2\pi x_1 + \frac{j\pi}{n})^2\right]$$

$where\ J_1 = \{j|3 \le j \le n, and\ j-1\ is\ a\ multiplication\ of\ 3\}, J_2 = \{j|3 \le j \le n, and\ j-2\ is\ a\ multiplication\ of\ 3\},$
$J_3 = \{j|3 \le j \le n, and\ j\ is\ a\ multiplication\ of\ 3\}$

UF9

$$f_1(x) = 0.5\left[\max\left\{0,(1+\in)(1-4(2x_1-1)^2\right\} + 2x_1\right]x_2 + \frac{2}{|j_1|}\sum_{j\in j_1}(x_j - 2x_2\sin(2\pi x_1 + \frac{j\pi}{n})^2)$$

$$f_2(x) = 0.5\left[\max\left\{0,(1+\in)(1-4(2x_1-1)^2\right\} + 2x_1\right]x_2 + \frac{2}{|j_2|}\sum_{j\in j_2}(x_j - 2x_2\sin(2\pi x_1 + \frac{j\pi}{n})^2)$$

$$f_3(x) = 1 - x_2 + \frac{2}{|j_3|}\sum_{j\in j_3}(x_j - 2x_2\sin(2\pi x_1 + \frac{j\pi}{n})^2)$$

$where\ J_1 = \{j|3 \le j \le n, and\ j-1\ is\ a\ multiplication\ of\ 3\}, J_2 = \{j|3 \le j \le n, and\ j-2\ is\ a\ multiplication\ of\ 3\},$
$J_3 = \{j|3 \le j \le n, and\ j\ is\ a\ multiplication\ of\ 3\}, \in = 0.1;$

UF10

$$f_1(x) = \cos(0,5x_1\pi)\cos(0,5x_2\pi) + \frac{2}{|j_1|}\sum_{j\in J_1}\left[4y_j^2 - \cos(8\pi y_j) + 1\right]$$

$$f_2(x) = \cos(0,5x_1\pi)\cos(0,5x_2\pi) + \frac{2}{|j_2|}\sum_{j\in J_1}\left[4y_j^2 - \cos(8\pi y_j) + 1\right]$$

$$f_3(x) = \sin(0,5x_1\pi) + \frac{2}{|j_3|}\sum_{j\in J_3}\left[4y_j^2 - \cos(8\pi y_j) + 1\right]$$

$where\ J_1 = \{j|3 \le j \le n, and\ j-1\ is\ a\ multiplication\ of\ 3\}, J_2 = \{j|3 \le j \le n, and\ j-2\ is\ a\ multiplication\ of\ 3\},$
$J_3 = \{j|3 \le j \le n, and\ j\ is\ a\ multiplication\ of\ 3\}$